UNIVERSITAT AUTÒNOMA DE BARCELONA
INSTITUT DE CIÈNCIA I TECNOLOGIA AMBIENTALS

Radionuclides in the Arctic Ocean : tracing sea ice origin, drifting and interception of atmospheric fluxes

Patricia Cámara Mor

PhD thesis, 2012

Advisors:

Dr. Pere Masqué Barri

Dr. Jordi Garcia Orellana

UNIVERSITAT AUTÒNOMA DE BARCELONA
INSTITUT DE CIÈNCIA I TECNOLOGIA AMBIENTALS

Radionuclides in the Arctic Ocean : tracing sea ice origin, drifting and interception of atmospheric fluxes

Patricia Cámara Mor

PhD thesis, 2012

Advisors:

Dr. Pere Masqué Barri

Dr. Jordi Garcia Orellana

Dr. Pere Masqué Barri Dr. Jordi Garcia Orellana Patricia Cámara Mor

A la yaya, papis y tato

Acknowledge

De nuevo una página en blanco, pero ésta no es igual que las anteriores, es la última! Su punto y final significa el cierre de una aventura que comenzó hace ya unos años.

Esta aventura no habría sido posible sin que mis dos directores, Pere Masqué y Jordi Garcia Orellana, depositaran su confianza en mi. Vosotros sois quienes habéis hecho que me encuentre hoy aquí. Pere, gracias por animarme a seguir adelante, por tu pragmatismo y por subirme el listón en cada momento. Jordi, no sé como agradecerte todo tu apoyo, hacerme ver la luz al final del túnel y darme fuerzas para continuar en los momentos de flaqueza. Muchas gracias a los dos por los momentos compartidos durante estos años.

Quiero aprovechar esta ocasión que se me brinda para poder agradecer a todas aquellas personas que han compartido conmigo de una u otra manera esta aventura. Algunos vivisteis como comenzó, otros como acaba pero a todos vosotros: Eli, Ester, Cesar, Carolina, Núria, Valentí, Viena, Pep, Montse y Joan Manuel, quiero agradeceros los momentos compartidos durante la infinidad de horas encerrados en el laboratorio, despacho, etc., por aguantarme en los períodos duros y sobretodo por vuestra amistad. Quiero hacer extensivo el agradecimiento a los científicos que estuvieron de paso por el lab, Maria Villa, Pepe Mas, Karina Kammer, Tom Church, Claudia Benitez-Nelson,… a las satélites, Ester y Marta, así como a la gente del ICTA, tanto personal de administración como compañeros, y al departamento de Física, Manel y Jordi, que hacen posible que las cosas ocurran.

Ein besonderer Dank gilt den Kollegen des AWI, insbesondere der Geochemie Abteilung. Ihr mich am Anfang dieses Abenteuers empfangen und dessen Entwicklung auf die eine oder andere Weise verfolgt. Ingrid und Michiel, vielen Dank für eure Undetstútzung, Hilfe und Beratung vor, während und nach der Kampagne an Bord des Polarsterns. Ich wage zu bezweifeln, ob ich diese Zeit ohne Euch überstanden hätte. Jana und Claudia, vielen Dank für die lange Gesprächen an den Freitagen, wenn ich nach Bremerhaven kam und während den Aufenthalten mit Euch. Und auch vielen Dank an alle Doktorandinnen und Docktoranden, Sven, Tobias, Celia un Oli dafür, dass ihr die Stunden im Lab so angenehm gestaltet habt.

My acknowledge to Kirk Cochran for hosting me at SUNY-Stony Brook Univeristy (USA) and for providing me constructive comments that helped to enrich the manuscripts. And also thanks to Tim Kenna for teaching me everything he knows about

Pu isotopes and its quantification with ICP-MS and for welcoming me in his lab as another more. It was a great experience!

I would also like to express my gratitude to all those involved in producing the publications presented as part of this PhD dissertation, both to co-authors and all others who helped in producing the relevant material. To complete this list with all names would take large space. In particular, I would like to thank the staff of the RV Polarstern, who helped me in solving many practical problems and to all scientists who participated in the ARK XXII/2 cruise for providing a really nice environment for working out on the ice and in the labs and making that experience unrepeatable.

A Pepe Mas y Elena Chamizo, de la Universidad de Sevilla, gracias por las medidas de los isotopos de Pu, vuestras sugerencias y enseñarme los entresijos del AMS.

I would also like to thank to Walter Geibert and Jana Freidrich, for reading this thesis, for their comments to improve it and for writing the stand form for the European doctorate mention and as well as to Claudia Hanfland for providing me the needed letter for that mention. I would also like to thank to Michiel Rutgers van der Loeff, Antonio Tovar, Jordi Dachs, Pere Puig and Sergi Rossi for agreeing to be members of my PhD committee.

Mas allá de esta aventura, quiero agradecer a mis papis y tato, pilares fundamentales en mi vida, su apoyo incondicional (especialmente durante la primavera del 2011). Sin ellos, jamás hubiera podido conseguir lo que hasta ahora. Su tenacidad y lucha incansable han hecho de ellos mi gran ejemplo a seguir. Gracias! A mi yaya que desde donde estés sé que me cuidas. No quiero dejar de nombrar a los que han cuidado de mi desde que puse el pie en Barcelona, mi Padrino y Lina. Gracias por hacerme sentir como en casa y por ser mis segundos padres.

A vosotras, ya sabéis quienes sois, por vuestra amistad, por los todos los momentos vividos durante estos años: viajes, risas y lloros. Por ayudarme a evadirme de la ciencia, a ver que hay algo más allá que las cuatro paredes de la universidad y por aconsejarme en los precisos momentos. Gracias chicas!

Per últim i no menys important vull agrair al Victor la seva paciència en els darrer anys, els més difícils sense dubte. Gràcies per allargar-me la teva mà per tirar endavant, per recolzar-me en cada decisió i per saber treure la meva millor part. Gràcies per començar amb mi una altra aventura, la nostra aventura. T'estimo!

El presente trabajo ha sido posible gracias a beca FPU, AP2006-03071, otorgada a Patricia Cámara Mor por el Ministerio de Educación y Ciencias y gracias a la financiación de los proyectos IPY-Geotraces a l'Àrtic: Radionúclids com traçadors del paper de gel marí en el transport, dispersió i acumulació de material particulat i espècies associades a l'Oceà Àrtic, Ministerio de Educación y Ciencia (POL2006-00449) y Action ES0801: The ocean chemistry of bioactive trace elements and paleoclimate proxies, European Cooperation in the field of Scientific and Technical Research (COST ES0801) por el Ministerio de Educación y Ciencias y la Unión Europea, respectivamene.

Table of contents

List of Figures

List of Tables

Preface

At high latitudes the ocean is characterized by being covered by sea ice, its extent presenting a large degree of variability from summer to winter the year. In the Arctic Ocean, the average sea ice extent in summer and winter for the period 1979-2000 was of $1.28 \cdot 10^6$ and $15.86 \cdot 10^6$ Km^2, respectively. Nowadays, the Arctic Ocean is experimenting a strong impact of global warning, of which some obvious signs are the decline of sea ice extent, with a rate of 3% per decade for the period 1979 – 2007, and the shrinking of the sea ice thickness, with an average rate of -18 $cm \cdot y^{-1}$ [*Stroeve et al*., 2008; *Kwok and Rothrock*, 2009]. Some studies predict that the Arctic Ocean will be a free ice ocean in summer seasons by 2030 [e.g. *Holland et al*., 2006; *Maslowski et al*., 2007].

Sea ice is a key component of the Arctic Ocean. It is a thin, fragile, heterogeneous and dynamic layer, which acts as a barrier between two of the major Earth fluids: the ocean and the atmosphere. The presence or absence of sea ice controls the climate through the interactions between the atmosphere and the ocean, limiting heat and energy flux, as well as the interception of solar light contributes to limit the arctic primary production. Sea ice also modifies the amount of solar radiation absorbed by the surface ocean, as a fraction of it is reflected back to the atmosphere as a consequence of its high albedo. The freezing-melting processes cause vertical redistribution of salts in the ocean, leading to the formation of deep bottom water or the stratification of the surface water during melting [*Dieckmann and Hellmer*, 2003].

The dynamic character of sea ice makes it a relevant agent for the transport and distribution of chemical species and particulate matter [*Kempema et al*., 1989; *Pfirman et al*., 1989; *Dethleff and Kuhlmann*, 2010]. During its formation, mainly in the continental shelves, it incorporates particulate matter (sea-ice sediments) and is exported to the central Arctic Basin. During the drifting sea ice also incorporate chemical species. Subsequently, all incorporated components, both SIS and chemical species, are released to the water column by sea ice melting. Therefore, sea ice melting would markedly dictate biogeochemical element distribution in the water column in the ablation area.

Given the swiftly changes that Arctic sea ice is facing and the projections of sea ice extent in the future, as well as the poor understanding of the interaction of chemical species between the different compartments (ocean, sea ice and atmosphere) and the magnitude of these interactions [*Melinkov*, 1991; *Grankrog*, 2003; *Lannuzel et al*., 2010; *Tison et al*., 2010], it is of special interest to improve the knowledge of the role of sea ice in the biogeochemical cycling of chemical species (trace metals, radionuclides and other chemical species) and the transport and distribution of these chemical species

and particles. These shifts may entail several implications and effects: changes in sedimentation rates, enrichment of chemical concentration in surface waters in the ablation areas, impacts in the primary production, contaminant redistribution and perturbation of the biogeochemical cycling in the water column.

Scientific community has attracted by the Arctic Ocean due its extreme and inhospitable environment. In 1882-83, for the first time worldwide scientists banded together to organize exploring programs in the polar Arctic region: it was the first International Polar Year (IPY). 50 years later, the second International Polar Year took place and 75 years after the first IPY, the first International Geophysical Year was celebrated. Even though it was mainly focused on the geophysical and dynamic parameters of sea ice and meteorological research, it lead to a considerable improvement in the understanding of the Arctic Ocean and the Arctic sea ice. Notwithstanding, none of these programmes focused much efforts on the sea ice biogeochemistry, which have received more attention during the last decades, although still less than works on other sea ice aspects. During the International Polar Year (IPY) performed during 2007/09 (www.ipy.org), the GEOTRACES program (www.geotraces.org) proposed to study trace elements in the Arctic Ocean to establish the baseline of geochemical data for studying the constant changes and further shifts in the Arctic Ocean. Even though GEOTRACES focuses on the geochemistry in the water column of the ocean, some works were executed in relation to sea ice.

This dissertation is based on the consideration that all physical, chemical and structural processes that sea ice undergoes during the whole life cycle determine its role and the final fate of the sea-ice sediments and the chemical species dissolved or associated to particulate matter. The present rapid changes might disturb all these processes and the whole Arctic ecosystem as a consequence of sea ice feedbacks. Due to the large uncertainty about the presence of Arctic sea ice during summer in the coming years, it is essential to improve the knowledge on the interactions between the different compartments, atmosphere-sea ice-ocean, which shall allow to better understand the possible implications of the current shifts associated to climate change in the Arctic Ocean.

The different processes that sea ice undergoes (physical, chemical, geologic, biological, etc.) take place at the same time. Understanding, quantifying and predicting them may be benefit from using internal tracers, such as radionuclides. The radionuclides, natural or artificial in origin, are characterized by different half-lives and by having distinct chemical properties. As a result they participate in different degrees in those processes that control their distributions in the environment. Likewise, they are powerful tools to study all these processes that occur in the nature, in this case in the Arctic sea ice, at different time-scales. The variation in their concentrations, which are caused by transport, diffusion, association, decay, scavenging processes, allows attempting to answer the aims of the PhD dissertation.

Aims

The primary objective of this dissertation is to provide with some insight and evaluate the relevance of the Arctic sea ice as an agent of the transport and distribution of chemical species and particulate matter along the Arctic Ocean through the use of a set of radionuclides, both natural (^{7}Be, ^{210}Pb and ^{210}Po) and artificial (^{137}Cs, ^{239}Pu and ^{240}Pu). The specific aims are:

i) Study the feasibility of the use of this set of natural and artificial radionuclides to evaluate and quantify the importance of several processes that sea ice undergoes during its lifespan. These processes are related to interception, accumulation, transport and distribution of particulate matter and chemical species.

ii) Elucidate which are the main mechanisms by which radionuclides (^{7}Be, ^{210}Pb, ^{210}Po ^{137}Cs, ^{239}Pu and ^{240}Pu) are incorporated into sea ice, and ascertain which processes cause their enrichment in sea ice sediments (SIS): atmospheric inputs or scavenging from seawater.

iii) Use ^{137}Cs, ^{239,240}Pu and the ^{240}Pu/^{239}Pu atom ratio in SIS to assess the origin of sea ice floes.

iv) Understand the interaction of sea ice with the ocean and the atmosphere through the study of the interception of atmospheric fluxes of ^{7}Be and investigate the mechanisms and the efficiency by which sea ice accumulates chemical species from the atmosphere.

v) Determine the distributions of radionuclide with an atmospheric component, such as ^{7}Be, in the Arctic Ocean and investigate the processes that regulate their presence in the different compartments (sea ice, sea water, sea-ice sediments, atmosphere flux) in particular define the role that sea ice plays.

Thesis structure

This dissertation is organized in seven chapters. The first chapter details the most relevant aspects of the Arctic Ocean, in particular regarding Arctic sea ice. The first subsection frames the study area, presenting its general features on bathymetry, hydrology and water circulation. The second part summarizes the sea ice properties and the characteristics of drifting, extent, thickness and points to its role in the transport and redistribution of particulate matter along the Arctic Ocean.

General considerations on the sources and distributions of the radionuclides of interest (^{7}Be, ^{210}Pb and ^{210}Po and ^{137}Cs and ^{239,240}Pu) in the Arctic Ocean are given in the second chapter.

Chapter 3 is devoted to the description of the field protocols followed to sample sea ice, seawater, precipitation and sediments and the analytical methods used to determine and quantify the suite of analysed radionuclides: gamma emitters (^{7}Be and ^{137}Cs) by gamma-spectrometry, ^{210}Pb and ^{210}Po by alpha spectrometry and plutonium isotopes (^{239}Pu and ^{240}Pu) and the ^{240}Pu/^{239}Pu atom ratio by mass spectrometry.

In chapter 4, we present and discuss the data on ^{137}Cs and ^{239,240}Pu activities and the ^{240}Pu/^{239}Pu atom ratio in SIS in the Arctic Ocean, including previously published data. We show that the distribution of both ^{137}Cs and ^{239,240}Pu concentrations in SIS mirrored the main sea ice drift patterns, reflecting the transport of particulate matter by sea ice. Through a direct comparison of the concentrations measured in SIS samples against those reported for the potential source regions, the usefulness of these radionuclides as tracers of sea ice origin is studied. The ^{240}Pu/^{239}Pu atom ratio is a fingerprint of the Pu source, and it is used to distinguish between different continental shelves, and ^{137}Cs data permitted to constrain the source of SIS[1].

The efficiency by which sea ice intercepts atmospheric inputs is studied by using the data on ^{7}Be in Chapte 5 ^{7}Be, an atmospheric natural radionuclide with a short half-life and well-known sources, is analysed in all compartments of the sea ice system: surface sea ice, sea-ice sediments, water beneath ice, surface water and atmosphere, and the efficiency of interception-accumulation is assessed through a mass balance of ^{7}Be, The data is also used to estimate the amount of sediments that are transported and released by sea ice in the Fram Strait at/on an annual basis[2].

Chapter 6 focuses on the discussion of the mechanisms of radionuclide enrichment in SIS. Previous work has suggested that scavenging from surface seawater is the main source of ^{210}Pb in SIS, while other studies claimed atmospheric deposition to be the main mechanism. In order to do that, a set of

[1] Cámara-Mor P., P. Masqué, J. Garcia-Orellana, J.K. Cochran, J.L. Mas, E. Chamizo, C. Hanfland (2010). Arctic Ocean sea ice drift origin derived from artificial radionuclides. Science of the Total Environment 15: 408(16):3349-58.

[2] Cámara-Mor P., P. Masque, J. Garcia-Orellana, S. Kern, J.K. Cochran and C. Hanfland (2011). Interception of atmospheric fluxes by Arctic sea 1 ice: evidence from cosmogenic ^{7}Be. Journal Geophysical Research 16:C12041,doi:10.1029/2010JC006847.

radionuclides, natural and artificial in origin, with different sources, half-lives and geochemical characteristics, is used to assess the relative significance of each process

The general and most significant conclusions of this work are synthesized in Chapter 7.

Chapter 1.

The Arctic Ocean and Sea ice

The first studies related to Arctic sea ice were mainly focussed on its geophysical properties and its dynamics. However, in the recent years other environmental questions have become relevant, and studies on ecological and biogeochemical aspects of sea ice are increasingly receiving attention by the scientific community. In this first chapter we provide with an introduction to the main characteristics of the Arctic Ocean, with especial emphasis on those aspects that are directly related to our thesis. Firstly, Arctic Ocean features: bathymetry and circulation; secondly, sea ice, as a key component of the Arctic Ocean, describing its properties such as salinity and temperature, thickness and drift patterns.

1.1. The Arctic Ocean

The Arctic Ocean, also called Mediterranean, occupies $14 \cdot 10^6$ km^2. It is surrounded by several shallow marginal seas with depths lower than 500 m, comprising about 1/3 of the total area. These shallow areas are the Eurasian Seas (Barents, Kara, Laptev, East Siberian) and the North American Seas (Chukchi, Beaufort, and Lincoln). The central Arctic Basin consists of two main basins, the Eurasian and Canadian Basins, with depths up to 4200 m and 3900 m, respectively. Both basins are separated by the Lomonosov Ridge, which stretches from Siberia to Greenland through the North Pole. Both basins are further divided by others ridges: the Gakkel Ridge divides the Eurasian Basin into the Amundsen and Nansen Basins, and the Alpha-Mendeleyev Ridge subdivides the Canadian Basin into the Canada and Makarov Basins (Figure 1.1).

The Arctic Ocean is connected with the Pacific and the Atlantic oceans mainly through the Bering and the Fram Straits, respectively (Figure 1.1). Both straits have quite distinguishable features. The Fram Strait reached,3000 m of depth and is approximately 440 km wide, being the only deep passage in the Arctic Ocean. The majority of water mass exchange with the world oceans takes place through it; furthermore it is the only place where deep-water mass exchange occurs. The Bering Strait is only 50 m deep and 85 km wide, and the water exchange is reduced to surface waters. The Barents Sea and the narrow straits in the Canadian Arctic archipelago are other connections with the Atlantic Ocean, without deep-water exchange

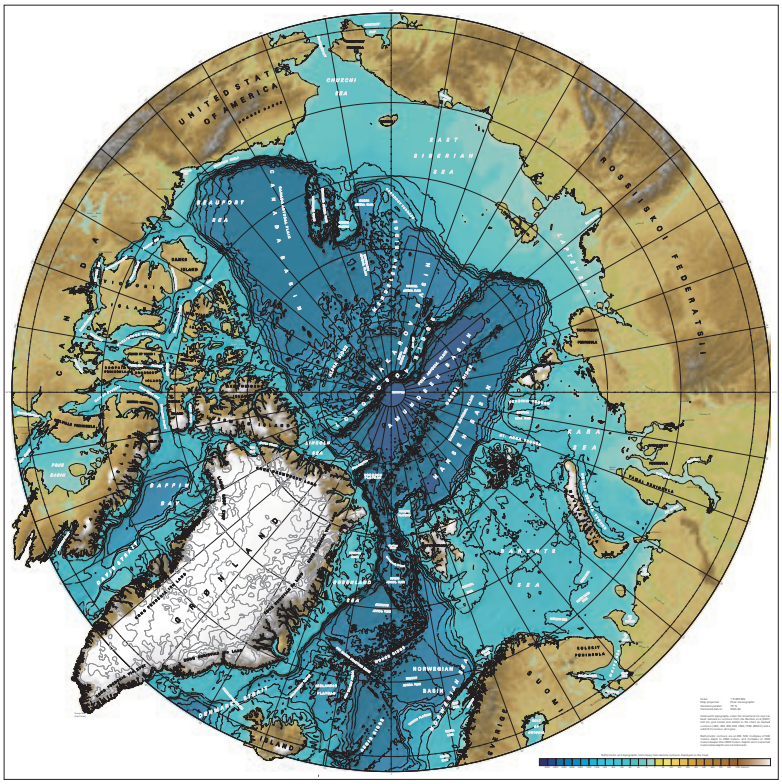

Figure 1.1 Topography and bathymetry of the Arctic Ocean based upon the data set, *IBCAO* [2004].

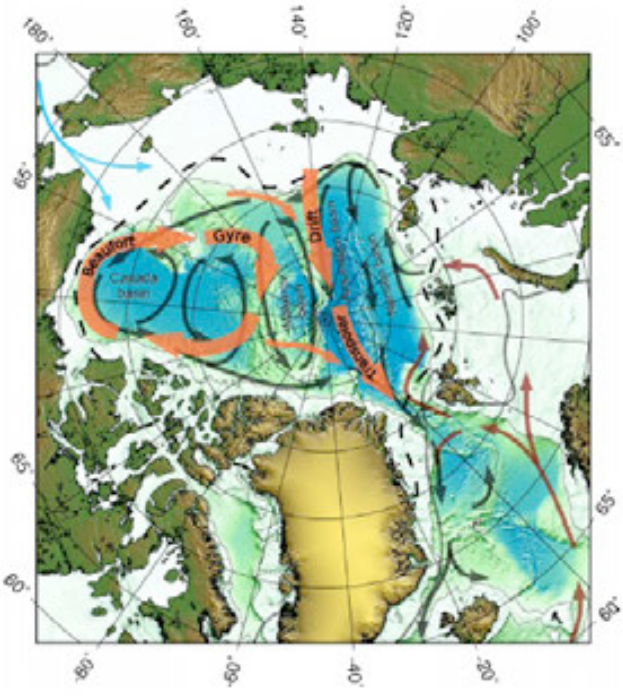

Figure 1.2 Circulation of the surface waters in the Arctic Ocean (Beaufort Gyre and Transpolar Drift), represented in orange arrows. Warm Atlantic Currents are indicated in red, Pacific water inflow in light blue and re-circulated currents in green. The typical winter and summer sea ice extent of the recent years are represented as black dashed and dots lines, respectively. [*Gunnar*, 2009].

The Atlantic water is the main inflow of water into the Arctic Ocean (Figure 1.2). This water mass is characterized by being a warm (temperature above 0ºC) and saline (35) inflow and the major oceanic heat source for the Arctic Ocean. It enters into the Arctic Ocean divided in two branches: the West Spitzbergen Current (WSC), which goes through the Fram Strait, and the Norwegian Atlantic Current (NAC), which enters through the Barents and the Kara Seas (Figure 1.2) [*Gerdes and Schauer*, 1997]. The Pacific water enters through the Being Strait into the Arctic Ocean, presenting a seasonal cycle: its inflow is greater in summer than in winter. This water mass is characterized by being less dense and fresher (32.5) than the Atlantic water and supplies water to the Chukchi Sea and to the upper layers of the Canadian Basin (Figure 1.2) [*Coachman and Barnes*, 1961]. This Pacific inflow is approximately 10% of the Atlantic water inflow.

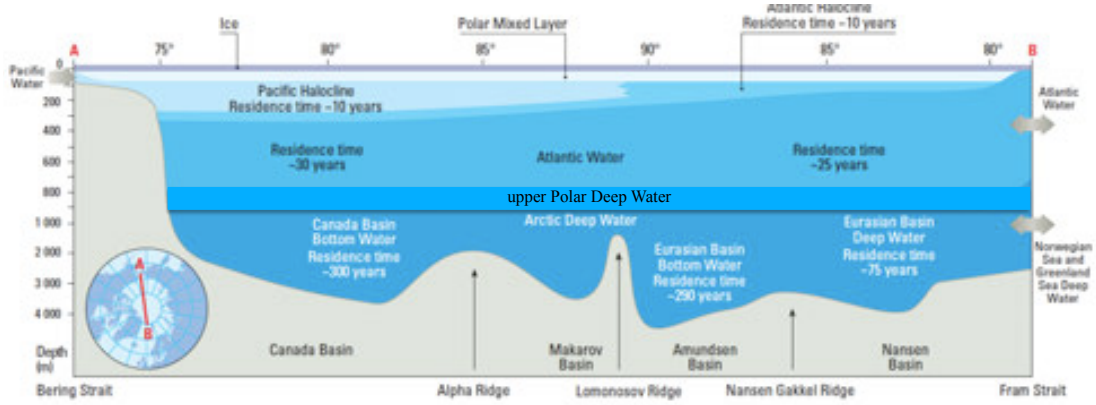

Figure 1.3 A schematic representation of the three-layer structure of the Arctic Ocean, the Arctic Surface Water (Polar Mixed Layer and Halocline) above the Atlantic Water and Arctic Deep Water [*Aagaard and Carmack*, 1989]. The residence time of each water mass is also shown [*Bönisch and Schlosser*, 1995]. Figure from *AMAP* [1998].

A scheme of the vertical structure of the water column in the Arctic Ocean is shown in Figure 1.3. The Arctic Ocean is normally divided in three layers, characterized by different water masses and circulation patterns: the Arctic Surface Water, the Atlantic Water and the Deep Water [*Aagard et al*., 1985; *Carmack,* 1990; *Anderson et al*., 1994].

The Surface Water (0-200 m) is subdivided in the Polar Mixed Layer (PML) (upper 30-50 m) and the Halocline (50-200 m). This water layer constitutes 17% of the total volume of the Arctic Ocean [*Aargaard et al*., 1985]. The PML is characterized by a temperature close to the freezing point due to presence of the sea ice cover. Its salinity exhibits a seasonal fluctuation as a consequence of sea ice melting and freezing and the inputs from the river runoff. The salinity varies geographically, being lower in the Canadian Basin (30-31) than in the Eurasian Basin (32-33) [*Rudels,* 2001]. The Halocline is markedly characterized by being stratified, insulating the Atlantic Water. This implies advective sources [*Schlosser et al*., 1995] and inhibits vertical transport of properties such as heat [*Carmack* 1990; *Rudels et al*., 1996]. The Halocline is subdivided in the Pacific Halocline Water (PHW) and the Atlantic Halocline Water (AHW). The PHW is originated in the Bering Strait and the Chukchi Sea. It is less saline (33.1) and thicker (200 m) than the AHW, whose thickness reaches 100-150 m depth and its salinity is 34.2. This water mass is originated in the Eurasian shelves (Figure 1.3).

Surface water circulation has been deduced from the sea ice drift [Carmack and Swift, 1990; Rudels 2001]. The main surface patterns are the Transpolar Drift (TPD) and the Beaufort Gyre (Figure 1.2). The TPD is a current that flows from the Siberian shelves along the Eurasian Basin, close to the North Pole, to the Fram Strait. Velocity in the TPD increases towards the Fram Strait, being the mean drift speed 5-20 $cm \cdot s^{-1}$, where the water leaves the basin to become part of the East Greenland Current [Carmack, 1986]. The Beaufort Gyre has a clockwise motion within the Canadian Basin, with a drift velocity of 1-3 $cm \cdot s^{-1}$ [Thornike, 1986]. This circulation pattern depends upon atmospheric circulation and is restricted to the upper surface layer.

Below the upper layer are the intermediate water that comprises the Atlantic Water (AW) and the upper Artic Deep Water (uPDW) (Figure 1.3). The AW extends from 200 to 900 m, representing 46%

of the total volume of the Arctic Ocean. When the AW enters into the Arctic Ocean, its temperature is above 3 ºC and its salinity is 35; nonetheless its temperature decreases along its path through the Arctic Ocean: at the Canadian Basin the maximum temperature is below 1 ºC and decreases down to 0.5 ºC in the Canada Basin, reaching the lowest temperature just before existing through the Fram Strait. These alterations are caused by diffusion and mixing with shelf waters and the overlying halocline water [*Schauer et al*., 1997]. The uPDW is the intermediate water placed below the AW and above the Deep Arctic Water. It is colder than 0 ºC and its salinity is greater than 34.85 [*Rudels,* 1994]. In this layer, salinity increases while temperature decreases with depth, as a result of the merging of entraining shelf plumes and the Arctic water column [*Rudels*, 2001]. Geographically, it is warmer and more saline in the Canadian Basin than in the Eurasian Basin (Figure 1.4).

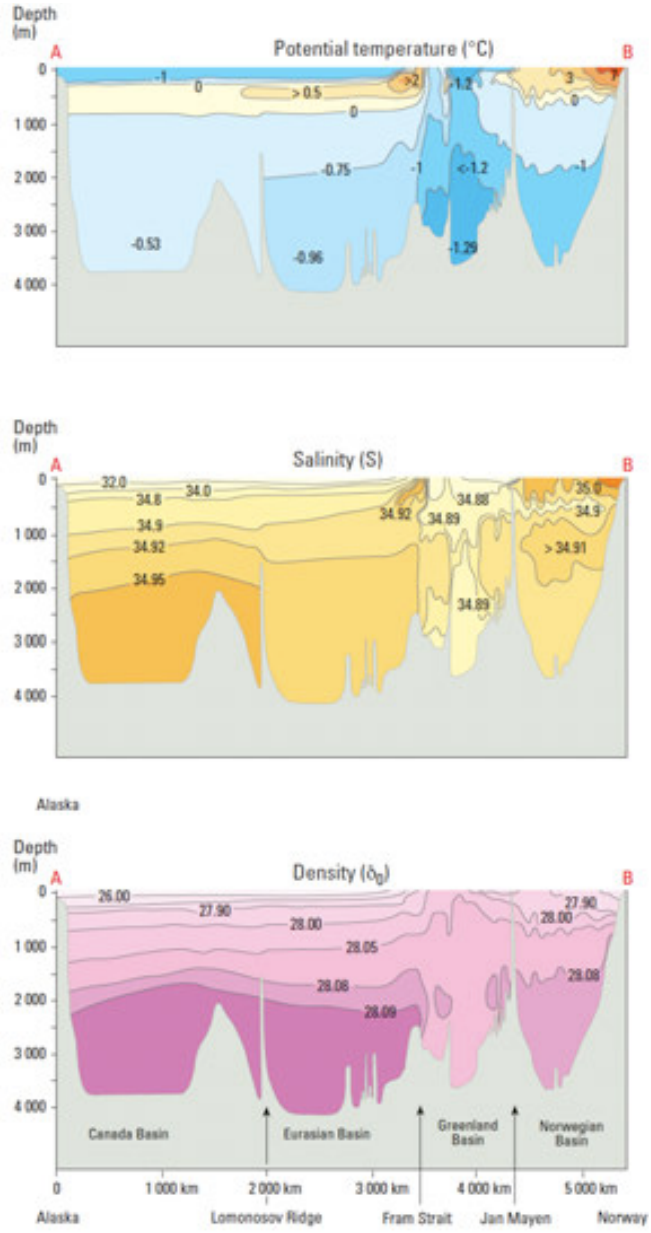

Figure 1.4 Schematic representation of the distribution of the potential temperature, salinity and density in the section across the Arctic Ocean from Alaska (A) to Norway (B). [*AMAP*, 1998].

A schematic representation of the AW and the intermediate water circulation is given in Fig. 5. The AW enters into the Arctic Ocean through the Fram Strait and the Barents Sea (1 - 3 Sv, [*Rudels*, 2001])

and flows eastward along the Eurasian Basin. At the eastern part of the St. Anna Trough both branches merge [*Rudels et al*., 1994] and continue flowing eastward as a boundary current, although a fraction, predominantly of the branch that entered through the Fram Strait, returns toward the Fram Strait within the Nansen Basin [*Coachman and Barnes*, 1963; *Anderson et al*., 1989]. At the Lomonosov Ridge 50% of the boundary current turns northward to the Fram Strait into the interior of the Amundsen Basin and the rest goes eastward [Aagaard, 1989]. At the Mendelev Ridge and further in the Chukchi Cap, the boundary current is again divided [*Aagaard et al*., 1996; *Carmack et al*., 1997]. The boundary current continues flowing along the American continental slope, in which is again splits at the Alpha Ridge and the Lomonosov Ridge. North of Greenland, one fraction of the boundary current returns to the Eurasian Basin and the rest flows toward the Fram Strait into the East Siberian Current [*Coachman and Barnes*, 1963, *Aagaard*, 1989]. The boundary current formed by the AW mass gets denser by cooling while it travels cyclonically around the perimeter of the Arctic Ocean and sinks down, mainly in ice growth regions as a result of the additional brine rejection input that contributes to the intermediate waters and also modified them (Figure 1.5). Finally, the boundary current formed by the AW mainly leaves the Arctic Ocean again via the Fram Strait, being now colder and fresher than the surrounding waters [*Rudels et al*., 2000] (Figure 1.4).

The temperature and salinity characteristics of the Arctic Deep Waters continue to diverge in both basins. The Arctic Deep Water is subdivided into the Canadian Basin Deep Water (CBDW) and the Eurasian Basin Deep Water (EBDW) [*Aagaard et al*., 1985]. This water layer represents 60% of the total volume in the Artic Ocean, and it is the oldest water of the Arctic Ocean [*Schlosser et al*., 1995] (Figure 1.3). The EBDW is again subdivided in the Deep and the Bottom Waters [*Aagaard et al*., 1981]. The main difference is that the CBDW is warmer and salty (-0.5ºC, 34.95) than the EBDW (-0.75, 34.92 and -0.95 ºC, 34.93 for deep and bottom, respectively) (Figure 1.4). The difference between bottom waters, >2000 m, in the Canadian and the Eurasian Basins is shown in Fig. 1.4. That difference is caused because the Lomonosov Ridge prevents deep-water exchange below the crest and only shallow, warmer and deeper waters of the Eurasian Basin can enter into the Canadian Basin [*Coachman and Aagaard*, 1974]. However, *Rudels* [2001] and *Woodgate et al*. [2001] stated that colder water from the EBDW passes into the Makarov Basin through gaps in the central part of the Lomonosov Ridge.

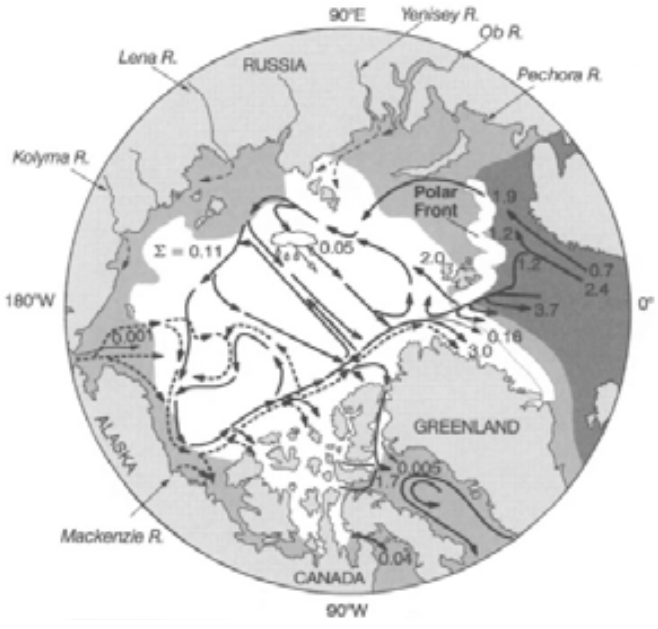

Figure 1.5 Schematic representation of main currents entering in the Arctic Ocean and their circulation along the Arctic Ocean [Macdonals *et al*. 2000] Atlantic and intermediate waters are shown as solid arrows. The dashed arrows indicate runoff from the major rivers. The numbers given are the estimated inflows and outflows in Sverdrups ($1Sv=10^6\ m^3 \cdot s^{-1}$). Sea ice extent is also represented. White colour represents permanent pack ice, light grey identifies seasonal ice and dark grey indicates permanent open water.

The Arctic Deep Water circulation follows the same pattern than the Arctic Intermediate oceanic circulation in the Arctic Ocean, which is controlled by: i) the boundary current along the continental shelves, which flow cyclonically around the basin [*Rude*ls, 2001], ii) the topography features of the Arctic Ocean, as parallel ridges split the basins and cause flows into their interior [*Rude*ls, 2001] and iii) the thermohaline forcing, in contrast to the major oceans. The exception is the strong influence of the Lomonosov Ridge in blocking any direct flow between the deep basins [*Woodgate et al*., 2001; *Rudels,* 2001].

1.2. Sea ice

Arctic sea ice has been studied since the Nansen expedition in the earlier 1900s. At the beginning studies were only focused on the geophysical and dynamic properties of the sea ice, such as salinity, temperature, thermodynamic and dynamic processes. Since 1980s a number of studies evidenced the importance of sea ice as a transport agent of particulate matter [e.g. *Pfirman et al*., 1990; *Reimnitz et al*., 1991]. Nevertheless, the role of sea ice in cycling of chemical species has received poor attention. Recently, some works have studied the content of nutrients, metals and radionuclides in sea ice, the role of sea ice sediments (SIS) as a significant source of Fe, for instance, when those are released into surface waters, the implications of the transport of chemical species and particulate matter along the Arctic Ocean by sea ice, etc. [e.g. *Garkrong*, 2003; *Measures*, 1999; *Masqué et al*., 2007; *Tovar-Sanchez et al*. 2010]. In order to appreciate the relevance of sea ice in cycling of chemical species and transport agent, a general introduction of the main aspects of sea ice is provided here.

1.2.1. Growth and classification

According to the World Meteorological Organization [*WMO*, 1970] sea ice consists of all forms of ice found at sea that have been originated from freezing of seawater. The main characteristics of the sea ice differ significantly from fresh water ice due to presence of salt in the seawater. Salt content in seawater influences the freezing points and maximum density of seawater, as shown in the Figure 1.6.

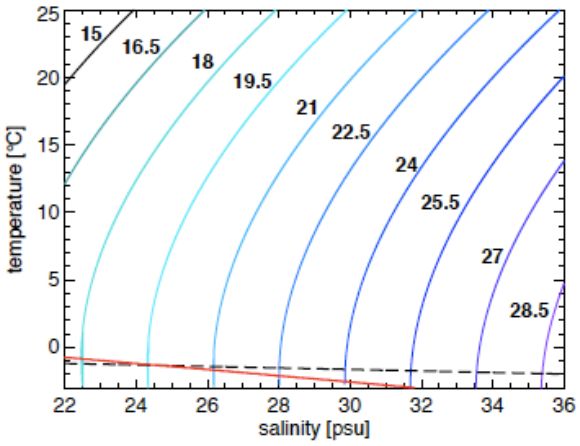

Figure 1.6 Temperature of the density maximum and the freezing points of the seawater are function of the salinity. Seawater density is shown in blue lines. The black dashed line is showing the seawater freezing point and in red the maximum density line is marked. Adapted from Maykut, [1985].

Among all sea ice types, the most common are summarized in Table 1.1. These categories reflect the sea ice age, the forms and the thickness at various stages of its development. The Arctic sea ice is categorized into three main categories; new sea ice, first year-ice or multiyear-ice. The new sea ice is a generalist category that gathers frazil, slush, etc. The first year ice is a floating ice younger than one year's growth developing or that has not survived one summer season. The multiyear ice corresponds to ice that has survived at least one melting period. After the first summer, sea ice is then called residual

first-year ice until 31 December of that year. As from the next year it is called second-year ice and all following years multi-year ice.

Table 1.1 Most common sea ice types for different stages of development, WMO [1989].

Development	Ice type	Ice thickness
New ice/nilas	frazil ice, grease ice, dark nilas	< 5 cm
	light nilas	5 – 10 cm
	pancake ice	up to 10 cm
Young ice	grey ice	10 – 15 cm
	grey-white ice	15- 30 cm
First-year ice	thin first-year ice	30 – 70 cm
	medium first-year ice	70 – 120 cm
	thick first-year ice	20 – 200 Cm
Old ice	second-year ice	approx. 250 cm
	multi-year ice	300 cm or more

Formation

As the temperature of the upper ocean drops below the freezing point, approximately between -1.8 and -1.9ºC for salinity of 34, ice crystals begin to form (Figure 1.6). Instantaneously to first ice crystals formation, salts are rejected to the surrounding waters, increasing salt concentrations and the water density, while the freezing point drops simultaneously. The first type of sea ice forming under turbulence conditions is frazil ice, small ice needles and plates suspended in the water [*Osterkamp*, 1978]. If freezing continues, frazil ice coagulates to form grease ice (transition zone). The next kind of ice growth depends upon the ocean swell. On the one hand, under calm conditions like in leads, frazil crystals freeze together to form a continuous thin, closed ice cover called nilas (congelation ice). At the beginning these forms are transparent, however, when ice grows thick, nilas take on a grey colour and finally a white appearance. On the other hand, if swells prevail by wind action, small ice floes, called pancake ice, form from grease ice or nilas [*Eicken*, 2003] (Figure 1.7).

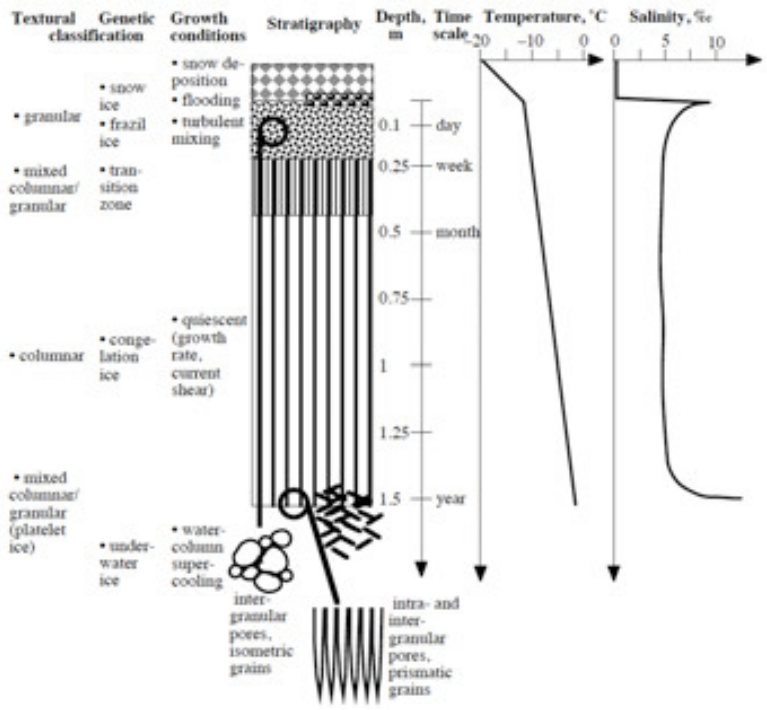

Figure 1.7 Schematic summarizing the main sea ice textures, growth conditions and time scales, and also typical Winter temperatura and salinity profiles for first-year ice [*Eicken*, 2003].

Once this first layer of sea ice is formed, turbulence by wind and thermohaline mixing are reduced and a solid ice cover is formed by freezing of seawater at the ice-water interface (static conditions). Sea ice changes its microstructure and texture since both rely on the growth rate and boundary conditions (Figure 1.7). The feature of ice growth under static conditions is the establishment of a super-cooled layer beneath sea ice, formed as a consequence of the advancing of the ice-water interface. Sea ice grows into ordered patterns of lamellae structure: blades of ice separated by narrow layers of brine, which are the supersaturated liquid inclusions entrap within the solid ice matrix (Figure 1.8) [*Maykut*, 1985]. This structure is also called congelation ice, hence grown is determined thermodynamically and ice crystals become vertically aligned [*Eicke*n, 2003].

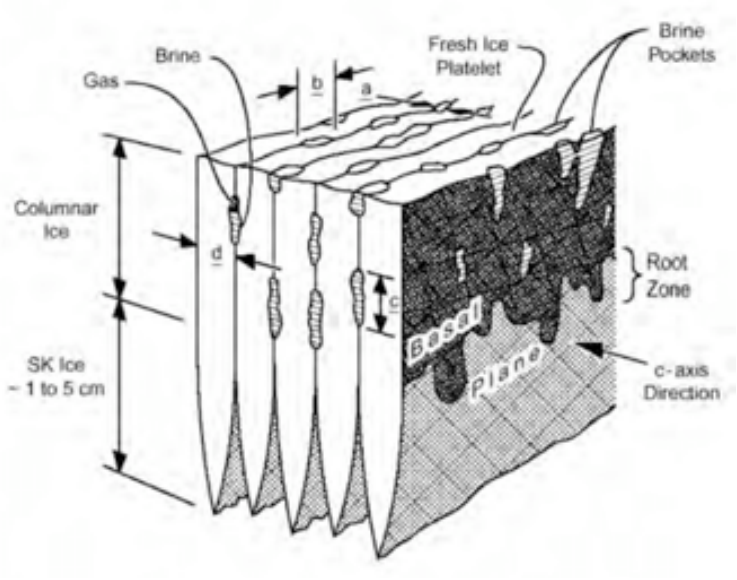

Figure 1.8 Sea ice structure with the main components; brine pockets, lamellae interface, brine. From *Kovacs* [1996].

Another type of ice derives from snow and it is called superimposed ice. It is formed by freezing of the snow (precipitation) at the ice-snow interface on the top of an existing sea ice sheet [*Haas et al*., 2001]. Normally this sea ice presents low porosity and thereby low brine volume fraction.

1.2.2. Properties: Salinity and temperature

The ice crystal lattice structure is responsible of the most relevant properties of sea ice and determines its role in the environment. The exceptional and the most important property of sea ice is its lower density than seawater, approximately 10% of it. Its geophysical properties (thermal, mechanical, electromagnetic) are governed by its temperature and salinity that control the brine volume fraction, morphology of the brine inclusions and microestructure [*Weeks and Ackley,* 1986; *Eicken*, 2003].

Sea ice is a heterogeneous medium in which solid, liquid and gas phases coexist at the same time. The phase relations in sea ice are function of bulk salinity and temperature [*Assur,* 1960]. Figure 1.9 shows the phase relations in sea ice assuming a close system and a thermodynamic equilibrium between all phases all time [*Assur,* 1960]. When ice fraction increases, the temperature drops whilst the brine salinity increases steadily due to salt rejection. At the same time, the freezing point of the brine decreases, co-evolving with the increasing of salinity of the liquid phase, and therefore density increases. At one point, the brine solution is supersaturated respect to a chemical component as a result of the increase of salt concentration in brine, causing its precipitation. Unfrozen liquid within ice matrix is always present, being essential for the microorganisms as it allows their survival during the overwintering.

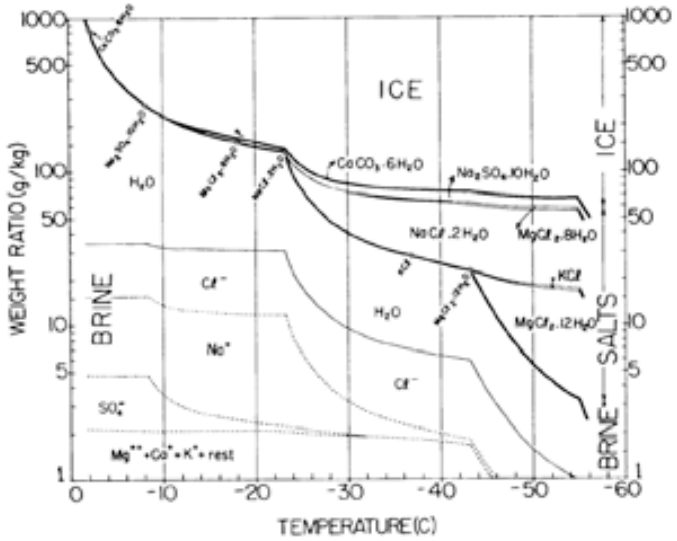

Figure 1.9 Representation of the brine, salts and ice phase relation in function of tem-perature.

The sea ice properties (mechanical, electrical, optical and acoustical, thermal conductivity, etc.) are function of the phase relations that are controlled by both salinity and temperature. Comprehending how these properties, in particular mechanical ones, change with salinity and temperature variations is essential to improve the understanding of the role of the sea ice in biogeochemical cycling and as agent for transport, redistributing and cycling of chemical species and particulate matter.

Salinity

Bulk salinity is a fundamental property of sea ice. Sea salt ions dissolved in seawater cannot be incorporated into the ice crystal lattice structure. Although a large fraction of the ions is rejected into the underlying water column, some are trapped in liquid inclusions in the solid ice matrix (brine) (Figure 1.8). Other chemical species are expected to behave similarly and these would be neither entrained in sea ice crystal [*Weeks and Ackley*, 1986]. Isolated brine inclusions are e called brine pockets, with usually present an ellipsoid shape (Figure 1.8).

The sea ice bulk salinity is a function of different processes that contribute to the loss of salt from sea ice during all stage of its life cycle: formation, growth and melting. Salinity evolves from an initial C-shape to lineal shape at the end of melting season (Figure 1.10).

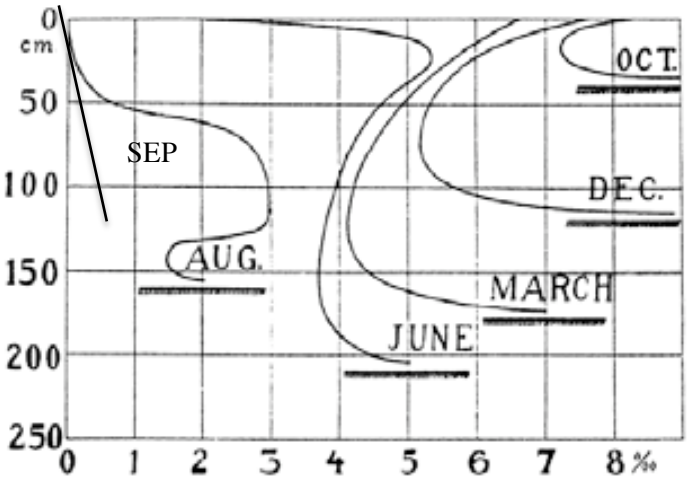

Figure 1.10 Salinity profiles evolution for first year Arctic sea ice. During the winter, the salinity profile presents C-shape, with higher salinity on the top and bottom parts. Salinity decreases on surface and its shape changes to S-shape (August) and finally lineal shape when the season advances. Adapted from *Malmgren* [1927].

The first process in determining salt content in sea ice is the segregation at the ice-ocean interface that is controlled by growth rate [*Weeks and Ackley,* 1986]. It is constant in new sea ice and proportional to the ice-growth rate in columnar ice [*Nakawo and Sinha*, 1984; *Cox and Weeks*, 1983]. At high growth rate, ice platelets are randomly orientated, and more brine and gas are trapped within ice crystals. This growth rate is related to low segregation coefficients and, therefore, high ice salinity [*Wakatsuchi*, 1983]. At low growth rate, ice platelets are ordered and can grow wider, thus less brine is trapped among the ice crystals.

After the initial fractionation of salt at the ice-ocean interface, other mechanisms contribute to the loss of salt within sea ice consolidation and ageing. These are gathered in two groups: cold (brine diffusion, brine expulsion and brine drainage) and warm (flushing) conditions.

The first mechanism that contributes to desalination after initial formation is brine diffusion or brining pocket migration [*Whitman*, 1926]. It is based on the fact that all sea ice phases trend to be in equilibrium. Sea ice temperature gradient, cold in the upper part and warm in the bottom part, is translated in a salinity gradient within brine pockets, in which salinity increases toward its top. That causes downward diffusion of salt ions within brine pockets. Since its velocities are too small, its relative significance in the total sea ice desalination is low [*Notz and Worstern,* 2009].

Brine exclusion consists on any change in temperature that causes changes in the brine volume fraction, by freezing or melting, originating a pressure gradient within sea ice. In the growth season, decrease in temperature triggers the freezing of the brine, resulting in a build-up of pressure in isolated pores. This pressure increase drives brine downward through microcracks or microscopy pore networks. This process is independent of ice porosity and it is considered to be the dominant mechanism of desalination during the first stage of sea ice formation [*Notz and Worstern,* 2009].

Gravity drainage is the most effective desalination mechanism under cold conditions [*Eicken*, 2003]. Sea ice is cooled in the upper parts during aging, causing changes in brine pockets to maintain phase equilibrium. As a result, brine density profile is unstable, decreasing density downward. This gradient causes a displacement of cold and saline brine by warmer and less saline seawater or brine. This process relies mainly on the connectivity and size of pores, which in general are proportional to the brine volume fraction [*Weeks and Ackley*, 1986; *Golden et al*., 1998].

The combination of the segregation coefficient and these three processes leads to the C-shape, typical for first year ice before the summer season (Figure 1.10). The most effective process of losing salt is under warm conditions. Sea ice porosity and permeability become greater as brine pockets are connected. The hydrostatic head produces surface melting that is capable to percolate downward into the ice cover, displacing high salinity brine from within ice. Thus salinity profile changes from a C-shape typical for cold season to the characteristic lineal shape in summer, with values close to zero at the surface as of a few per mil in the lower ice layers (Figure 1.10). That is the reason why multi-year ice is less saline than young and first-year ice [*Untersteiner*, 1968].

These mechanisms would likely affect the distribution of dissolved chemical species, such as tracer metals, nutrients, PCBs, radionuclides in the sea ice, as it happens with salts. In fact, *Tisson et al*. [2008] and *Lannuzel et al*. [2010] studied Fe distribution in Antarctic sea ice and found a relation between Fe distribution and the different stage of sea ice.

Temperature

Ice temperature is also a controlling factor of the relation amongst phases, solid, brine and salts, and of the entire ice physical properties. *Cox and Weeks* [1983] described the brine volume fraction, which is a key parameter to deduce transport properties and ice microstructure, as function of ice temperature. Other parameters, such a density of pure ice, brine salinity and brine density, are also function of temperature.

Ice temperature varies annually, with a nearly linear profile in winter season, with low values on the top and higher temperature at the bottom part where temperature is the freezing point, to the inverse profile in summer (Figure 1.11). When sea ice begins warming, the morphology of the ice microstructure is modified, particularly brine size enhances. Given that all phases tend to

thermodynamic equilibrium, brine salinity and chemical contents are also affected. However, ice macrostructure does not vary until when ice temperature is higher than the freezing point, when sea ice starts melting and its thickness begins declining. Sea ice can melt from top by solar radiation and from bottom parts when seawater is warmer than the freezing point. Sea ice is considered permeable when ice temperature and salinity are greater than 5ºC and 5, respectively, as brine inclusions converge into vertical brine channels.

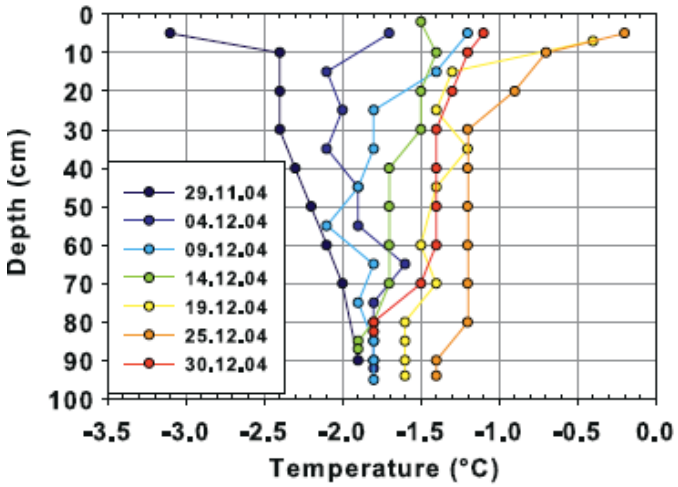

Figure 1.11 Temperature profiles in Antarctic sea ice from November to December 2004. Temperature in the upper part changes from cold to warm during summer season. Bottom temperature remains almost constant. From *Tison et al*. [2008].

1.2.3. Sea Ice Circulation

Drift of sea ice is mainly driven by local surface winds and ocean currents, tending to drift about 35º to the right of the direction of the surface wind. *Thorndike and Colony* [1982] indicated that geostrophic wind-stress explains more than 70% of the variance of daily sea ice motion away from coastal boundaries in both winter and summer, whereas seasonal drift variations have been related to changes in the sea level pressure and the Arctic Oscillation (AO) and the North Atlantic Oscillation (NAO), parameters derived from the difference and variability of sea level pressure in the Arctic and at lower latitudes [*Thompson and Wallace*, 1998, *Rigor et al*., 2002].

The mean sea ice large-scale drift patterns are the TPD over the Eurasian Basin and the anticyclonic Beaufort Gyre in the Canadian Basin [*Thorndike,* 1986] (Figure 1.2). Both drift patterns are fed by sea ice formed in the continental shelves and then exported to the central Arctic Basin. The continental shelves are the main source of sea ice. Identifying sea ice origin is relevant to estimate the most probable drift path of an ice floe from a particular area, such as potential pollution source, validate sea ice drift models or assess the relevant sources of sediment transport. Figure 1.12 shows the approximately net annual exchange flux of sea ice from shelves to the central Artic and through the Fram Strait. The TPD transports sea ice to the West Arctic Ocean over the Eurasian Basin across the North Pole to the North Atlantic through the Fram Strait, which is one of the main sea ice ablation areas. The transit time of sea ice from shelves to the Fram Strait is approximately 2 to 4 years [*Pavlov et al*., 2004]. The Eurasian shelves, principally the Laptev Sea following by the Kara Sea, are considered the main source areas of the sea ice that constitutes the pack ice of the TPD [*Pfirman et al*., 2004; *Pavlov et al*., 2004] (Figure 1.12). Sea ice formed in the Eastern Arctic Ocean is largely influenced by the presence of the Beaufort Gyre. Sea ice incorporated within the Beaufort Gyre remains there for 5 to 15 years before joining the TPD through the Polar Branch and arriving finally to the Fram Strait [*Thorndike*, 1986]. The East Siberian Sea can contribute to both regimes depending upon atmospheric conditions [*Pfirman et al*., 2004].

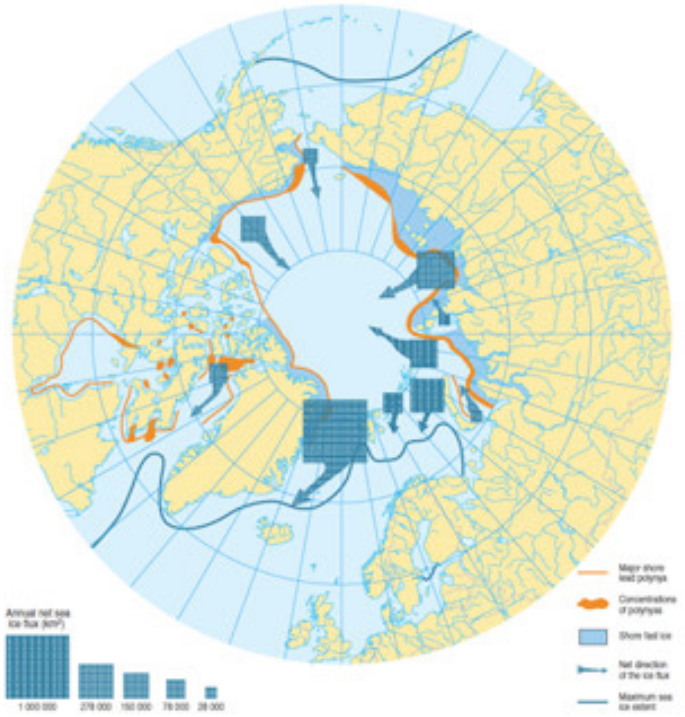

Figure 1.12 Estimates of the annual net flux of sea ice (km^2) exchange in the Arctic Ocean. Size of the squares indicates the annual flux exported and arrows indicate the export direction. [*AMAP*, 1998].

Both motion drifting regimens change the typical localization, extent, strength and transit time required to arrive to the Fram Strait according to variations in the pressure fields that in turn are function of the polarity of the AO and the NAO (Figure 1.13) [*Rigor et al*., 2002*, Walsh et al*., 1996, *Kwok,* 2000].

Under low-index AO conditions, a high-pressure cell is placed over the Beaufort Sea (anticyclonic phase). The Beaufort Gyre is rather strong and occupies a large area of the Arctic Ocean, reaching the North Pole, whilst the TPD is restricted to the Eurasian Basin (Figure 1.13 a). Under these conditions, sea ice in the Beaufort Gyre takes at least a year longer from the west to the east than under high-index conditions (Figure 1.13 b). This anticyclonic circulation favours a convergent sea ice motion [*Walsh et al*., 1995; *Mysak,* 2001; *Rigor et al*., 2002, *Rigor and Wallace,* 2004].

When high-index AO conditions are present, the anticyclonic circulation of the Beaufort Gyre reduces its size, becomes weaker and its influence in the Eurasian Arctic decreases. Thereby less sea ice recirculates within it. The TPD, instead, is strengthened and its influence moves westward, resulting in an advection increase of multi-year ice away from the Eurasian coast towards the Canadian Arctic and out through the Fram Strait. The sea ice transit time into the Eurasian Basin decreases as a consequence of the increase of the TPD strength (Figure 1.13 c and d) [*Polyakov and Johnson*, 2000; *Mysak*, 2001; *Rigor et al*., 2002]. This dominant cyclonic circulation of the sea ice is related to divergent ice motion, being able to create open water areas over the central Arctic Ocean. Thus albedo is reduced, favouring sea ice melting [*Walsh et al*., 1996]. This phase favours the thinning of sea ice in the Eurasian Basin and the increase of the sea ice areal flux through the Fram Strait. For example, between 1994 and 1995 (under high-index AO) sea ice areal flux rose up to 4700 $km^3 \cdot y^{-1}$ due to old and thick sea ice being exported. Instead, under low index AO, sea ice effluxes were around 2050 and 2700 $km^3 \cdot y^{-1}$ for the period 1990-1991 and 1986-1992, respectively [*Vinje et al*., 1998; *Kwok and Rothrock*, 1999; *Rigor and Wallace*, 2004; *Nghiem et al*., 2007].

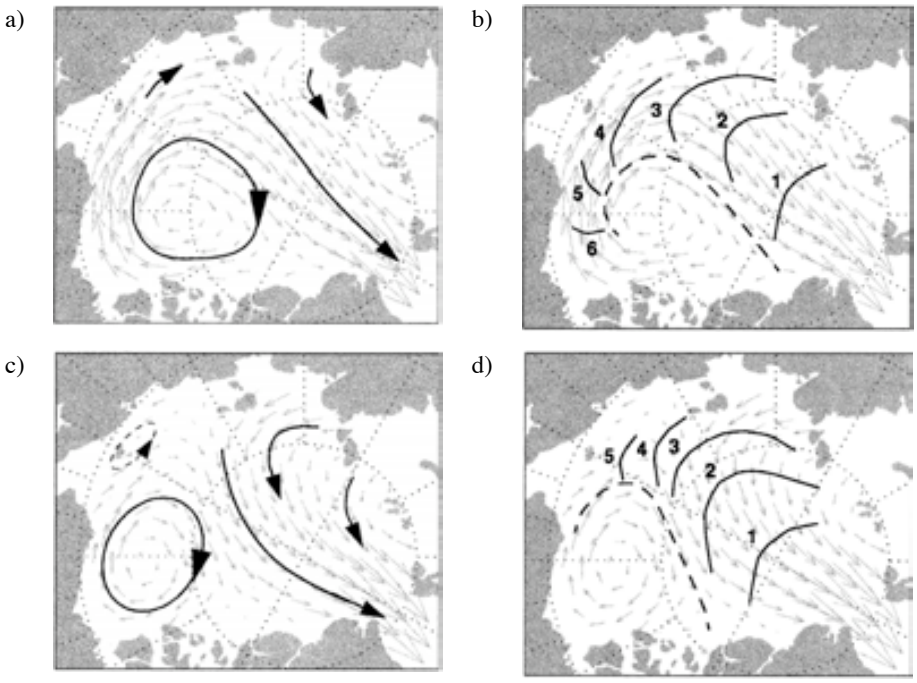

Figure 1.13 Sea ice drift pattern under low-index AO and high-index AO. a) Geographical distribution of the TPD and Beaufort Gyre under low-index AO; b) transit time in year to reaching the Fram Strait area under low-index AO; circular line indicates the recirculation of sea ice within the Beaufort Gyre; c) geographical distribution pattern under high-index AO; d) transit time in year in reaching the Fram Strait under high-index AO. Figures *Rigor et al*. [2002].

These variations in the AO index have relevant implications in the whole Arctic Ocean, since any slight change is translated into variations in the drift patterns which are in turn translated to changes in sea ice thickness distribution, sea ice extent, sea ice mass balance, sea ice transit time and to all processes related with sea ice. The amount of ice transported, the localization and the main production areas that fed each drift pattern, transport of particulate matter, chemical species of sea ice would result disturbed [*Zhang et al*., 2000, *Rigor and Wallace*, 2004; *Pfirman et al*., 1997].

1.2.4. Sea ice extent and thickness- age

Sea ice extent has been monitored since the 1970s using satellite-based sensors. It is characterized by presenting a seasonal variability between winter and summer (averages of $15.7 \cdot 10^6$ and $7.0 \cdot 10^6$ km^2 in sea ice extent for the period 1979-2000, respectively, National Snow and Ice Data Center, NSIDC). Its maximum extent is in March, at the end of the freezing season, and the minimum extent is in September, at the end of the melting season. This monitoring has shown that the sea ice extent has been decreasing for the past few decades, being one of the most obvious signs of climate change. Annual sea ice extent has decreased by approximately 4% per decade from 1979 to 2007. This decrease is more significant in the summer, with a decrease rate of 10% per decade (1979-2007). In September 2007, sea ice reached its minimum extent, 23% lower than the previous minimum record in 2005 and 39% lower than average extent for the period 1979-2000 [*Comiso et al*., 2008; *Stroeve et al*., 2008] (Figure 1.14).

The sea ice extent is controlled by the effects of the atmosphere and the ocean on the sea ice at different time scales. Variations on scales of days and weeks can be related to the wind stress from storms that can create ridges of sea ice or open water [*Shy and Walsh*, 1996]. On seasonal time scales, the AO explains most of the variation in sea ice drift and, therefore, in sea ice extent [*Thompson and Wallace*, 1998]. *Rigor and Wallace* [2004] stated that more than half of the variance in summer sea ice extent is explained by the age or thickness of the sea ice, which also declined in the last years [*Kwok and Rothrock*, 2009].

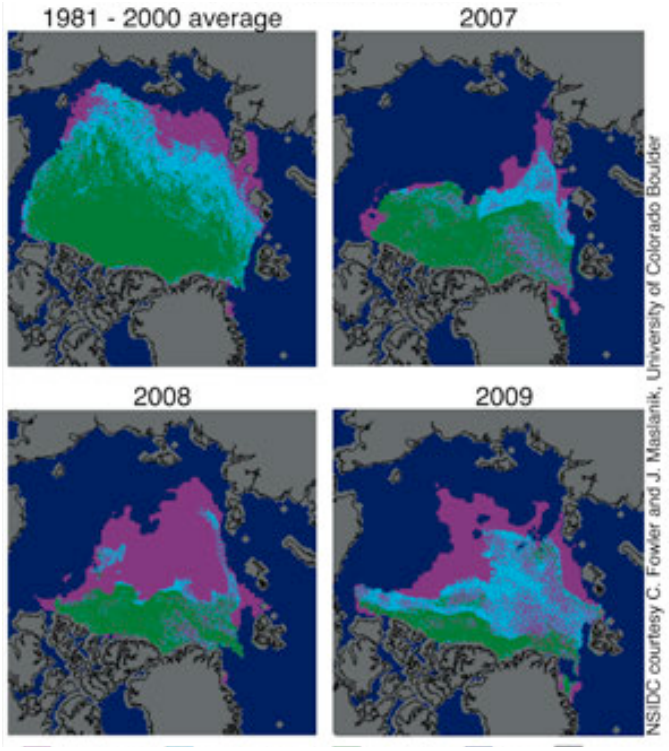

Figure 1.14 Sea ice age at the end of the melting season (September) and minimum sea ice extent. Sea ice age is represented in colours: purple corresponds to first year ice (<1 year old), second year ice is represented with light blue, older ice (>2 years) with green and dark blue represents open water (NSIDC).

Sea ice thickness also presents large seasonal and spatial variations. The sea ice drift pattern controls the sea ice regional thickness: the thickest sea ice is mostly concentrated in the western Arctic Basin, under the influence of the Beaufort Gyre, while the thinnest ice is located in the Siberian shelves, from where sea ice is permanently exported into the TPD [*Haas*, 2003].

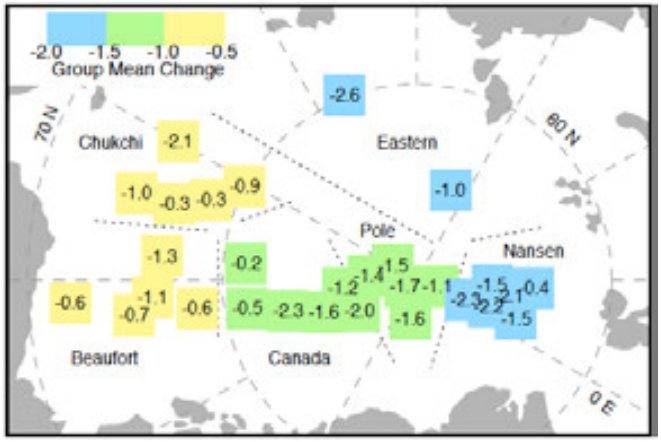

Figure 1.15 Changes in mean draft from 1958-1976 to 1993-1997. The change at each crossing is shown numerically. Each square covers about 150 km, the typical sample size. Figure from *Rothrock et al*. [1999].

All available ice thickness measurements from submarines, drilling and electromagnetic sounding reveal that the Arctic sea ice has thinned substantially since the late 1950s [*Rothrock et al*., 1999; 2003; 2008; *Wadhams and Davis,* 2000; *Haas,* 2004; *Tucker et al*., 2001]. A comparison of draft, sea ice thickness below the waterline, acquired from submarine measurements indicated that mean sea ice draft at the end of the melt season has decreased in about 1.3 m between 1958-1976 and 1993-1997. This

decline corresponded to a reduction of 42% of ice thickness and to a trend of -0.10 $m \cdot y^{-1}$ (Figure 1.15). Recently, time series of satellite measurements (ICESat) have shown that sea ice is thinning with an average rate of -0.18 $m \cdot y^{-1}$ [*Kwok and Rothrock*, 2009]. Nonetheless, it has not declined equally in all regions. The largest reduction has been observed in the North Pole and the Canadian Basin, as a consequence of the decrease of multi-year ice cover by the increased export of older ice out of the Fram Strait and ice compression toward the western Arctic [*Nghiem et al*., 2007; *Comiso,* 2002].

Each kind of sea ice is defined by ice growth and thickness, which are closely related to sea ice age. The sea ice extent and age at the end of the melting season along different years is shown in Fig 1.14. After the minimum record in 2007, sea ice extent seems to recover even though extent much less than the average for the period 1979-2000, but sea ice age has decreased (NSIDC). The region covered by old and thick sea ice has dropped substantially and was replaced by younger and thinner ice. At the end of the melt season in 2009, the fraction of thin–one year ice increased up to 49% of the ice extent, whereas the old sea ice represented an average of 48% of the sea ice extent during the period 1981-2000 and only 19% in 2009. The presence of thin, young ice entails significant consequences, because it is more vulnerable to survive the following summer, contributing to the shrinking of the sea ice cover extent [*Rigor and Wallace*, 2004].

The decrease of sea ice extent, the shrinking of the sea ice thickness and the warming of the water has wide physical, biological, political, social to economical, etc. implications. Physically, one of the first effects is a shift in the albedo, and the atmosphere-ice-ocean feedbacks would be drastically disturbed: a larger influx of solar radiation into the surface water will change the characteristics of the mixed layer and the ocean stratification. When heat penetrates below the ice draft, it warms the boundary layer and is available for melting the bottom ice, declining sea ice thickness. If heat remains above the draft, it will contribute to melting the ice edge, which could cause a shrinking of the sea ice extent and an increase of lead – open waters. Furthermore, freeze-up is delayed in the season and ice breaks-up earlier, water is less salty and warmer, etc. These changes in the Arctic marine physical environment are also generating changes in the marine ecosystems related to primary production, carbon export to the deep sea and biodiversity [*Grebmeier et al*., 2004]. The reduction in extent and sea ice thickness causes an increase in the total phytoplankton production in the Arctic, since greater light penetration favours ice algae growth [*Pabi et al*., 2008]. However, the ice metazoans community decreases since they rely on the occurrence of multi-year ice for their development stages. All these shifts can be translated in a profound impact in the structure of the marine ecosystem and the Arctic biodiversity that might be substantially reduced. A number of studies have denoted that a strong stratification of the ocean can reduce nutrients availability, causing a reduction in primary production [*Carmack et al.*, 2006; *Murray et al.,* 2010] The warming of seawater can benefit the invasion of warmer water species in the Arctic Ocean, replacing cold adapter species, as it has been observed with copepods [*Hirche and Kosobokova*, 2007]. These changes in biota have effects in the biogeochemical cycles: for example, *Damm et al*. [2009] pointed out that biota changes modify the biogases concentration in ice and water. Other shift is the acceleration of sea ice drift, as a consequence the sea ice flux through the Fram Strait has increased. This is probably the cause of an increase sedimentation rate in that area, since large amount of particulate matter is related to the arrival of the sea ice edge when sea ice melts [*Hebbeln and Wefer*, 1991]. From the point of view of social implications, the Inuit community is vulnerable to this sea ice changes, since its culture, subsistence and economy depends principally on the natural resources of marine and terrestrial systems. These shifts are causing a decoupling between freeze-up, ice break-up and caribou calving, seal whelping, etc. and could not only impact the reproductive success of the species, but also can hamper the ability of the communities to obtain food by hunting and fishing. The predictions of summer free ice in the near future has increased the interest for natural resources exploitations together with the shipping routes across the Arctic Ocean from the Atlantic to the Pacific Ocean, activities that might largely disturb the Arctic ecosystem [*Perovich and Richter-Menge*, 2009].

1.2.5. Sea Ice Sediments

Sea ice Sediments (SIS) are widespread over the Arctic Ocean [*Nürnberg et al*., 1994; *Pfirman et al*., 1990; *Dethleff et al*., 1998; *Lisitzin*, 2002]. Its presence is not homogenous along the Artic Ocean: in areas close to the Siberian continental shelves SIS is present on about 10% of the total ice, and its concentration increases along the TPD until occupying 50 - 70% of the total sea ice extent at the Fram Strait [*Nürnberg et al*., 1994; *Pfiman et al*. 1989].

SIS are essentially entrapped within sea ice during its formation in the shallow continental shelves during late fall and winter under turbulence conditions. Among all entrainment mechanisms, suspension freezing is identified as the most effective process [e.g. *Kempema et al*., 1989; *Reimnitz et al*., 1992, *Eicken et al*, 2005; *Dethleff,* 2005]. Recently, *Dehtleff and Kempema* [2007] identified the Langmuir circulation, a wind driven helix circulation in the ocean with the axis almost parallel to the wind, as an important contributor to the process of the suspension freezing. It promotes the entrainment of silt and clay-sized particulate material into the newly formed ice cover. Other incorporation processes are the slush ice formation and the anchor ice formation [*Kempema et al.,* 1989; *Reimnitz et al*., 1993]. This last process leads to the incorporation of coarse particles, and it requires that the whole water column is supercooled [*Kempem*a *et al*., 1989; *Reimnitz et al*., 1992; 1993; *Dethleff et al*., 1993].

Aeolian deposition might be another source of particulate matter in sea ice. Nevertheless, its contribution to particulate matter amount is insignificant, since the deposited amount of aerosols are orders of magnitude lower compare to the high particulate load observed in sea ice [*Nürnberg et al*., 1994; *Pfirman et al*., 1989]. Some studies have measured the fluxes of atmospheric dust, varying from 3.3 to 21 $\mu g \cdot cm^{-2} \cdot y^{-1}$ [*Windom*, 1969; *Muller et al*. 1972; *Darby et al*., 1974]. Therefore, the presence of SIS indicates that sea ice has been formed in the continental shelves since those are entrained into sea ice during its formation in shallow areas and therefore, one can used them to identify sea ice source areas [*Pfirman et al*., 1989; 2004].

Sea ice contains large amounts of particulate matter, ranging from 5 to 56000 $g \cdot m^{-2}$ [*Nürnberg et al*., 1994; *Eicken et al*., 1995; 1997; *Pfirma*n *et al*., 1995], or from a few mg per liter to maximum concentrations of 3000 $mg \cdot L^{-1}$ [*Kempema et al*., 1989; *Reimnitz et al*., 1993; *Stierle and Eicken*, 2002]. The average SIS concentration is considered to be 20-30 $mg \cdot L^{-1}$, similar to the average concentration of suspension matter in the waters of the Arctic rivers, and several orders of magnitude higher than the suspension matter in the Arctic seawater, 5 $\mu g \cdot L^{-1}$ [*Bacon et al*., 1989; *Lisitzin*, 2002]. This wide variability in sediment load and concentration is related to the different entrainment processes, as well as to meteorological and ocean conditions. SIS consists mainly of silt and clay (<63 μm), representing approximately the 60-90% of the total weight [*Reimnitz et al*., 1987; *Kempema et al*., 1989; *Eicken et al*. 2005].

1.2.6. Sea ice as a transport and redistribution agent

Sea ice is considered the major mechanism of transport and distribution of particulate matter and chemical species in the Arctic Ocean [*Pfirman et al*., 1999; *Hebbeln and Wefer*, 1991; *Eicken et al*., 2005; *Dethleff and Kuhlmann*, 2010]. Some processes during sea ice transit may enhance the intitial concentrations of chemical species incorporated during sea ice formation such as the interception of atmospheric fluxes by sea ice and in a less extent scavenging from surface waters by SIS contributes to increase their concentrations while the brine flushing contributes to decrease their concentrations [e.g. *Grankrog*, 2003; *Masqué et al*., 2007; *Baskaran,* 2005].

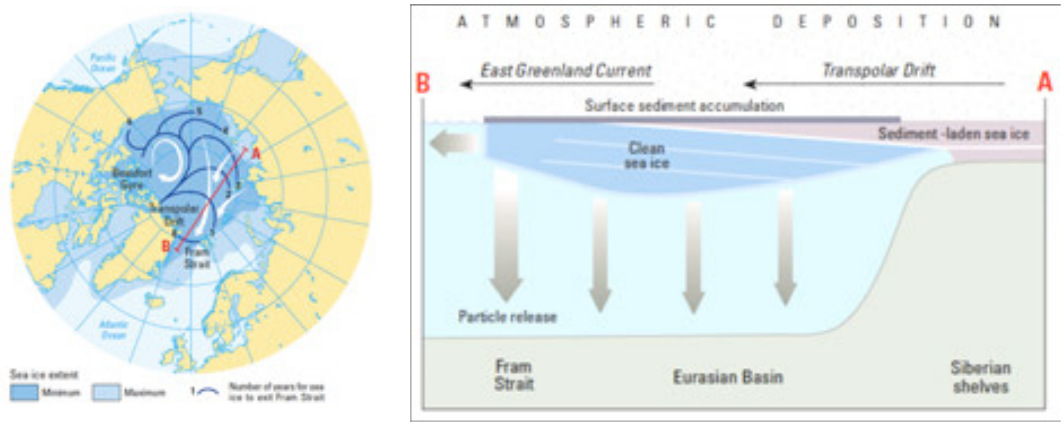

Figure 1.16 Arctic Ocean with average maximum (blue) and minimum sea ice extent (dark blue). The numbered line denotes the expected transit time in years that sea ice needs to reach the Fram Strait, based on drifting buoy data during 1979-1990. Schematic representation of different processes that sea ice undergoes from its formation in Laptev Sea (A) to melting in the Fram Strait (B). [*AMAP,* 1998].

During its drifting, sea ice undergoes continuous melting and freezing cycles, apart from intercepting and accumulating atmospheric fluxes. Each summer, surface and bottom ice melts. That melted water can i) percolate downward through brine; ii) accumulate in melt ponds; iii) run off the ice floe; or iv) refreeze inside the ice floe. The flushing is the most relevant process of losing salt, and other chemical species would be also removed from ice and released to the underneath water. One would also expect that particulate matter would be removed from ice too, but, given that particle are accumulated on surface ice as a result of this seasonal melting and freezing cycles [*Barrie et al*., 1998; *Pfirman et al*., 1989], SIS release along the drift path seems to be unlikely [*Pfirman et al*., 1989] (Figure 1.16). Thus, the greatest potential deposition of the vast majority of transported particulate matter and chemical species associated to them takes place in the marginal areas and in the ablation areas, such as the Fram Strait.

Eventually, sea ice melts and thus SIS and chemical species transported by sea ice are discharged onto the surface water, linking their final fate to that of sea ice (Figure 1.16). That happens in relatively short-time scales, releasing a massive particle and chemical species flux onto surface water. Besides, that process coincides usually with biological blooms [*Melnikov,* 1991]. One effect of this transport and release is the redistribution of transported chemical species and particulate matter from one area to other area. According to *Wollenburg* [1993], *Larssen et al*. [1987] and *Dethleff and Kuhlmann* [2010], between 7 and 158 Mt of SIS are annually exported through the Fram Strait, contributing significantly to the sedimentation rate in that area [*Hebbeln and Wefer*, 1991]. As a reference, the discharge of sediment load from Arctic rivers is of about $115 \cdot 10^6$ tons per year [*AMAP*, 1998]. In fact, sedimentation traps placed at the Fram Strait have registered these events [*Hebbeln and Wefer*, 1991]. Another effect is the potential increase in the concentration of released chemical species in surface waters: in the case of nutrients this can promote or increase biological production, and contaminants (PCBs, etc.) can inhibit biological productivity and be accumulated by organisms.

Chapter 2.

Radionuclides in the Arctic Ocean

Radionuclides have both natural and artificial sources. The natural radionuclides, produced in the environment without human intervention; are formed by interaction of cosmic rays in the atmosphere (cosmogenic radionuclides) or produced during Earth formation (primordial radionuclides) or by disintegration of them (including the natural decay chains). Artificial radionuclides have been introduced in the Earth by human activity.

2.1. Natural Radionuclides (^{7}Be, ^{210}Po and ^{210}Pb)

2.1.1. ^{7}Be

^{7}Be is a cosmogenic radionuclide produced in the upper part of the atmosphere, mostly in the stratosphere (70%) and in the upper part of the troposphere (30%). It is the result of the interaction of cosmic rays with nitrogen, carbon and oxygen nuclei when they absorb protons and even neutrons of the primary component of cosmic radiation (reference within *Papatefanou*, [2008]) (Figure 2.1). Be-7 is produced continuously and globally. However, its production rate does not remain constant owing to variations in the flux of cosmic rays [*Lal et al*., 1958; *Lal and Peters*, 1962]. The fact that the flux of cosmic rays is anti-correlated with solar activity makes that ^{7}Be production rate varies according to the 11-yeas solar cycle [*Lal and Peters*, 1962, 1967]. ^{7}Be production is also affected by latitude and altitude, increasing its production rate as latitude increases, and for all latitude production rate decreases approximately two orders of magnitude between the lower stratosphere and the surface air [*Lal and Peters*, 1962].

^{7}Be has a relatively short half-life, 53 days, and decays to ^{7}Li by electron capture emitting gamma rays (477.6 keV, 10.4% yield). Once it is produced in the atmosphere, it is rapidly attached to submicronsized aerosols particles (reference within *Papatefanou,* [2008]). The mean residence time of ^{7}Be in the troposphere is 21 days, although this value varies as a function of the region, with shorter residence time for the tropic (10-15 days) and longer in polar and dry regions (25-40 days)[*Koch et al*.,

1996, *Yu and Leem,* 2002]. In the stratosphere, the ^{7}Be residence time is about 1 year, which is much longer than its half-life and thus equilibrium between decay and production is assumed to occur [*Staley*, 1982].

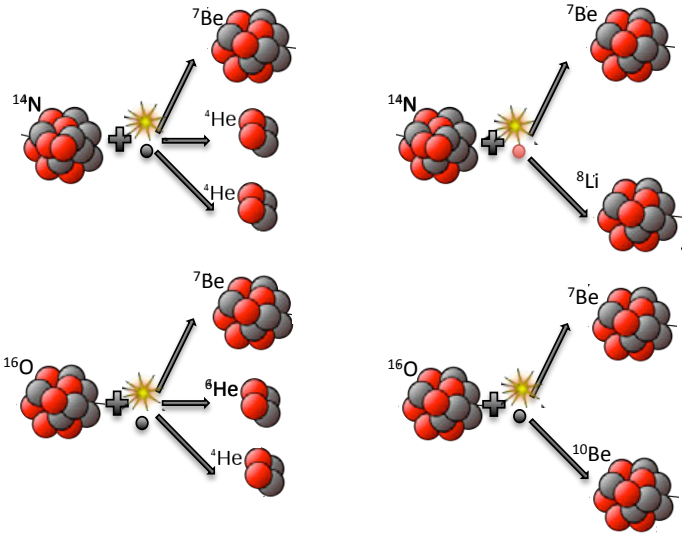

Figure 2.1 Some diagram of the ^{7}Be formation through the interaction of cosmic rays with nitrogen and oxygen nuclei.

Table 2.1 Average ^{7}Be surface air concentration at different localcations.

Localization	**Latitude**	**^{7}Be (mBq·m^{-3})**	**Period**	**Study**
Jungfraujoch, Switzerland	46ºN	7.0	1996/99	*Gerasopoulos et al*. [2001]
Nagaro, Japan	36ºN	6.4	2000/05	*Muramatsu et al* [2008]
Midway, North Pacific	28ºN	2.9	1985	*Uematsu et al*. [1994]
Enewetak, North Pacific	11ºN	1.7	1985	*Uematsu et al*. [1994]
Nauru, South Pacific	1ºS	1.4	1985	*Uematsu et al*. [1994]
Fiji South Pacific	18ºS	1.6	1999/00	*Garimella et al*. [2003]
Hokitika, New Zeland	42ºS	3.1	1985/86	*Harvey and Mathews* [1989]

The concentration of ^{7}Be in surface air is not homogeneous neither latitudinally nor temporally, since it depends on production rate, mean residence time in the atmosphere and decay rate. Greater values are present in the middle latitudes of both hemispheres, and lower concentrations are observed at high latitude sites, and also at sites in the Pacific under the inter-tropical convergence zone (Table 2.1). The troposphere and stratosphere exchange, vertical mixing within the troposphere, air mass transport from middle latitudes to high latitudes or rainfall cause a seasonal variability in surface air concentration. The average concentration in the troposphere is 12.5 mBq·m^{-3} [*UNSCEAR*, 2000], while in surface air in temperate zones is 3 mBq·m^{-3} [*UNSCEAR*, 1982].

^{7}Be enters to the marine and terrestrial environments via wet or dry deposition. Wet deposition is the most efficient removal process, accounting for approximately 90% or more of the total ^{7}Be deposition in temperate zones [*Ioannidou and Papastefanou*, 2006].

Following deposition, ^{7}Be trends to associate rapidly with particle material (it is a particle-reactive element, K_d>10^{5} L·kg^{-1}, [*You et al*., 1989]). In terrestrial environment, ^{7}Be is concentrated in the first centimetres of the soil and in the surface ocean, ^{7}Be is diluted within the mixed layer and the attachment to particles produces its distinct depletion in open surface waters. At the SHEBA station (Arctic Ocean), *Kadko et al*. [2004] observed in as ^{7}Be concentration drops substantially downward the mixed layer depth.

Distribution in the Arctic Ocean

Given that ^{7}Be has not been routinely measured in the Arctic Ocean, sparse data is available. One of the first studies of ^{7}Be in the Arctic Ocean was performed by *Dibb* [1990], who estimated an atmospheric flux of ^{7}Be ranging from 0.31 to 0.36 and from 0.45 to 0.89 Bq·m^{-2}·d^{-1} from June to July 1989 at the Dye 3 and at the Summit stations (Greenland), respectively. *Kadko* [2000] reported an atmospheric flux of 0.33 Bq·m^{-2}·d^{-1}, with daily values ranging from 0.0083 to 0.53 Bq·m^{-2}·d^{-1}, in October 1997 at the SHEBA station, located in the Canada Basin. At the same station, the ^{7}Be atmospheric flux varied from 0.46 to 3.8 Bq·m^{-2}·d^{-1} from July to August in 1998, with a mean value of 2.03 Bq·m^{-2}·d^{-1} [*Kadko and Swart*, 2004]. *Cooper et al*. [2005] reported fluxes ranging from 0.95 to 1.04 Bq·m^{-2}·d^{-1} between July 19th and August 21st 2002 in the Chukchi Sea.

The first measurements of ^{7}Be in seawater were carried out in 1997 at the SHEBA station by *Kadko* [2000] and *Kadko and Swart* [2004]. They quantified ^{7}Be activities in a seawater profile in one lead. It showed a rapid decline of activity with depth, from 44 Bq·m^{-3} at 0.5 m depth to 0.8 to 1.5 Bq·m^{-3} at 7 - 10 m depth. *Kadko* [2000] stated that mixed layer depth is a critical parameter that largely determines the ^{7}Be surface activity, since ^{7}Be is mixed the in mixed layer with respect to its radioactive decay. Below the mixed layer depth, ^{7}Be activities were lower due to its isolation from its input.

Sea ice present the highest ^{7}Be concentrations in the upper parts (42 Bq·m^{-3} in the brine of the upper 10 cm), and decrease downward the ice core since these layers have not been exposed to the atmosphere for at least several months (8.3 Bq·m^{-3} at 1.2 m depth) [*Eicken et al*., 2002]. Melt ponds presented similar concentrations as brine channels (16 - 183 Bq·m^{-3}), although the activities changed between early July and early August. A time series study at the SHEBA station between early July and early August 1998 revealed that the ^{7}Be activities in melt ponds decreased due to input of old ice and the drainage, and in late August those increased in one order of magnitude because the formation of a stratified surface layer derived from surface heating and meltwater input [*Eicken et al*., 2002]. *Cooper et al*. [1991] measured snow samples from the Chukchi Sea in which ^{7}Be activities ranged between 41 and 123 Bq·m^{-3}. ^{7}Be is also associated to the particulate matter present in the sea ice. Concentration in SIS showed variability from 20 to 212 Bq·kg^{-1} that can be ascribed to time exposed to the atmosphere [*Masqué et al*., 2007].

2.1.2. ^{210}Pb and ^{210}Po

^{210}Pb and ^{210}Po are natural radionuclides that belong to the ^{238}U decay chain. ^{210}Pb is produced by the decay of ^{222}Rn ($T_{1/2}$ = 3.8 y) through its short-lived daughters (^{218}Po, ^{214}Pb, ^{214}Bi and ^{214}Po) (Figure 2.2). ^{210}Pb decays to ^{210}Bi by beta decay with a half-life of 22.3 years, which in turn produces the alpha emitter ^{210}Po, with a half-life of 138.4 days.

^{210}Pb is formed in the atmosphere as a decay product of the ^{222}Rn exhaled from the Earth crust after alpha decay of ^{226}Ra. ^{222}Rn can escape to the atmosphere either by diffusion or alpha recoil following radium decay. In addition, ^{222}Rn produced in water column of the oceans or lakes can also escape to the atmosphere. However, given that the ^{226}Ra concentration in seawater is several orders of magnitude lower than in soils, the ^{222}Rn flux from the water bodies to the atmosphere is considered to be negligible [*Turekian and Graustein*, 2003].

The distribution of ^{210}Pb in the atmosphere depends upon the landmass distributions in the Earth. Thus, the greatest ^{210}Pb activities are mostly measured in the Northern Hemisphere [*Turekian et al*., 1989]. Once in the atmosphere, ^{210}Pb is rapidly associated to aerosols due to its strong affinity for particles (K_d = 1·10^{7} L·kg^{-1}, [*IAEA*, 1985]) and is removed from the atmosphere in days or weeks by dry and wet deposition. Wet deposition drives approximately 90% of the total ^{210}Pb depositions on the surface earth [*Turekian et al*., 1989].

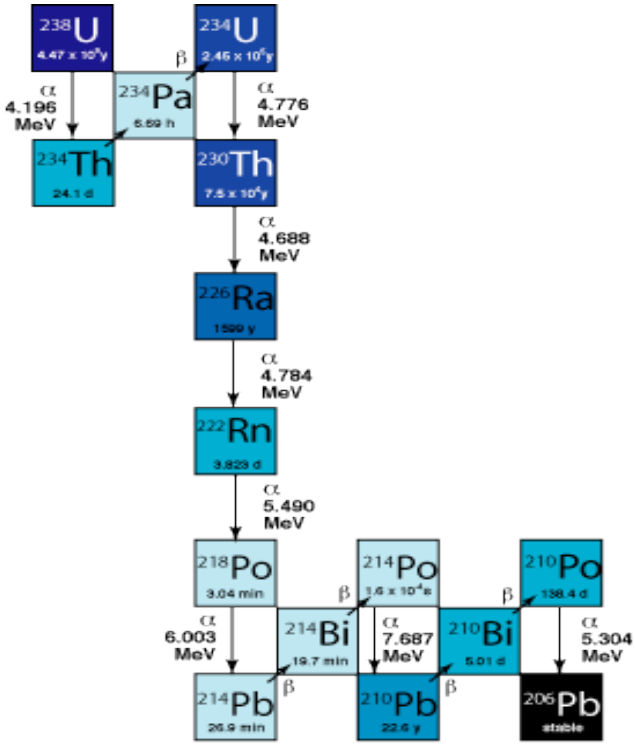

Figure 2.2 Schematic diagram of the natural ^{238}U decay chain. Vertical arrows indicate alpha-decay, while diagonal arrows indicate beta-decay. The half-lives of each radionuclide is noted below the name of the isotope. Energies of emission are also indicated..

In seawater, ^{210}Pb is produced by *in situ* disintegration of ^{226}Ra, which has a conservative behaviour. In shallow waters of coastal areas *in situ* production of ^{210}Pb is almost negligible compared to the atmospheric flux, while this via represents a much greater contribution in the open water ocean, although excess of ^{210}Pb respect to ^{226}Ra can be influenced by atmospheric flux [*Cochran et al*., 1992].

Concerning ^{210}Po, and since the residence of ^{210}Pb in the atmosphere is shorter compared to the half-life of ^{210}Po, this isotope has little time to grow towards equilibrium with its parent, and thus the atmospheric flux to the Earth surface is of about 10 to 20% that of ^{210}Pb [*Lambert et al.,* 1982]. Likewise, the main source of ^{210}Po in the surface Earth is the *in situ* decay of ^{210}Pb.

Distribution in the Arctic Ocean

Atmospheric deposition rates of ^{210}Pb in the Arctic Ocean are very low compared to other regions due to the reduced exhalation of ^{222}Rn from the limited soil coverage and the low precipitation rates [*Dibb*, 1992]. Near Point of Barrow, the atmospheric ^{210}Pb flux was 13.3 $Bq \cdot m^{-2} \cdot y^{-1}$ in 1979 [*Weiss and Naidu*, 1986]. Atmospheric fluxes ranging from 6.67 to 45 $Bq \cdot m^{-2} \cdot y^{-1}$ were estimated in several Arctic lakes and in Greenland ice cores in 1975-1987 [*Kipphut,* 1978; *Cornwel*l, 1985; *Baskaran and Naidu*, 1995]. *Dibb et al*. [1990] estimated ^{210}Pb fluxes in Greenland between Juny - July 1989 of 8.7 ± 0.7 $Bq \cdot m^{-2} \cdot y^{-1}$ at the Summit station and of 12.5 ± 6.5 $Bq \cdot m^{-2} \cdot y^{-1}$ at the DYE-3 station. Lower atmospheric fluxes were measured in the interior of the Canada Basin, 4.2 $Bq \cdot m^{-2} \cdot y^{-1}$ in 1985 [*Moore and Smith*, 1986], and *Huh et al*. [1997] determined a ^{210}Pb atmospheric flux of 10 $Bq \cdot m^{-2} \cdot y^{-1}$ in the central Arctic Ocean.

Once can expect that atmospheric fluxes are intercepted by sea ice. Thereby sea ice would show the highest ^{210}Pb and ^{210}Po activities in the upper layers, as shown by *Masqué et al*. [2007], that reported concentrations ranging from 43 to186 and from 45 to 90 $Bq \cdot m^{-3}$ in the upper 10 cm of sea ice, respectively. The interception of atmospheric fluxes is corroborated by low salinity values found in these sections. Downward the sea ice cores their activities dropped down to 1-2 $Bq \cdot m^{-3}$. The ^{210}Pb and ^{210}Po activity profiles mostly mirror the salinity, with the exception of the first 20 cm, suggesting that

the same processes that regulate salt contents do apply to ^{210}Pb and ^{210}Po [*Masqué et al*., 2007]. ^{210}Pb concentrations in SIS showed a large variability, ranging from 19 to 3000 Bq·kg^{-1} [*Baskaran*, 2005; *Masqué et al*., 2007].

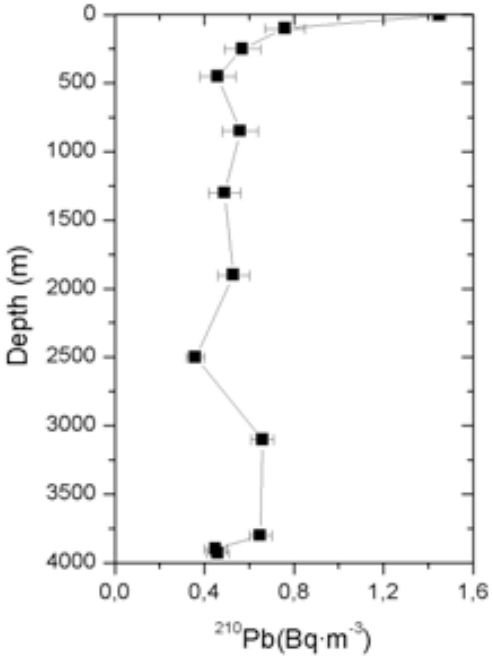

Figure 2.3 Concentration profile of ^{210}Pb in seawater at the Nansen Basin. *Cochran et al*. [1995a].

^{210}Pb and ^{210}Po activities in surface seawater range from 0.6 to 0.9 Bq·m^{-3} (Moore and Smith, 1986; Smith *et al*., 1995; 2003), decreasing from the Eurasian Basin (0.67 Bq·m^{-3}) across the Makarov Basin to the continental slope of the Chukchi Sea (< 0.083 Bq·m^{-3}) [*Smith et al*., 2003]. The typical ^{210}Pb and ^{210}Po seawater profile showed in the upper part concentration decrease as depth increasing, reaching a minimum approximately at 200 m from in which activities remain fairly constant in deep waters (0.5 Bq·m^{-3}) (Figure 2.3) [*Smith et al*., 2003, *Cochran et al*., 1995a].

^{210}Pb in seawater is scavenged and transported downward by sinking particles. Its concentration in bottom sediments varies according to the water column depth, sedimentation rate and decay rate. High activities in the central Arctic Basin and the Fram Strait, of up to 1400 Bq·kg^{-1} [*Masqué et al*., 2003; *Not et al*., 2008] contrast to those measured in continental shelves: in the Kara Sea, activities in the upper 3 cm varied from below detection limit to 109 Bq·kg^{-1} and in the Chukchi Sea ranged from 24 to 127 Bq·kg^{-1} [*Lepore et al*., 2008, *Baskaran et al*., 1996; 2000]. The ^{210}Pb inventory is correlated to water column depth, although boundary scavenging might alter it [*Lepore et al*., 2009]. Focussing factors showed greater values in the Makarov Basin and lower in the Eurasian Basin, indicating a net lateral export of ^{210}Pb between both basins (Smith *et al*., 2003). At the North Western Polynya, *Robert et al*. [1997] compared the ^{210}Pb in excess in bottom sediments to the *in situ* production and atmospheric deposition: lateral ^{210}Pb inputs might account for the observed difference, but they suggested the contribution of ^{210}Pb associated to sea ice as the most likely cause. This was further investigated by *Masqué et al*. [2007].

2.2. Artificial Radionuclides (^{137}Cs and ^{239,240}Pu)

Since the 1950s, anthropogenic radionuclides such as ^{137}Cs and Pu isotopes amongst others have been introduced and distributed worldwide, including the Arctic Ocean. During the past two decades numerous national and international programs have been carried out to study the distribution, sources,

transport and behaviour of anthropogenic radionuclides in the Arctic Ocean [e.g. *JNREG*, 1994, 1996; *AMAP*, 1998].

The main source of anthropogenic radionuclides in the Arctic Ocean has been global stratospheric fallout [*JNREG*, 1996; *Oughton et al.,* 2004]. However, secondary sources have also been significant. Regional or tropospheric fallout resulted from nuclear weapons tests carried out by the former Soviet Union (FSU) at the Novaya Zemlya archipelago (85 atmospheric, 3 underwater, 2 surface water tests between 1955 and 1990) and at Semipalatinsk (86 atmospheric, 30 ground surface and 340 underground tests; [*Salbu*, 2001]). Nuclear wastes from reprocessing facilities also contributed to the overall inventories of ^{137}Cs and Pu in the Arctic Ocean, including discharges from Sellafield (UK) and, to a lesser extent, from La Hague (France) [*Holm et al.,* 1994; *Aarkrog*, 2003]. Also, the Ob and Yenisey rivers contribute terrestrial run-off which has received radionuclides from weapons testing at Semipalatinsk and discharges from nuclear facilities located near or on the rivers (Tomsk-7 and Mayak) [e.g. *JRNC*, 1994, 1996, *Oughton et al.,* 1999; *Smith et al*., 1995]. For example, it has been documented the release of about 100 TBq of liquid waste from Mayak, including about 2 TBq of alpha emitters, to the Techa River during 1948-1951 [*Christensen et al.,* 1997; *Vorobiova et al.,* 1999]. Other reprocessing plants such as Krasnoyarsk-26, located close to the Kara Sea discharged about 30 to 100 TBq of ^{137}Cs into the Kara Sea between 1958 and 1993 [*Vakulovsky et al.,* 1995]. Finally, the FSU also carried out dumping of liquid and solid radioactive wastes into the Barents and Kara Seas between 1960 and 1991. Overall, the total amount of nuclear waste dumped in the Arctic Ocean was estimated by *IAEA* [1998] to be approximately 37 PBq. Nuclear accidents have also contributed artificial radionuclide into the Arctic environment, such as those occurred in Kyshtym in 1957 and in Tromsk-7 in 1993 [*Kabakchi et al.,* 1995; *Waters et al.,* 1999].

2.2.1. Plutonium isotopes (239 and 240)

Plutonium is the most abundant transuranium radionuclide into the environment (Goldberg *et al.,* 1980). Trace amount of Pu isotopes are produced naturally in uranium ores by neutron capture however, in environmental studies those concentrations can be considered negligible compare to the amount of Pu injected by human activities. Pu isotopes are produced by the activation of ^{238}U present in the nuclear combustible with neutrons.

Among all 20 isotopes, the most abundant are ^{239}Pu ($T_{1/2}$ = 24110 y) and ^{240}Pu ($T_{1/2}$ = 6563 y). Both isotopes are alpha-emitters with energies of 5.157 MeV (70.8% yield) and 5.168 MeV (72.8% yield), respectively.

Distribution of ^{239,240}Pu isotopes from the global fallout, material injected to the stratosphere, showed latitudinal dependence [*Hardy et al.,* 1973]. Pu was mainly deposited in the North Hemisphere since most of the atmospheric tests took place there, and the highest values are also found there. Temperate regions also presented large deposition given the preferential air exchange between stratosphere and troposphere in the mid-latitude and the air circulation pattern in this troposphere, whereas deposition decreases in the equatorial and polar regions by a factor of two [*UNSCEAR*, 2000]. However, the integrated ^{240}Pu/^{239}Pu atom ratio in soil is 0.18 remaining constant along the Earth [*Kelley et al.,* 1999] since it depends upon the weapon design and the parameters of the test. Some exceptions, for example, are the place around 35º due to Nevada Test Site, Novaya Zemlya, Semipalatinsk, etc. where tropospheric nuclear test took place whose deposition is confined regionally to those areas proximal to the test site [*Smith et al*., 2000; *Yamamoto et al*., 2001].

In the marine environment, Pu entered mostly by deposition and as secondary source as runoff from rivers. However, nowadays, the atmospheric flux of Pu is negligible, but it was relevant in the last decades [e.g. *UNSCEAR*, 1982; *AMAP*, 2000; *Masqué et al.,* 2003]. Once in the ocean, Pu is associated to particles due to its particle reactive behaviour (K_d $1 \cdot 10^5$ $L \cdot kg^{-1}$; [*IAEA*, 1985]). The fraction of Pu associated to particles ranges from 1 to 10 % of the total amount of Pu [*Hirose et al.,* 2001b; *Livington et al.,* 1987]. As a result, Pu moves downward with sinking particles and finally it is deposited in the seabed [*Fowler et al.,* 1983]. The Pu distribution profile shows a surface minimum, a mid-depth maximum and, thereafter, a decrease with increasing water depth. Physical processes, such as advection

and upwelling, also affect Pu distribution [*Hirose et al.,* 2002]. The residence times for ^{239,240}Pu in the water column varies from tens of days in turbid shallow coastal systems to tens of years in open ocean waters [*Hirose et al.*, 2001].

The relative abundance of the Pu isotopes depends upon the practices and sources of Pu during production, reactor type and nuclear fuel burn-up. Thus the isotope ratio is used to identify the specific Pu source, since in the environment it is not affected by differential geochemical behaviour (Table 2.2). However, the isotope ratio can vary as a function of the localization and time. Given that each isotope has a different half-life, the isotope ratio can vary with time, excepting ^{240}Pu/^{239}Pu atom ratio. For example, the ^{239}Pu/^{241}Pu or ^{238}Pu/^{239,240}Pu atom ratios have changed throughout the time since ^{241}Pu and ^{238}Pu have shorter half-lives (14.3 y and 87.7 y, respectively) than ^{239}Pu and ^{240}Pu.

Table 2.2 ^{240}Pu/^{239}Pu atom ratios for different sources and reactor type.

	^{240}Pu/^{239}Pu	**Study**
Weapon Pre 1960	0.01	*Rokop et al.*, [1995]
Weapon modern	0.055-0.065	*Rokop et al.*, [1995]
Weapon grade	<0.075	*Rokop et al.*, [1995]
Power Water Reactor	0.43	*Carlson et al.*, [1988]
Boiling Water Reactor	0.40	*Carlson et al.*, [1988]

Distribution in the Arctic Ocean

Current ^{239,240}Pu concentrations in the Arctic waters are dominated by the contribution from global fallout, except for some areas, like the Novaya Zemlya archipelago, where local sources have had a significant impact [*Livingston et al.,* 1984; *Holm et al.,* 1996; *Mitchell et al.,* 1998; *Smith et al.*, 2000]. The total concentrations of ^{239,240}Pu in seawater have changed with time. For instance, at the LOREX station situated in the North Pole (Makarov Basin), the surface activity was 14 mBq·m^{-3} in 1979 [*Livingston et al.,* 1984], eight year later the ^{239,240}Pu activity was 17 - 18 mBq·m^{-3} in the Nansen Basin [*Cochran et al.,* 1995]. In 1996, the ^{239,240}Pu activity dropped to 4.2 - 9.8 mBq·m^{-3} in the Eurasian Basin [*Josefsson*, 1998]. *Holm et al.* [1991] calculated an effective half-life of 7 - 8 yeas for the surface plutonium in the northeast Atlantic Ocean, which was in good agreement with the activity decrease from 1987 to 1996 in the Nansen Basin. Along the Eurasian Shelf, the ^{239,240}Pu activities in the PML decreased in an eastward direction: from 7 - 9 mBq·m^{-3} in the eastern Barents Sea [*Herrmann et al.,* 1998], to average concentrations of 3.0 ± 0.9 mBq·m^{-3} and 2.6 ± 0.7 mBq·m^{-3} in the Kara and Laptev Seas, respectively, and 1.5 ± 0.7 mBq·m^{-3} in the East Siberian Sea [*León Vintró et al.,* 2002]. This pattern was attributed primarily to losses of Pu to bottom sediments via vertical transport in these shallow waters.

Concentration profiles of ^{239,240}Pu in the water column show a depletion in the surface due to scavenging by particle matter and a subsurface maximum as a result of remineralization below the halocline. A secondary maximum of ^{239,240}Pu is associated to the Atlantic Water, derived from Sellafield (Figure 2.4): the ^{239,240}Pu concentrations in the Atlantic Water at the LOREX station in 1979 was 10.2 - 18.3 Bq·m^{-3} [*Livingston et al.,* 1984], while they were of 24.2 mBq·m^{-3} and 28.3 mBq·m^{-3} in the Nansen Basin and the Barents Sea in 1987 [*Cochran et al.,* 1995a], and ranged from 14 to 22 mBq·m^{-3} in 1996 in the central Arctic Ocean [*Jossefson*, 1998]. This distribution was attributed to the advection of Atlantic Water contaminated by both global fallout and discharges from the European reprocessing plants (mainly Sellafield) along the same path. A comparable trend has been found for ^{137}Cs [*Kershaw and Baxter*, 1995; *Holm et al.,* 1996].

Overall, the ^{240}Pu/^{239}Pu atom ratios in surface waters are approximately 0.18 [*Josefsson*, 1998; *Cooper et al.*, 1999; *León-Vintro et al.,* 2002], consistent with global fallout [*Krey et al.,* 1976] and with the discharge-weighted from Sellafield ratio during 1966-1985 [*Cooper et al.,* 1999]. However, ^{240}Pu/^{239}Pu atom ratios lower than global fallout were measured in the less saline waters of the Laptev Sea, likely revealing the impact of the Russian rivers discharge [*Cochran et al.*, 1995b; *Josefsson,* 1998, *Cooper et al.*, 1999].

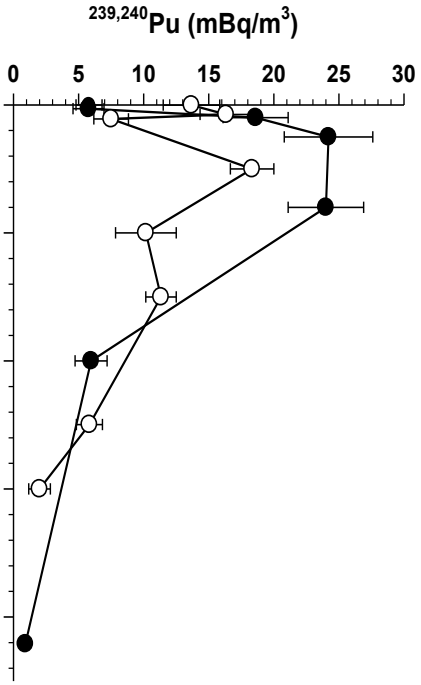

Figure 2.4 Concentration profiles of ^{239,240}Pu in the water column at the North Pole in 1979 (white circles) and in 1994 (black circles).

The ultimate sink for Pu present in the marine environment is bottom sediments. The ^{239,240}Pu concentrations in sediments decrease with depth, although it is mostly concentrated in the first cm. The Pu inventory should increase with time as more Pu is scavenged to the bottom sediments from the water column. In Arctic bottom sediments the ^{239,240}Pu in the shelves and slopes (27.4 - 48.5 Bq·m^{-2}) were two orders of magnitude greater than in the deep basins (0.15 - 0.74 Bq·m^{-2}) [*Huh et al.,* 1997]. That is consistent with low scavenging rates in the central Arctic Basin. *Masqué et al*. [2003] reported inventories ranging from 1.90 to 16.7 Bq·m^{-2} at the Fram Strait, with the exception of one core with an inventory as high as 35.9 Bq·m^{-2}. Concerning to the ^{240}Pu/^{239}Pu atom ratios, all Arctic continental shelves exhibit ratios comparable to global fallout [*Skipperud et al.,* 2004] except some areas of the Kara Sea, Laptev and Barents shelves where lower ratios have been measured [*Smith et al*., 1995; 1999; *Oughton et al*., 2004]. Slightly higher values than global fallout have been found in the Chukchi shelf [*Cooper et al*., 2000]. The ^{240}Pu/^{239}Pu atom ratio decreased from global fallout to values down to 0.10 with increasing latitude. *Huh et al*. [1997] suggested that this is due to a mixture of global fallout inputs, which decreases with increasing latitudes, and discharges from reprocessing plants in Russia and in the Atlantic area. At the Fram Strait, the distribution of ^{240}Pu/^{239}Pu atom ratio in bottom sediments mirrors the sea ice drift patterns. Each drift pattern is fed with sea ice formed in the continental shelves and thus it is labelled with distinct ^{240}Pu/^{239}Pu atom ratios. Low ^{240}Pu/^{239}Pu atom ratios were measured in the area of the Fram Strait where the ice transported by the TPD melts [*Masqué et al*., 2003], consistent with the general patterns of sea ice formed in the Siberian continental shelves and the Kara Sea, characterised by low ^{240}Pu/^{239}Pu atom ratios [e.g. *Pfirman et al*., 1999; *Smith et al*., 2000], and that feed the TPD.

In sea ice, there is any data about the concentration of Pu and ^{240}Pu/^{239}Pu atom ratios however, several studies [*Landa et al*., 1998; *Cooper et al*., 1998 and *Masqué et al*., 2003; 2007] measured Pu and ^{240}Pu/^{239}Pu atom ratios in SIS. Specific activities of ^{239,240}Pu SIS ranged over four orders of magnitude, from 18 up to 1824 mBq·kg^{-1}. The highest activities were mainly measured in SIS samples collected in the Eurasian Basin, with the exception of two SIS samples that were collected in the Canada Basin. The back-trajectory analysis indicated that these samples were formed in the Western Arctic Ocean. The ^{240}Pu/^{239}Pu atom ratios in SIS ranged from 0.138 to 0.201. Most of the ^{240}Pu/^{239}Pu atom ratios are comparable to the typical global fallout ratio (0.18), suggesting that source areas for most of the

sampled sea-ice sediments are only affected by fallout-global. Geographically, the $^{240}Pu/^{239}Pu$ atom ratios lower than global fallout were measured in the Eurasian Basin, while the higher $^{40}Pu/^{239}Pu$ atom ratios in the Canadian Basin. In fact, bottom sediment in the Arctic continental shelves also reflected this distribution.

2.2.2. ^{137}Cs

Caesium-137, with a half-life is 30.07 y, is the major product produced by fission of the nucleus (fission yields: 6-7%) [*UNSCEAR*, 2000]. ^{137}Cs decays to ^{137m}Ba ($T_{1/2}$= 2.6 min) by emitting β particles and ^{137m}Ba decays by γ emission (661.7 keV, 85.0 %).

Global fallout is the main responsible of the presence of ^{137}Cs in the Earth [*UNSCEAR*, 2000]. Its deposition on the surface has not been homogenous, being higher in the Northern Hemisphere due to the occurrence of most nuclear weapon tests in the 50s and 60s. The deposition also presented differences by latitude driven by the air exchange between the stratosphere and the troposphere and the global circulation patterns. In particular, the band between 40-50 received the highest ^{137}Cs deposition in both hemispheres (3600 $Bq \cdot m^{-2}$ in the north and 810 $Bq \cdot m^{-2}$ in the south), whereas the lowest inputs were registered in the band 60-70º (1600 and 400 $Bq \cdot m^{-2}$ in the north and the south, respectively) [*UNSCEAR*, 2000; *Aoyama et al*., 2006]. Nuclear accidents, like Chernobyl, and nuclear weapons tests in the troposphere also contributed to increase the ^{137}Cs deposition locally [*AMAP,* 1998; *UNSCEAR*, 2000].

The incorporation of ^{137}Cs in the marine environment is mostly driven by deposition as well as through rivers runoff. Given that ^{137}Cs is characterized by a high solubility and low affinity to particles in seawater, it is mainly present in dissolved form, and only 0.1% of the total activity in the seawater is associated to particulate matter [*Livingston et al*., 1977]. The ^{137}Cs distribution in the marine system is function of the mechanisms that governs the vertical transport of soluble substances, mainly mixing and advection of water masses. The combination of these processes makes that the typical ^{137}Cs seawater profile shows a continuously decreasing activity with depth. Bottom sediments are the ultimate fate for ^{137}Cs present in the marine environment. Activity concentrations and inventories of ^{137}Cs in bottom sediments are function of sedimentation rates, water column depth and type of particles.

Distribution in the Arctic Ocean

The main sources of ^{137}Cs in the Arctic Ocean are global fallout, the Chernobyl accident in 1986 and discharges from the Sellafield reprocessing facility [*Livingston et al.,* 1984; Cochran *et al.,* 1995]. Nowadays atmospheric deposition of ^{137}Cs can be considered negligible [*UNSCEAR*, 2000; *AMAP*, 1998].

The activity of ^{137}Cs in seawater has changed with time due to different processes; vertical transport, advection, mixing and decay. Surface ^{137}Cs activities in the central Arctic Basin showed high activities in the Eurasian Basin and low activities in the Canadian Basin [*Josefsson*, 1998]. In the Eurasian Basin at about the Gakkel Ridge, a gradient from low activities (5.1 $Bq \cdot m^{-3}$) in the south to high activities in the north (11.3 $Bq \cdot m^{-3}$) was observed in 1994 [*Ellis et al*., 1995]. The same pattern was observed in 1996 in the same area, increasing from 5.2 to 10.7 $Bq \cdot m^{-3}$ [*Josefsson*, 1998]. These differences reflect the input derived from Chernobyl and the releases from nuclear reprocessing plants. Concentrations of ^{137}Cs in surface seawater have decreased with time, but punctuated with the increase after Chernobyl accident. For instance, ^{137}Cs concentrations ranged from 9 to 14 $Bq \cdot m^{-3}$ in the Nansen Basin in 1987 [*Cochran et al*., 1995] and from 11 to 14 $Bq \cdot m^{-3}$ in 1994 [*Ellis et al*., 1995] and in 1996 dropped to the similar values than those observed at the North Pole in 1979 (around 6.5 $\cdot m^{-3}$) [*Josefsson*, 1998]. Comparable results were observed in the Canadian Basin, even through ^{137}Cs concentrations were lower than in the Eurasian Basin [*Smith et al*., 1995a; 1998; *Livington et al*., 1988; *Cooper et al*., 1999].

All published concentration profiles of ^{137}Cs seawater in the open Arctic are characterized by fairly similar patterns, with a continuous decrease in activity with depth (Figure 2.5), even though with slight differences between basins: concentrations in the Atlantic Water in the Eurasian Basin were about 5

Bq·m^{-3} higher than in the Canadian Basin [*Jossefso*n, 1998]. Still, the AW represented the highest percentage of ^{137}Cs in the water column in both cases, more markedly in the Makarov Basin than in the Nansen basin.

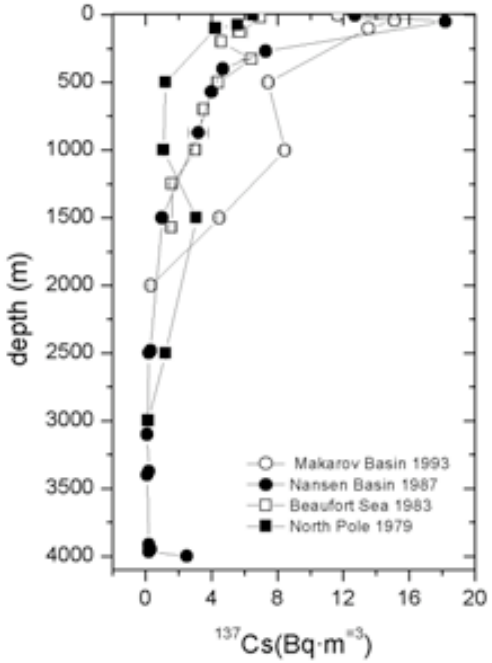

Figure 2.5. Concentration profiles of ^{137}Cs in the water column in the North Pole [*Livingston et al*., 1984], the Beaufort Sea [*Cooper et al*., 1999], the Nansen Basin [*Cochran et al*., 1995] and the Makarov Basin [*Smith et al*., 1998].

Studies in the distribution of ^{137}Cs in bottom sediments have been mainly devoted to continental shelves. Its distribution in the Siberian continental shelves showed a decrease in the eastward direction: the highest activities in surface sediments have been determined in the Kara Sea, with an average of about 15 Bq·kg^{-1}, with the exception of the Novaya Zemlya Archipelago where reported concentrations of up to 100 Bq·kg^{-1} have been measured [*AMAP*, 1998]. These high activities reflect the impact of the nuclear testing (85 atmospheric-tropospheric, 3 underwater, 2 surface water tests from 1955 to 1990) and nuclear waste dumping that took place in this area [*JNREG,* 1994; *Baskaran et al*., 1996; *Smith et al*., 1995b; 2000]. Average concentrations in surface sediments of the shelves of the Laptev and the East Siberian Seas averaged 7 and 4 Bq·kg^{-1}, respectively [*Johson-Pyrtle et al*., 2001]. The average concentrations in the Chukchi-Bering Seas were of about 1.5 Bq·kg^{-1} [*Cooper et al*., 1998]. In general, ^{137}Cs is concentrated in the first cm of the sediment; however, mixing due to bioturbation leads to detect ^{137}Cs at deeper layers of the sedimentary column. The ^{137}Cs inventories in bottom sediments from estuary areas tend to be higher than in marine sediments: the ^{137}Cs inventory in the Kara Sea was on average 580 Bq·m^{-2}, while it was of 1600 and 515 Bq·m^{-2} in the estuaries of the Ob and Yenisey rivers respectively [*Baskaran et al*., 1996]. A similar pattern was observed in the Laptev Sea, where an average of about 1000 Bq·m^{-2} was estimated in the estuary, slightly higher than in marine sediments (875 Bq·m^{-2}) [*Johson-Pyrtle et al*., 2001]. Elevated inventories were also measured in the Kolyma River in the East Siberian Sea (695 Bq·m^{-2}), while in the east Chukchi and East Siberian marine sediments it was of about 350 Bq·m^{-2} [*Cooper et al*., 1998; *Baskaran and Naidu,* 1995].

In the sea ice compartment, the only available data of ^{137}Cs is in SIS [*Meese et al*., 1997; *Landa et al*., 1998; *Cooper et al*., 1998; *Masqué et al*., 2003 and 2007, Baskaran, 2005; *Cota et al*., 2006]. SIS contained a large variability of ^{137}Cs activity, varying from measured <0.2 up to 2522 Bq·kg^{-1}. Although most of the samples, 85%, contained ^{137}Cs concentrations lower than 40 Bq·kg^{-1}. The highest activities, > 40 Bq·kg^{-1}, were mainly measured in SIS samples collected in the Eurasian Basin, along the TPD, although *Cota et al*. [2006] found two SIS samples with highest ^{137}Cs activities in SIS, > 2000 Bq·kg^{-1},

in the Canadian Archipelago. These ^{137}Cs activities in SIS were accountable for enrichment during sea ice drifting, however other authors indicated that concentration of ^{137}Cs in SIS is predominantly a function of the radionuclide load of bottom sediments in the region where sea ice was formed [*Cooper et al*., 1998 and *Landa et al.,* 1998]. .

Chapter 3.

Sampling and analytical methods

A detailed description of the field protocols for sampling during the ARK XXII/2 cruise in the Arctic Ocean in 2007 and the analytical methods used to analyse and quantify the natural and artificial radionuclides studied here (^{7}Be, ^{210}Po, ^{210}Pb, ^{137}Cs, ^{239}Pu and ^{240}Pu) is presented in this chapter, divided in two sections. We first address the methods and equipment used to sample each compartment of the Artic sea ice system; in the second part we describe the analytical methods: ^{7}Be, ^{137}Cs (and ^{226}Ra) by gamma-spectrometry and ^{210}Po and ^{210}Pb by alpha-spectrometry at UAB, and ^{239,240}Pu and the ^{240}Pu/^{239}Pu atom ratio by ICP-MS and AMS at the Woods Hole Oceanographic Institution (WHOI), the Centro Nacional de Aceleradores (CNA) the and Lamont Doherty Earth Observatory (LDEO).

3.1. Sampling

In summer 2007, from 28th July to 7th October, the ARKXXII/2 Arctic expedition took place on board the German research vessel Polarstern during which we gathered samples of surface sea ice, sea ice cores, sea-ice sediments, surface sea water, melt ponds, water beneath sea ice (Figure 3.1, Table 3.1).

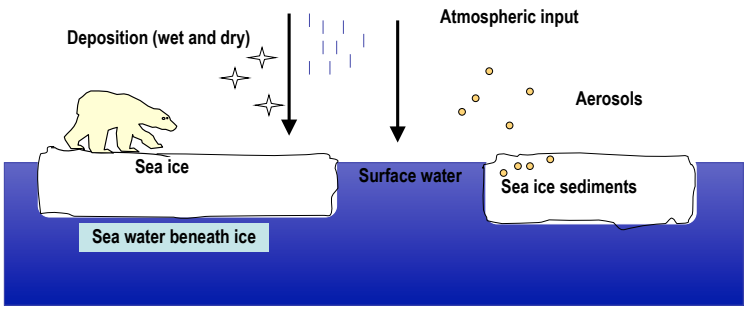

Figure 3.1 Schematic representation of the compartments of the Artic sea ice system from which samples for analyses were collected

Table 3.1 Number of samples and radionuclides analysed for each type of sample.

Matrix	Number of samples	Radionuclides
Melt ponds	10	^{10}Pb,
Surface sea ice	20	^{7}Be and ^{137}Cs
Sea ice cores	14	^{10}Pb
Sea-ice Sediments	64	^{7}Be, ^{234}Th, ^{210}Pb, ^{137}Cs, ^{240}Pu and ^{240}Pu/^{239}Pu atom ratio
Surface water	56	^{7}Be and ^{137}Cs
Water beneath ice	11	^{7}Be
Precipitation	16	^{7}Be and ^{210}Pb

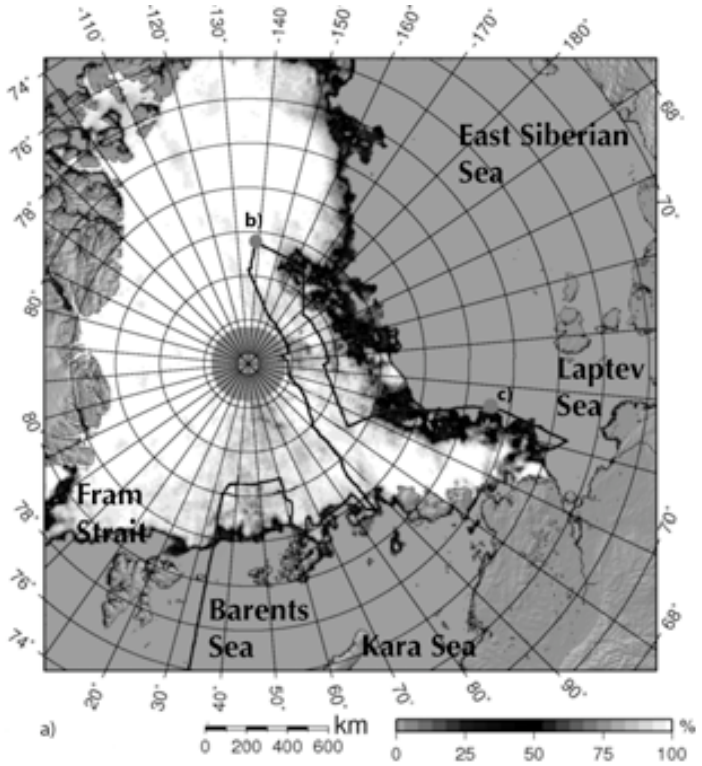

Figure 3.2 Cruise track of the ARK XXII/2 expedition in the Arctic Ocean (blak line). Sea ice extent and concentration in September 2007 is also shown.

The study area comprises the Eurasian Basin of the Arctic Ocean, from the shelves of the Barents, Kara and Laptev Seas across the Nansen, Amundsen and Makarov Basins beyond the Alpha Ridge and the Canada Basin (cruise track is shown in Figure 3.2). Sea-ice sediment samples from previous cruises ARK XIV/1a (n= 12, 1998), ARK XIV/2 (n=13, 2001) and ARK XIX/4 (n=23, 2003) were also analysed. These samples were obtained from the Nansen Basin and the Fram Strait.

3.1.1. Sea Ice Station

Samples of surface sea ice, melt ponds, sea ice cores and seawater beneath ice were collected at several ice stations. In order to minimize any alteration and contamination due to the vessel activities (particularly by fumes), samples were collected at distances of about 200 m away from the vessel. Given the low concentrations of ^{7}Be, ^{210}Pb, ^{137}Cs, ^{239}Pu and ^{240}Pu in these matrixes, sampling of large volumes was necessary. Other participating teams measured sea-ice thickness by drilling and also by

towing a kayak over the sea ice in whose interior electromagnetic sounding equipment was installed [*Haas et al.,* 2003] [*Schauer*, 2008].

Surface sea ice was sampled to determine the concentrations of ^{7}Be, ^{210}Pb and ^{137}Cs in order to study the interception and accumulation of atmospheric flux by sea ice. We assumed that the atmospheric deposition is accumulated in the upper 10 cm of sea ice, on the basis of previous test carried out by us (unpublished data). Before sampling the sea ice, the snow thickness was measured using a calibrated pole and then it was removed. Approximately between 60 and 100 L of sea ice from the upper 10 cm were collected using stainless shovels and transferred to 30 L polypropylene containers. Once onboard, ice was transferred to a 120 L polypropylene container and left to thaw at room temperature for analysis.

A representative integrated ice core sample was sampled to determine the amount of ^{210}Pb. This integrated ice core sample consisted of approximately between 4 and 8 ice cores which were collected within an area of 1 m^2 using a stainless steel ice corer of 10 cm of diameter. Firstly the upper parts of the sea ice cores (first 90 cm) were sampled and immediately transferred to plastic bags to minimize brine loss. There after, bottom parts were drilled following the same procedure as upper parts. Once on-board, sea ice cores were transferred to a 120 L polypropylene container to be processed as an integrated sample. Sea ice cores were thawed at room temperature for several days.

Water beneath sea ice (1 m depth) was sampled using a peristaltic pump through a hole drilled in the sea ice with a stainless steel ice corer. Samples volumes were of about 100 L, and were collected in 30 L polypropylene containers and once onboard were transferred to 120 L polypropylene containers.

Melt ponds were also collected to measure ^{210}Pb. Between 15 and 25 L of water from melt ponds were sampled from the closer melt pond to where the rest of sea ice samples were collected.

3.1.2. Sea-ice sediments

Most sea-ice sediments were sampled in heli-stations that were reached with helicopter, after detecting dirty ice during recognition flights. Between 10 and 200 g of SIS were collected from the upper surface of the ice floes, usually from ridges or cryoconites holes. Sampling was carried out by scraping with a stain-steel shovel or an ice-hammer in order to obtain blocs of turbid sea ice. Once on-board, samples were thawed and SIS were isolated from the supernatant liquid by careful decantation. Afterwards, SIS samples were stored in plastic bags and kept frozen until their analysis in the laboratory. A fraction of each sample was dried to constant mass in an oven at 60 ºC for 48 - 72 hours and subsequently grounded to a powder before analysis.

3.1.3. Seawater

Approximately 100 L of water were collected using the water intake line of the RV Polarstern, placed at 8 m depth. for determination of ^{7}Be and ^{137}Cs concentrations in surface seawater.

3.1.4. Precipitation

Samples of atmospheric deposition were collected using two precipitation collectors placed on the top of the RV Polarstern's bridge. Each collector consisted in a polypropylene container in which a plastic funnels with an effective surface area of 0.19 m^2 was connected to a polyethylene bottle placed beneath the funnel.

One of the collectors remained opened at all times to obtain total (dry and wet) precipitation, whilst the wet precipitation was collected in the second system, which was only opened at the beginning of every rain-snow event. At the end of each rain-snow event both collectors were closed. the collectors taken to the laboratory and the surfaces of the funnels and interior walls of the collection bottles washed with a known volume of 1 N HCl. Samples were stored in 500 mL polypropylene bottles.

3.2. Analytical methods

This subsection describes the methods used to determine ^{7}Be, ^{210}Pb, ^{226}Ra (natural radionuclides) and ^{137}Cs, ^{239,240}Pu and the ^{240}Pu/^{239}Pu atom ratio (artificial radionuclides) in the samples studied here. The analytical procedures to determine ^{210}Pb and the gamma emitters such as ^{7}Be, ^{226}Ra and ^{137}Cs and are based on methods developed in our research group [*Merino*, 1997; *Sanchez-Cabeza et al.*, 1998; *Masqué*, 1999]. The analyses of Pu were carried out in collaboration with other institutions and the methods were adapted as required depending on the matrices of the samples.

3.2.1. ^{7}Be

Liquid samples

The concentrations of ^{7}Be in seawater and sea ice were determined in approximately 100 L of sample, while volumes precipitation samples were more variable, ranging from 12 to 202 mL. Samples were acidified with HCl (37%) to pH of about 1 – 2 and spiked with a known amount of stable Be (10 mg) as an internal tracer of the analytical procedure. 300 mg of Fe^{3+} were added as carrier. Then samples were vigorously stirred and stored for 12 - 24 hours for chemical equilibration, after which the pH was adjusted to 8.5 with NaOH to allow the precipitation of Fe-hydroxide ($Fe(OH)_2$), that scavenges ^{7}Be from solution. Once the precipitate settled down, the supernatant was carefully removed by siphoning and the precipitate was transferred to 250 mL polypropylene bottles and stored until analysis in the laboratory.

Once in the laboratory at UAB, the iron precipitates were centrifuged for 5 minutes and the supernatants were carefully removed by siphoning. The precipitate was rinsed twice with Mili-Q water to remove salts, it was centrifuged again and transferred to polypropylene vials and dried for gamma measurement.

Sediment samples

Samples of sea-ice sediments were dried in an oven at 60ºC until constant mass. Aliquots of 0.5–11 g of each dried, ground sea-ice sediment sample were placed into plastic vials for gamma spectrometry.

3.2.2. ^{210}Pb

Liquid samples

The analytical method followed for liquid samples to determine the concentrations of ^{210}Pb was described by *Masqué* [1999]. Once samples were collected, they were immediately acidified with HCl (37%) to pH ~1 – 2, spiked with a known amount of ^{209}Po ($T_{1/2}$ = 102 y, 100 µL, 0.8446 ± 0.0339 Bq·mL^{-1}) and stable Pb^{2+} (85 mg) as yield tracers. Fe^{3+} (300 mg) was added as a carrier. After storing them for 12 - 24 hours for chemical equilibration, pH was adjusted to 8.5 with NaOH to allow the precipitation of Fe-precipitate ($Fe(OH)_2$) that amongst others, scavenges ^{210}Pb and ^{210}Po from solution. The supernatant was removed and the precipitate was poured to 250 mL bottles.

Radiochemical purification and measurement were conducted in the laboratory at UAB. Once in the laboratory, samples were always analyzed within 6 months after its collection. Samples were centrifuged and supernatants were carefully removed by syphoning. The precipitates were rinsed twice with Mili-Q water and were dissolved with HCl (37%). Samples were evaporated without boiling and were digested adding 2 mL of HCl (37%) for 3 times. Afterwards, samples were evaporated and preconditioned with 80 mL 1M HCl. An aliquots of 1 mL was taken from the solution and diluted with mili-Q water to a volume of 10 mL for determination of stable Pb. The solutions were heated at 80 ºC under stirring. Given that the solutions can contain dissolved iron that could be deposited onto the silver discs and interfere in the quality of the spectra, ascorbic acid was added to the warm solution until that became transparent, uncoloured. At this point the solutions were ready for Po auto-deposition onto

lacquered silver discs. Auto-deposition was carried out at 80 ºC for 8 hours under constant stirring. The Po auto-deposition isolates it from other alpha-emitting radionuclides and elements of the matrix. After that, the discs were dried at room temperature, being ready for measuring. In order to remove any Po left in solution, although it is typically less than 1%, the remaining solutions were re-plated onto another silver disc for another 8 hours at 80 ºC. The remained solutions were poured to a 125 mL polypropylene bottle and they were re-spiked with a known amount of ^{209}Po (100 µL, 1.0447 ± 0.0089 Bq·mL^{-1}). Solutions were stored for at least 6 months for ^{210}Po ingrowth, and , the same procedure as first plating was performed in order to determine the ^{210}Pb concentration in the sample.

Sediment samples

^{210}Pb and ^{210}Po are in secular equilibrium in sediment samples at the time of analysis. The analytical procedure used to determine ^{210}Pb in sediment samples was published by *Sanchez-Cabeza et al*. [1998]. Briefly, about 150 - 200 mg of sample to which a known amount of ^{209}Po (100 µL, 1.0447 ± 0.0089 Bq·mL^{-1}) was added as yield monitor, were heated and acid digested by using a commercial MDS-2000 microware sampler preparation system. Sediments were digested using two steps: first an acid mixture digestion HNO_3:HCl:HF:H_2O (5:2:3:10 mL) and then boric acid was added to complex the Fe ions of the solution. The resulting solution was transferred into 125 mL Teflon beakers and evaporated to dryness without boiling and was processed as described in the above sections.

3.2.3. ^{137}Cs and ^{226}Ra

For solid sample, the same analytical method applied to determine ^{7}Be in SIS was used for ^{137}Cs and ^{226}Ra.

In liquid samples, the analytical method followed was described by Merino [1997]. After treating the sample to scavenge ^{7}Be onto the Fe-precipitate ($Fe(OH)_2$), the supernatant was then transferred into a second barrel since cesium stays in solution. By addition of 65% HNO_3, the pH was lowered again and subsequently stable Cs was added as a chemical yield tracer. Then, a pre-weighed sample of ammonium molybdophosphate (AMP) was added while stirring thoroughly. This produced a yellow precipitate that scavenges Cs. The precipitate was left to settle and then transferred into vials for gamma spectrometry.

3.2.4. ^{239,240}Pu and ^{240}Pu/^{239}Pu atom ratio

The most used analytical method for the determination of the concentrations of plutoniu m in environmental samples is alpha spectrometry, even through mass spectrometry techniques is receiving increasing interest, since it allows determining the ^{240}Pu/^{239}Pu atom ratios. Three different methods were used to determine the ^{239}Pu and ^{240}Pu concentrations here: a magnetic-sector inductively coupled plasma mass spectrometer (MS-ICPMS) at WHOI; accelerator mass spectrometry (AMS) at the can; and inductively coupled plasma mass spectrometer (ICP-MS) at LDEO.

Masqué *et al*. (2003) described the procedure used to determine ^{239}Pu and ^{240}Pu activities in SIS samples by MS-ICPMS at, based on the methods developed by *Buesseler* [1986] and *Kenna* [2002]. Briefly, a known amount of ^{242}Pu was added as an internal yield tracer to 2 - 25 g of sample that was incinerated at 550 ºC for 24 h. The ashes were digested with 8 M HNO_3. Pu was separated by ion exchange, and samples underwent several purification steps in order to obtain an adequate separation from other transuranic nuclides. Pu was eluted from the final ion exchange column with 10% HNO_3/1% HF and the solution was evaporated to 1 mL.

The chemical procedure for SIS samples measured by AMS is detailed by *Chamizo et al*. [2008a, 2008b]. About 2 g of dried sample were spiked with 10 pg of ^{242}Pu as a yield monitor, were incinerated at 600 ºC for 6 hours and acid digested with HNO_3 (65%), H_2O_2 (30%) and HF (40%). The supernatant was separated from the residue after centrifuging. Prior to ion exchange purification, the solution was prepared to contain Pu (IV) by adding 0.18 g of $NaNO_3$. Ion exchange separation was performed using TEVA-columns. The Pu fraction was isolated from the other actinides by washing the column with 6 M

HCl and 8 M HNO_3 to remove Th and U, respectively. Pu was eluted with a mixture of 0.002 M HF/0.02 M HNO_3 and the eluate was evaporated to 3 mL. To each sample 0.5 mg of Fe^{3+} (as $Fe(NO_3)_3$) were added, and after evaporation the sample was mixed with pure Al powder (2 mg), making sample. Then the sample was pressed into Al holders and finally mounted on a sample wheel.

The method used to quantify Pu isotopes in sediment samples by ICP-MS at LDEO was modified after Maxwell (1997) and Kenna (2002). About 2 g of dry sediment were spiked with ^{242}Pu as a yield monitor. Sediments were completely digested using a mixture of HNO_3 (65%) and HF (40%) under heating at 180ºC. After matrix dissolution, $HClO_4$ was added in order to remove HF by fuming. This step was repeated three times and the solution was evaporated to dryness. After that, Pu was co-precipitated with $Fe(OH)_3$. After centrifuging the solution, the supernatant was separated from the residue. The iron precipitated was dissolved with HNO_3 (65%). Prior to ion exchange purification, the solution was prepared to contain Pu in the IV oxidation state by adding 1.3 g of $FeSO_4 \cdot 7\ H_2O$ and 2.2 mL 4.2 M $NaNO_2$. Ion exchange separation was carried out with TEVA- resins and TEVA-pre-filter resin placed on a vacuum system. The Pu fraction was isolated from the other actinides by washing the column with 9 M HCl and 8 M HCl to remove Th and 8 M HNO_3 to remove U. Before Pu was eluted, a pre-filter resin was placed between column and solution collector to minimize the contribution of other components and then Pu was eluted with 0.13 M HF and 0.02 M HNO_3. The elute was prepared for a second purification adding 0.65 g of $FeSO_4 \cdot 7H_2O$ and 2 ml 4.2 M $NaNO_2$. After collecting the final Pu fraction, a drop of $HClO_4$ was added to remove the resin, the solution was evaporated to dryness and adjusted to an acid concentration of 1% HNO_3/0.1% HF.

3.3. Spectra analysis and activity quantifications

Several spectrometry systems for gamma, alpha and mas, were used for radionuclide determination. Each radionuclide was measured and quantified considering accuracy, time consumption and economical costs.

3.3.1. Gamma spectrometry

For gamma spectrometry we used well-type, low-background, high-resolution, high-purity germanium detectors (HPGe) coupled with a multi-channel pulse height analysis was used to measure gamma emitters (^{7}Be, ^{137}Cs and ^{226}Ra). Detectors were calibrated for energy and efficiency using a MCR 2009-018 solution standard supplied by the CIEMAT in several counting geometries. This solution consists in a cocktail of a mixture of ^{241}Am, ^{109}Cd, ^{139}Ce, ^{57}Co, ^{113}Sn, ^{85}Sr, ^{88}Y, ^{60}Co and ^{137}Cs.

All spectra were quantified using the Genie 2000 Gamma Analysis Software. That includes a set of algorithms for processing the acquired gamma spectra. Each spectrum can be analysed manually following a step-by-step sequence. The algorithms allow identifying and locating individual peaks, calculating net peak areas and making efficiency corrections. Once the analytical sequence is completed, the software provides with a report with the specific activities for each radionuclide present in the sample. All activities were decay-corrected to the date of collection and the uncertainties were calculated according to the theory of quadratic propagation quadratic of the uncertainty and is expressed at 1σ.

^{7}Be

Measurements of ^{7}Be through its emission line at 478 keV (10.4% yield) were conducted within two months after collection of the samples to minimize decay. Counting times were set to ensure a maximum uncertainty of 15% in the concentrations. Chemical recoveries of Be were determined through measurement of stable Be in aliquots of each sample by optic absorption spectrometry at the Servei d'Anàlisi Química (SAQ) at UAB. Table 3.2 summarizes the average recoveries of Be for each type of sample.

Table 3.2 Average recoveries of stable Be for different type of samples.

Sample	Stable Be recovery (%)	Range (%)
Surface sea ice	71 ± 5 (n= 20)	61 - 83
Surface seawater	63 ± 5 (n= 29)	52 - 72
Water beneath ice	62 ± 9 (n= 11)	54 - 72
Precipitation	62 ± 13 (n= 16)	32 - 77

^{137}Cs

Cs-137 was determined in SIS and liquid sample samples through its gamma emission at 661.6 keV. In order to reach an activity uncertainty lower than 10%, samples were measured for 2 to 7 days.

^{226}Ra

The ^{226}Ra activity was quantified based on photopeaks from its daughters (^{214}Pb at 295 KeV and 351 KeV and ^{214}Bi at 609 KeV) in secular equilibrium. Secular equilibrium is reached after 3 weeks since polypropylene vials are sealed with parafilm to avoid ^{222}Rn escape.

3.3.2. Alpha spectrometry

Polonium emissions from the platted disks were counted by alpha spectrometry using silicon surface barrier detectors SSB (EG&G Ortec Mod. SSB 450 R) coupled to a multi-channel pulse height analysis system. Discs were measured long enough to achieve uncertainties derived from counting lower than 5%.

The analysis of the spectra was performed using the software MAESTRO™ II vs. 1.40 and Genie 2000, for the Ortec and Cmaberra model, rexpectively. The polonium spectrum consists in two single peaks, which correspond to ^{209}Po and ^{210}Po emitting at 4.866 MeV and 5.305 MeV, respectively. Detector background and reagent blank contributions are subtracted conveniently. Quantification of the ^{210}Po activity [A_{210}] is calculated as:

$$A_{210} = \frac{(N_{210} \cdot A_{209})}{N_{209}} \qquad (3.1)$$

where [A_{209}] is the total activity of ^{209}Po added to the sample (Bq) and [N_{210}] and [N_{209}] are the net counts of ^{210}Po and ^{209}Po, respectively. The chemical recovery of ^{209}Po [ρ] was calculated as

$$\rho\ (\%) = \frac{N_{209}}{t \cdot \varphi \cdot A_{209}} \qquad (3.2)$$

where [N_{209}] is the net counts of ^{209}Po, [t] the counting time (s), [φ] the solid angle and [A_{209}] the total activity of ^{209}Po added to the sample (Bq). Table 3.3 summarizes the average and range recoveries of ^{209}Po for each type of sample.

Table 3.3 Average recovery of ^{209}Po for different types of samples.

Sample	Stable Pb recovery (%)	Range (%)
Surface sea ice	66 ± 12 (n=14)	43 - 83
Whole ice core	88 ± 20 (n=117)	60 - 116
Melt ponds	68 ± 21 (n= 10)	41 - 98
Precipitation	68 ± 13 (n= 16)	50 - 87

The ^{210}Pb activity is quantified with the second plating of the stored solution after at least 6 months of ingrowth of ^{210}Po, applying the adequate ingrowth-decay correctionz to calculate the ^{210}Pb activity at sampling time. The ^{210}Po concentration is determined from the first platting measurement, also correcting for decay and ingrowth [Sylvain et al. 2012]. Potential contamination from the Pb stable carrier and Pb recovery corrections are also taken into account. The uncertainty in the activity was calculated using the theory of quadratic propagation of uncertainty, expressed as 1σ.

The analytical recoveries of Pb were determined through measurement of stable Pb from an aliquot of each sample by atomic absorption spectrometry at SAQ (UAB). Table 3.4 summarizes the average analytical recoveries of Pb for each type of sample.

Table 3.4 Average recoveries of stable Pb for different types of samples.

Sample	Stable Pb recovery (%)	Range (%)
Surface sea ice	73 ± 9 (n= 20)	54 - 85
Whole ice core	56 ± 16 (n=14)	33 - 75
Melt ponds	83 ± 13 (n= 10)	51 - 96
Precipitation	73± 9 (n= 16)	54 - 93

3.3.3. Mass spectrometry

Mass spectrometry methods differ respect to decay-counting methods because it measures the amount of each radionuclide in the sample directly instead than waiting for individual decay events to occur. During the last decades this approach has received increasing interest due to the good sensitivity, low detection limits, short analysis time and, for Pu, because one can obtain isotopic information (^{239}Pu and ^{240}Pu) that otherwise it would be difficult to obtain by alpha spectrometry: ^{239}Pu and ^{240}Pu isotopes have alpha-particle energies that differ by only 11 keV in 5.25 keV, and thus the ^{240}Pu /^{239}Pu atom ratio, being an indicator of the source of the plutonium, is not available for low concentrations.

A solid matrix was used in AMS to minimize both isobaric interferences from polyatomic species and memory effects, while in ICP-MS a liquid matrix was used. Once sample is ionized, with plasma in the case of ICP-MS and with Caesium sputter source for AMS, ions are accelerated and mass analysed by different magnets. Eventually selected ions reach the ionization chambers.

Before measurements, torch position, gas flows and some optical setting of both ICP-MS and AMS were optimized to gain maximum sensitivity with respect to counts per second per concentration unit in tuning solution. A ^{238}U signal is normally used to optimize the ICP-MS and AMS. Switching between isotopes may be accomplished either by changing the magnetic field or by changing the energy of the ions in the magnetic field while the magnetic field is kept fixed. Each mass, 238, 239, 240, 241 and 242 was counted during different time (seconds) reflecting isotope abundance in the sample, and each mass was counted sequentially 25 times. In order to minimize memory effects and to clean the equipment between samples, a solution of 1% HNO_3/0.1% HF was run for ICP-MS. After each sample, a blank was measured and every 4-5 samples a ^{238}U standard with different concentrations was also run to determine tailing, interferences in 239 and 240 masses and also to control equipment stability.

The results are obtained as a ratio between masses, 239/242 and 240/242. These ratios were corrected taking into account the mass discrimination factor determined experimentally by measuring the U standard solution as well as UH+ and polyatomic species (combinations of Pb, Tl and Hg isotopes with isotopes of Cl and Ar) and background from instrument and solutions (laboratory and instrument blank). The combined uncertainty of the measured concentration was calculated taking into account standard deviations of the measured ratio, background (including instrumental background and interferences hydrate ions), uncertainty of mass discrimination factor and uncertainty associated with the activity of the internal standards of ^{242}Pu. The measured atom concentrations of ^{239}Pu and ^{240}Pu have been converted into activities (see Eq 3.3 for ^{239}Pu, it would be equivalent for ^{240}Pu) and expressed as ^{239,240}Pu in order to facilitate comparison with previous works:

$$A_{^{239}Pu} = \frac{^{239}Pu}{^{242}Pu} \cdot \frac{^{242}Pu \; T_{\frac{1}{2}}}{^{239}Pu \; T_{\frac{1}{2}}} \cdot A_{^{242}Pu} \qquad (3.3)$$

where [A^{239}Pu] is the activity of ^{239}Pu (Bq), [A^{242}Pu] is the total activity of ^{242}Pu added to the sample (Bq), [^{239}Pu/^{242}Pu] is the measured atom ratio and [$T_{1/2}$] is the half-life of each isotope.

Chapter 4.

Arctic Ocean sea ice drift origin derived from artificial radionuclides

4.1. Introduction

The Arctic Ocean is often considered as a pristine area, but it can not avoid the effect of industrialization and development. It is thus subject to inputs of contaminants such as heavy metals, persistent organic pollutants and anthropogenic radionuclides [*MacDonald et al*., 2005]. Since the 1950s, anthropogenic radionuclides such as ^{137}Cs and the Pu isotopes (e.g. ^{239}Pu, ^{240}Pu) have been introduced and distributed worldwide, including the Arctic Ocean. During the past two decades numerous national and international programs have been carried out to study the distribution, sources, transport and behaviour of artificial radionuclides in the Arctic Ocean [e.g. *Yablokov et al*., 1993; *JNREG*, 1994, 1996; *AMAP*, 1998]. The main source of anthropogenic radionuclides in the Arctic Ocean has been global stratospheric fallout [*JNREG*, 1996; *Oughton et al*., 2004]. However, secondary sources have also been significant. Regional or tropospheric fallout resulted from nuclear weapons tests carried out by the former Soviet Union (FSU) at the Novaya Zemlya archipelago (85 atmospheric, 3 underwater, 2 surface water tests between 1955 and 1990) and at Semipalatinsk (86 atmospheric, 30 ground surface and 340 underground tests) [*Salbu*, 2001]. Nuclear wastes from reprocessing facilities also contributed to the overall inventories of ^{137}Cs and Pu in Arctic Ocean, including discharges from Sellafield (UK) and, to a lesser extent, from La Hague (France) [*Holm et al.,* 1994; *Aarkrog*, 2003]. Also, the Ob and Yenisey rivers contribute terrestrial run-off which has received radionuclides from weapons testing at Semipalatinsk and discharges from nuclear facilities located near or on the rivers (Tomsk-7 and Mayak) [e.g. *JRNC*, 1994, 1996; *Oughton et al*. 1999; *Smith et al*., 1995]. For example, it has been documented the release of about 100 TBq of liquid waste from Mayak, including about 2 TBq of alpha emitters, to the Techa River during 1948-1951 [*Christensen et al.,* 1997; *Vorobiova et al.,* 1999]. Other reprocessing plants such as Krasnoyarsk-26 discharged about 30 to 100 TBq of ^{137}Cs into the Kara Sea between 1958 and 1993 [*Vakulovsky et al.,* 1995]. Finally, the FSU also dumped liquid and solid radioactive wastes into the Barents and Kara Seas between 1960 and 1991. Overall, the total amount of radioactive wastes dumped in the Arctic Ocean was estimated by the *IAEA* [1998] to be of

approximately 37 PBq. Nuclear accidents have also contributed artificial radionuclides into the Arctic environment, such as those occurred in Kyshtym in 1957 and in Tromsk-7 in 1993 [*Kabakchi et al*., 1995; *Waters et al*., 1999].

Once radionuclides are introduced into the sea they can be scavenged from seawater by particulate matter and be eventually deposited in sediments in the bottom floor [e.g. *Livingston and Bowen*, 1979; *Baxter et al*., 1995; *Aarkrog*, 2003]. In the Arctic Ocean, several studies have focussed on studying the distributions of ^{137}Cs and ^{239,240}Pu and the ^{240}Pu/^{239}Pu atom ratio (which is a useful indicator of Pu origin [*Masqué et al*., 2003]) in bottom sediments from the central Arctic Basin [*Huh et al*., 1997; *Cooper et al*., 2000] and from the Fram Strait [*Masqué et al*., 2003]. However, most studies have paid attention to the continental shelves, particularly along the Siberian shelves, as they are the most affected areas by introduction of artificial radionuclides [e.g. *Baskaran et al*., 1996, 2000; *Cochran et al*., 2000; *Smith et al*., 2000].

The Arctic continental shelves, especially in the Siberian area, are one of the main sources of sea ice (Figure 4.1). During sea ice formation in these shallow areas, sediments and suspended particles are mainly incorporated by suspension freezing into the ice. As a result, sea ice can contain a significant amount of sediments (sea-ice sediments, SIS) ranging from a few grams to tens of kilograms per cubic meter [*Nürnberg et al*., 1994]. Although aeolian deposition onto the ice is also possible, field evidence for such a process is very sparse and its deposition rate on the central Arctic ice cover appears to be several orders of magnitude less than the other contributions to SIS loads [*Pfirman et al*., 1989, 1990; *Nürnberg et al*., 1994]. Thus in general it is assumed that “dirty ice” (ice with high concentrations of sediment) has been formed on shallow shelves.

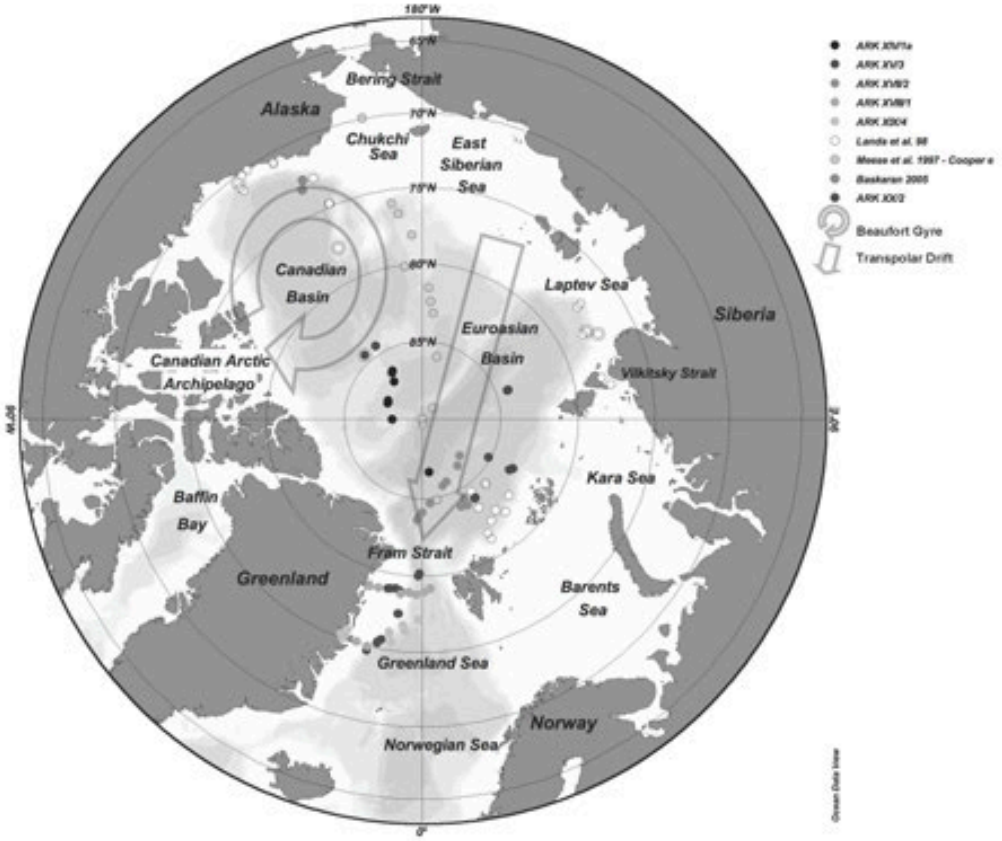

Figure 4.1 Arctic Ocean topography and sea ice drift pattern.

The particulate matter and the associated chemical species contained in sea ice are transported from continental shelf areas to the central Arctic basin in association with the physical circulation. The mean sea-ice drift patterns are controlled by the Transpolar Drift (TPD) over the Eurasian Basin and the

anticyclonic Beaufort Gyre in the Canada Basin [*Thorndike*, 1986]. Sea ice formed over the western Siberian shelves is carried by the TPD with a transit time of 2-4 years to the Fram Strait [*Thorndike and Colony*, 1982]. Sea ice which rotates in the Beaufort Gyre may circulate there for ~5 to 15 years, and is generally thought to be formed in the Beaufort, Chukchi and East Siberian Seas, although it is also possible to find sea ice from the TPD in the Beaufort Gyre [*Thorndike*, 1986]. As sea ice reaches ablation areas such as the Fram Strait and, to a lesser degree, also along the central Arctic Ocean or in the Canadian archipelago, it melts and releases the entrained particulate matter to the surface water [*Pfirman et al*., 1997; *Rigor et al*., 2002]. Hence, sea ice has been identified as playing a potentially important role in the redistribution and transport of particulate matter and chemical species in the Arctic Ocean [e.g. *Nürnberg et al*., 1994; *Landa et al*., 1998; *Masqué et al*., 2003].

In this work we use new and published data on concentrations of ^{137}Cs, ^{239,240}Pu and the ^{240}Pu/^{239}Pu atom ratio in SIS in the Arctic Ocean to assess the possible origin of the sea ice, which forms the ice pack.

4.2. Sampling

A total of 63 SIS samples were collected during several cruises of R/V Polarstern (Table 4.1). Samples were recovered from annual or multi-year sea ice and icebergs from the central Arctic Ocean, the Nansen Basin and the Fram Strait. Approximately 10 to 200 g of SIS were collected from the upper surface of the ice floes, from ridges and from cryoconites holes (small holes produced by aggregation of particles in the surface ice by absorption of solar energy) by scraping with stain-steel shovels or/an ice-hammer in order to obtain blocs of turbid sea ice. Once onboard, sea-ice samples were thawed and SIS were isolated from the supernatant liquid by careful decantation. Afterwards, SIS samples were kept frozen and stored in plastic bags until their analysis in the laboratory. Before radionuclide analysis, all samples were dried in an oven at 60 ºC and ground to a powder.

Table 4.1 Data on sampling cruises on board RV Polarstern, year, areas of study and number of SIS samples collected.

Name Cruise	Year	Expedition area	Number of samples
ARK XIV/1a	July 1998	Central Arctic Basin	12
ARK XV II/2	August-September 2001	Nansen Basin	13
ARK XVIII/1	July-August 2002	Fram Strait	10
ARK XIX/4	August-September 2003	Fram Strait	12
ARK XXII/2	July-October 2007	Along Transporlar Drift	16

4.3. Results

The specific activities of artificial radionuclides (^{137}Cs and ^{239,240}Pu) and the ^{240}Pu/^{239}Pu atom ratios in sea-ice sediments are summarized in Table 4.2.

Table 4.2 Specific activities (±1σ) of ^{137}Cs, ^{239,240}Pu and ^{240}Pu/^{239}Pu atom ratios in sea-ice sediments collected from the Arctic Ocean. n.m.: not measured.

Code	Date	Lat N	Long E	^{137}Cs (Bq·kg^{-1})	^{239,240}Pu (Bq·kg^{-1})	^{240}Pu/^{239}Pu
ARK XIV/2 –Central Arctic Basin						
5	08-jul-98	86.658	7.690	13.3 ± 0.7	0.26 ± 0.02	0.20 ± 0.04
8	10-jul-98	88.073	-89.887	9.9 ± 0.5	0.06 ± 0.03	n.m
11	12-jul-98	87.572	-115.094	13.2 ± 0.9	0.141 ± 0.008	0.19 ± 0.02
12	12-jul-98	87.578	-116.606	15.5 ± 0.9	0.183 ± 0.011	0.19 ± 0.02
14	12-jul-98	87.520	-118.825	14.3 ± 0.8	0.09 ± 0.02	n.m
15	13-jul-98	86.992	-143.379	8.3 ± 0.6	0.096 ± 0.009	0.17 ± 0.04

Table 4.2 (cont.)

Code	Date	Lat	Long	^{137}Cs (Bq·kg^{-1})	^{239,240}Pu (Bq·kg^{-1})	^{240}Pu/^{239}Pu
17	13-jul-98	86.457	-147.240	8.0 ± 0.9	0.29 ± 0.03	0.19 ± 0.04
18	14-jul-98	86.373	-148.478	12.9 ± 0.7	0.109 ± 0.006	0.18 ± 0.02
23	18-jul-98	85.673	-176.937	n.m	0.032 ± 0.011	n.m
25	18-jul-98	85.653	-177.862	n.m	0.16 ± 0.05	0.17 ± 0.11
27	21-jul-98	83.560	144.983	n.m	0.084 ± 0.014	0.18 ± 0.06
29	23-jul-98	81.473	145.065	n.m	0.169 ± 0.011	0.17 ± 0.11
ARK XV II/2- Nansen Basin						
217	05-aug-01	83.950	24.250	3.7 ± 0.3	0.136 ± 0.007	0.18 ± 0.02
0.02218	06-aug-01	85.633	17.313	4.15 ± 0.44	0.083 ± 0.010	n.m
220	08-aug-01	84.667	5.100	14.4 ± 1.1	0.97 ± 0.04	0.184 ± 0.016
222	10-aug-01	84.133	0.017	25.2 ± 1.6	1.23 ± 0.02	0.186 ± 0.008
223	11-aug-01	83.636	-2.975	11.9 ± 0.7	0.474 ± 0.011	0.189 ± 0.009
228	16-aug-01	83.791	-2.199	4.2 ± 0.4	0.211 ± 0.013	0.118 ± 0.019
270-2	27-sep-01	84.289	28.258	14.2 ± 0.8	0.54 ± 0.08	0.17 ± 0.05
270-3	27-sep-01	83.873	28.258	4.3 ± 0.3	0.246 ± 0.005	0.179 ± 0.008
270-4	27-sep-01	83.853	27.855	13.8 ± 1.4	0.94 ± 0.05	0.20 ± 0.02
Iceberg-1	21-aug-01	85.050	11.040	n.m	0.66 ± 0.03	0.18 ± 0.02
Iceberg-2	29-aug-01	86.333	37.767	1.79 ± 0.17	0.021 ± 0.002	0.18 ± 0.04
Iceberg-5	17-sep-01	86.720	46.653	4001 ± 77	31.9 ± 0.8	0.165 ± 0.009
Iceberg-6	23-sep-01	85.800	21.390	4.2 ± 0.3	0.205 ± 0.008	0.25 ± 0.02
ARK XVIII/1- Fram Strait						
01-1	30-jul-02	75.123	-16.528	n.m	0.044 ± 0.004	n.m
02-1	30-jul-02	75.009	-13.641	10.1 ± 0.4	0.24 ± 0.09	0.189 ± 0.015
03-1	8-aug-02	79.200	2.672	6.1 ± 0.7	0.223 ± 0.017	0.19 ± 0.03
05-2	12-aug-02	78.967	0.655	6.4 ± 0.5	0.71 ± 0.05	0.210 ± 0.024
06-2	13-aug-02	78.782	-2.002	3.459 ± 0.243	0.70 ± 0.03	0.217 ± 0.010
07-1	14-aug-02	78.943	-4.600	7.7 ± 0.3	0.086 ± 0.005	n.m
08-1	14-aug-02	78.756	-7.113	480.6 ± 2.3	7.69 ± 0.13	0.166 ± 0.007
08-3	14-aug-02	78.756	-7.113	651.7 ± 3.3	9.5 ± 0.4	0.187 ± 0.007
09-1	15-aug-02	78.909	-14.648	4.8 ± 0.5	0.75 ± 0.05	n.m
10-1	15-aug-02	78.844	-17.657	136.3 ± 0.9	2.52 ± 0.10	0.155 ± 0.009
ARK XIX/4- Fram Strait						
PS64 HELI02-2	15-aug-03	76.380	-4.654	3.9 ± 0.7	0.144 ± 0.008	0.187 ± 0.017
PS64 HELI04-1	16-aug-03	76.750	-5.480	5.4 ± 0.8	0.262 ± 0.017	0.19 ± 0.02
PS64 HELI04-2	16-aug-03	76.747	-5.459	4.2 ± 0.4	0.254 ± 0.012	0.193 ± 0.013
PS64 HELI05-1	20-aug-03	77.150	-1.172	5.6 ± 0.3	0.144 ± 0.011	0.17 ± 0.02
PS64 HELI06-1	20-aug-03	77.150	-1.201	5.6 ± 0.3	0.186 ± 0.015	n.m
PS64 HELI07-1	25-aug-03	75.586	-8.048	4.5 ± 0.6	0.124 ± 0.010	0.16 ± 0.03
PS64 HELI09-2a	29-aug-03	75.013	-20.101	22.4 ± 0.2	0.141 ± 0.012	n.m
PS64 HELI11-1	5-sep-03	76.115	-8.745	4.3 ± 0.6	0.44 ± 0.02	0.175 ± 0.012
PS64 HELI11-3	5-sep-03	76.216	-8.999	126.2 ± 8.4	2.92 ± 0.13	0.143 ± 0.009
PS64-HELI12.2	6-sep-03	75.622	-19.735	23.1 ± 0.2	n.m	n.m
PS64-HELI12.3	6-sep-03	75.261	-20.905	8.7 ± 1.5	n.m	n.m
PS64 HELI14-2	14-sep-03	73,357	-23,818	n.m	0.018 ± 0.005	n.m
ARK XXII/2- Along transpolar drift						
PS70/1.1	6-aug-07	83.994	34.026	31.8 ± 1.3	n.m	n.m
PS70/1.3	6-aug-07	83.994	34.026	29.9 ± 2.8	0.78 ± 0.03	0.157 ± 0.006
PS70/2.C.2	6-aug-07	83.993	34.385	29.6 ± 0.9	0.68 ± 0.02	0.177 ± 0.007
PS70/2.D.2	6-aug-07	83.993	34.385	19.2 ± 0.5	0.66 ± 0.02	n.m
PS70/4.1	12-aug-07	83.605	60.3989	4.8 ± 1.0	0.210 ± 0.018	0.21 ± 0.03
PS70/4.2	12-aug-07	83.605	60.399	9.7 ± 1.4	0.210 ± 0.011	0.188 ± 0.014
PS70/5	14-aug-07	83.423	61.986	4.5 ± 1.0	n.m	0.180 ± 0.018
PS70/3	11-aug-07	85.145	60.815	11.2 ± 1.9	n.m	n.m
PS70/6	7-sep-07	84.499	-138.389	15.1 ± 6.0	n.m	n.m
PS70/7.1.2	8-sep-07	84.450	-147.572	2.5 ± 0.3	0.229 ± 0.014	0.22 ± 0.02

Table 4.2 (cont.)

Code	Date	Lat	Long	^{137}Cs (Bq·kg^{-1})	^{239,240}Pu (Bq·kg^{-1})	^{240}Pu/^{239}Pu
PS70/7.2.2	8-sep-07	84.450	-147.572	5.148 ± 0.7	0.246 ± 0.017	n.m
PS70/7.3.2	8-sep-07	84.450	-147.572	2.7 ± 0.9	0.226 ± 0.018	0.20 ± 0.03
PS70/8.1	17-sep-07	84.261	108.746	16.6 ± 3.8	n.m	n.m
PS70/8.2	17-sep-07	84.261	108.746	8.1 ± 0.9	n.m	n.m
PS70/8.3	17-sep-07	84.261	108.746	7.2 ± 1.5	0.233 ± 0.012	0.224 ± 0.017
PS70/9.2	17-sep-07	84.215	108.916	20.4 ± 1.1	0.329 ± 0.018	0.216 ± 0.019

The ^{137}Cs activities showed a large variability, ranging from 1.8 to $4 \cdot 10^3$ Bq·kg^{-1}, although only 5% of the samples contained ^{137}Cs activities higher than 38 Bq·kg^{-1}. Outliers have been identified by box plot analysis, based upon inter-quartile differences. Median values were used since the data do not follow a normal distribution. Excluding these samples, the average ^{137}Cs activity was 9.1 ± 7.4 Bq·kg^{-1} (n=51). The highest ^{137}Cs specific activity, $4 \cdot 10^3$ Bq·kg^{-1}, was determined in sediments collected from an iceberg sampled from the waters near Franz Josef Land. This value is even greater than concentrations of ^{137}Cs reported by *Cota et al*. [2006] in sea-ice sediments from the Canadian Archipelago (~$2.5 \cdot 10^3$ Bq·kg^{-1}).

The ^{239,240}Pu specific activities also showed considerable variability, varying up to four orders of magnitude from 0.018 to 31.8 Bq·kg^{-1}, although most of the samples (95%) had ^{240,239}Pu activities <1.4 Bq·kg^{-1}. Excluding the samples with concentrations >1.4 Bq·kg^{-1}, activities of ^{240,239}Pu in SIS averaged 0.32 ± 0.25 Bq·kg^{-1} (n=45). The samples with ^{240,239}Pu concentrations >1.4 Bq·kg^{-1} were collected throughout the Nansen Basin, although mainly in the western part of the Fram Strait. In general, high ^{240,239}Pu concentrations are also characterised by high ^{137}Cs concentrations (>45 Bq·kg^{-1}) (Table 4.2).

The ^{240}Pu/^{239}Pu atom ratios ranged from 0.118 to 0.253 (Table 4.2). Most of the ^{240}Pu/^{239}Pu atom ratios in SIS samples were consistent with the atom ratio characteristic of global fallout (0.183 ± 0.009) measured in sediment samples collected at 70ºN by *Efurd et al*. [2005]. 25% of the samples had ^{240}Pu/^{239}Pu atom ratios lower than 0.174, and they had been mainly collected in the Fram Strait and north of Franz Josef Land. Another 25% of the samples had ^{240}Pu/^{239}Pu atom ratios >0.195, ranging up to 0.253, and in most cases were also collected in the Fram Strait. Samples with relatively low ^{240}Pu/^{239}Pu atom ratios (<0.174) also generally had relatively high concentrations of ^{240,239}Pu (>1 Bq·kg^{-1}) and ^{137}Cs (up to 45 Bq·kg^{-1}), except for samples 15, 228, 270-2 and PS70/3, which were collected in the Eurasian Basin. The samples with low ^{240}Pu/^{239}Pu atom ratios and high ^{137}Cs concentrations were collected in the Fram Strait and the Nansen Basin during summer in 2001 and 2002.

4.4. Discussion

In order to study the geographical distributions of ^{137}Cs and ^{239,240}Pu concentrations and ^{240}Pu/^{239}Pu atom ratios in SIS along the Arctic Ocean it is necessary to consider our data in the context of previous results such as those by *Meese et al*. [1997], *Landa et al*. [1998]; *Cooper et al*. [1998], *Masqué et al*. [2003; 2007] and *Cota et al*. [2006]. The combined dataset shall be sufficiently detailed to permit identification of areas of sea ice origin, by comparing the ^{240}Pu/^{239}Pu atom ratios and ^{137}Cs, ^{239,240}Pu concentrations in SIS with those reported in bottom sediments from the Arctic continental shelves.

The specific activities of anthropogenic radionuclides in SIS can be explained by multiple factors, including sediment source area, grain-size fractionation during sea-ice formation and addition of radionuclides to the ice from atmospheric deposition or scavenging from surrounding sea water during drift [*Landa et al*., 1998; *Cooper et al*., 2000; *Baskaran et al*., 2005]. At the time of collection of the samples considered here (1998-2007), the atmospheric fluxes of ^{137}Cs and ^{240,239}Pu were negligible. Another process, which might enhance the radionuclide concentration in SIS, is the direct uptake from ice during seasonal ice melting. However, this process is also likely to be insignificant because chemical compound solutes are generally excluded from the ice during formation due to the segregation of ions from the crystal ice (Weeks *et al*., 1984). Deposition of dust onto sea ice is generally regarded as unimportant [*Pfirman et al*., 1989, 1990]. Hence radionuclides associated with SIS are likely to reflect

dominantly the isotopic signature of sediments in source areas and thus might be used as a source signature or fingerprint of the area in which the ice incorporated its sediment.

4.4.1. Distribution of anthropogenic radionuclides concentrations in sea-ice sediments

The specific activities of both ^{137}Cs and ^{239,240}Pu in SIS in the Arctic Ocean range over four orders of magnitude, from 1.8 to $4{\cdot}10^3$ Bq·kg^{-1} for ^{137}Cs and from 0.021 to 31.8 Bq·kg^{-1} for ^{239,240}Pu (Figure 4.2). The highest activities of ^{137}Cs and ^{239,240}Pu were measured in the same SIS sample collected from an iceberg close to Franz Josef Land. High concentrations of ^{137}Cs were also measured at Resolute Bay (Canadian archipelago) (1785 and 2094 Bq·kg^{-1}), in two SIS samples collected from multi-year ice [*Cota et al*., 2006]. However, most of the SIS samples contained less than 1.4 Bq·kg^{-1} and less than 45 Bq·kg^{-1} of ^{239,240}Pu and ^{137}Cs, respectively (Figure 4.2). These values were identified as extreme-outliers values based upon box-quartile analysis, and thus they were used as criteria to identify samples with anomalously high activities.

Despite the large variation in activities of both radionuclides, three main sectors could be identified within the Arctic Ocean based on ^{137}Cs and ^{239,240}Pu activities: the Eurasian Basin (n=41), the Canadian Basin (n=30) and the Fram Strait (n=31) (Figure 4.2). The largest variability for both radionuclides was found in the Eurasian Basin, where ^{137}Cs and ^{239,240}Pu concentrations ranged from 1.8 to $4{\cdot}10^3$ Bq·kg^{-1} and from 0.02 to 31.8 Bq·kg^{-1}, respectively, and also in the Fram Strait, with ^{137}Cs and ^{239,240}Pu ranging from 2.2 to 651 Bq·kg^{-1} and 0.09 to 9.5 Bq·kg^{-1}, respectively. In contrast, activities in SIS in the Canadian Basin vary relatively less than in other sectors (0.10-1.82 Bq·kg^{-1} for ^{239,240}Pu and 1.7-73 Bq·kg^{-1} for ^{137}Cs). It is interesting to notice that these three sectors mirror the main patterns described from the mean field of sea ice motion: the TPD dominates in the Eurasian Basin, the Beaufort Gyre dominates in the Canadian Basin and the Fram Strait is the principal ablation area.

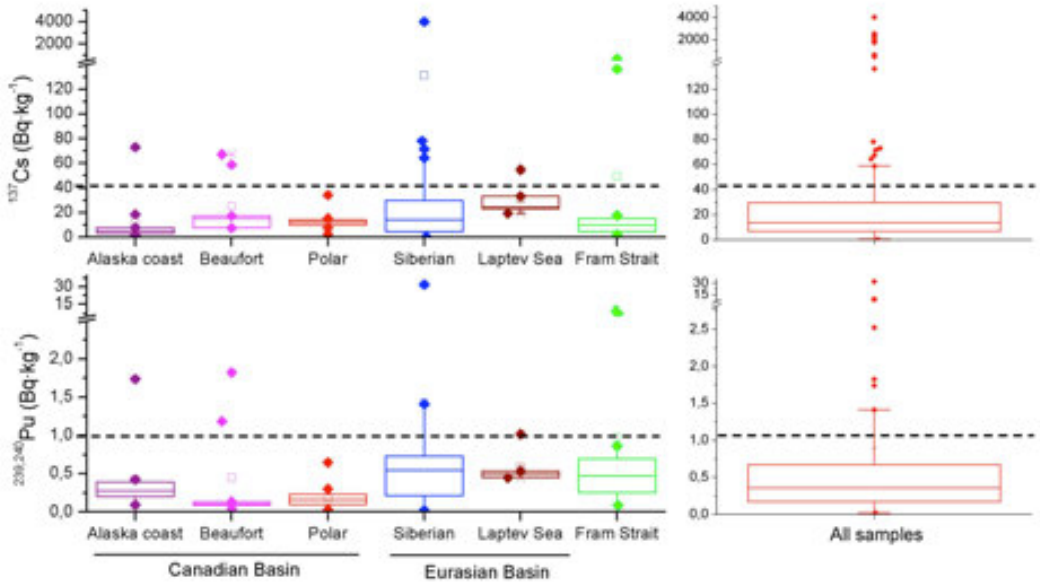

Figure 4.2 Box analysis of ^{137}Cs concentrations (a) and ^{239,240}Pu atom ratios (b) in sea-ice sediments in the Arctic Ocean (including data from this study and from *Meese et al*. [1997], *Landa et al*. [1998], *Cooper et al*. [1998], *Baskaran* [2005], *Masqué et al*. [2003, 2007] and *Cota et al*. [2006]. The median, first and third percentile, 95% percentile (vertical line), outliers (filled points), maximum and minimum values (stars) are indicated.

Within the Eurasian Basin, the highest variability of both radionuclides was found in the Siberian sector, in the Nansen and Amundsen Basins (from 0.4 to $4{\cdot}10^3$ Bq·kg^{-1} for ^{137}Cs and from 0.018 to 31.9 Bq·kg^{-1} for ^{239,240}Pu). This variability is explained by the fact that this area is a potential convergence

region of sea ice originated mainly in the Russian shelves, where comparable ^{137}Cs and ^{239,240}Pu activities have been reported in bottom sediments [*AMAP*, 2002]. Also, *Pavlov et al*. [2004], based on a sea ice drift model, identified the Kara Sea and the Novaya Zemlya archipelago as the most likely origin for sea ice surrounding Franz Joseph Land and Svalbard; this supports the comparison of ^{137}Cs and ^{239,240}Pu activities reported in SIS and surface sediments from the vicinity of the Novaya Zemlya archipelago [*AMAP*, 2002; *Smith et al*., 1995, 2000].

The Laptev Sea is an area where the highest median ^{137}Cs and ^{239,240}Pu activities in SIS were measured: 26 Bq·kg^{-1} and 0.515 Bq·kg^{-1}, respectively. Also, variability in concentrations is rather limited, ranging from 19.5 to 54.8 Bq·kg^{-1} for ^{137}Cs and from 0.45 to 1.012 Bq·kg^{-1} for ^{239,240}Pu, and compare well with reported concentrations in bottom sediments of the Laptev Sea shelf: from 0.01 to 2 Bq·kg^{-1} for ^{239,240}Pu [*AMAP*, 2002] and from 0.86 to 16 Bq·kg^{-1} for ^{137}Cs [*Johnson-Pyrtle and Scott*, 2001]. The only other possible source area of these sea-ice sediments is the Kara Sea, reaching the area through the Vilkitsky Strait. Indeed, SIS collected from a floe in the Vilkitsky Strait had activities as high as 54.8 Bq·kg^{-1} for ^{137}Cs and 1.02 Bq·kg^{-1} for ^{239,240}Pu [*Landa et al*., 1998]. Both values are comparable to those measured in bottom sediment from the Kara Sea and hence suggest that this particular ice floe incorporated the sediments in the Kara Sea.

In the Canadian Basin, a region dominated by the Beaufort Gyre, three subsectors could also be identified; the Alaskan coast (n=9), the Canada and Makarov Basins (identified as Beaufort in Figure 1.2) (n=8) and the central Arctic Ocean (n=13) (Figure 4.2). Despite the fact that ^{137}Cs and ^{239,240}Pu activities vary similarly, slight differences exist in relation to the median activities. For ^{137}Cs, the median activity in the Canada and Makarov Basins is approximately 3 times greater than that in the Alaskan continental shelves (4.9 Bq·kg^{-1}). In contrast, the median ^{239,240}Pu concentration in the Canada and Makarov Basins) is more than 2 times lower than in the Alaska continental shelves (0.28 Bq·kg^{-1}). These results suggest that the dominant source of sea ice is different for each of these regions. From comparison of ^{137}Cs activities in shelf-bottom sediments with those in SIS it can be inferred that sea ice in the Canada and Makarov Basins is more likely to be formed in the Siberian shelves, while sea ice in the Alaska continental shelves is formed along the Chukchi Sea and the Canadian archipelago.

Median activities of ^{137}Cs and ^{239,240}Pu in SIS from the central Arctic Basin were 12.4 and 0.16 Bq·kg^{-1}, respectively, which compare well with concentrations reported in SIS from the Alaska continental shelves and the Canadian and Makarov Basins, suggesting a mixture between both areas. This is in agreement with the findings of *Pfirman et al*. [1997], who stated that sea ice in the central Arctic Basin is formed by ice from diverse sources, identifying Alaska, the Canadian archipelago and the East Siberian Seas as main sources of sea ice.

The distribution of sea ice in the Fram Strait is governed by the oceanographic circulation, and is formed by a mixture of sea ice floes with distinct origins because the diverse trajectories for sea ice drift merge here. This fact is reflected in a large degree of variability in ^{137}Cs and ^{239,240}Pu activities in the Fram Strait (Figure 4.2). The highest range of activities of both radionuclides, 10-652 Bq·kg^{-1} for ^{137}Cs and 0.31-9.5 Bq·kg^{-1} for ^{239,240}Pu, were measured along the permanent ice covered region on the western side. The East Greenland Current flows through this area, and sea ice could have been formed in the eastern Arctic continental shelves and have been driven by the TPD [*Wadhams*, 1983]. This is in agreement with the fact that reported ^{137}Cs and ^{239,240}Pu activities in bottom sediments from the Siberian continental shelves are higher than those in the western Arctic Ocean [e.g. *Baskaran et al*., 1995; 2000; *Huh et al*., 1997; *Meese et al*., 1997; *Smith et al*., 2000; *Johnson-Pyrle et al*., 2001; *Oughton et al*., 2004]. ^{137}Cs and ^{239,240}Pu activities in the central-eastern side of the Fram Strait and in the Eastern Greenland continental shelves vary from 3.8 to 23 Bq·kg^{-1} and from 0.018 to 0.71 Bq·kg^{-1}, respectively. However, SIS samples from the Eastern Greenland area consisted mostly of sand (70%) (data not shown), in agreement with the description of bottom sediments by *Berner and Wefer* [1990], who reported that sand accounts for more than 50% of the sediments in the shelf areas of Greenland. Earlier sea-ice sediment studies carried out in the central Arctic Basin and in the Eurasian shelves [e.g. *Nürnberg et al*., 1994; *Dethleff et al*., 2005; *Eicken et al*., 2005] suggested that entrained materials consist of 60-90% fine-grained (<63 mm) silt and clay, with an essentially terrestrial origin. Therefore, the presence of either high or low concentrations of ^{137}Cs and ^{239,240}Pu associated with low fine-grained

content must be driven by the transport of particulate matter for long distances across the Arctic Ocean and not from Greenland.

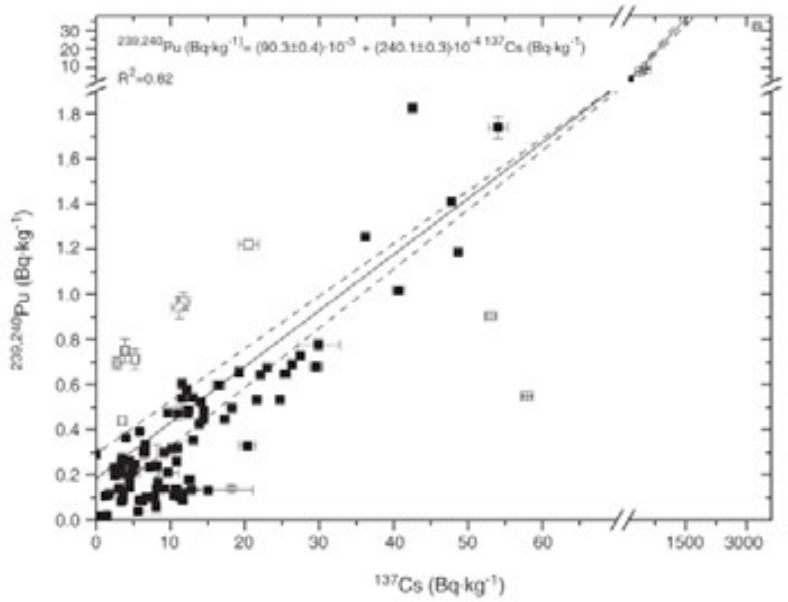

Figure 4.3 Relationship between all ^{239,240}Pu vs ^{137}Cs activities in sea-ice sediments from the Arctic Ocean (including data from this study and from *Meese et al*. [1997], *Landa et al*. [1998], *Cooper et al*. [1998], *Masqué et al*. [2003, 2007]. Confidence intervals at 95% are shown (R^2=0.82). Red points are considered as outliers and are not included into the regression.

Overall, and despite the large variability of ^{137}Cs and ^{239,240}Pu activities in SIS along the Arctic Ocean, a reasonable correlation exists between both radionuclides (R^2=0.80, Figure 4.3). As a general trend, most SIS samples contain ^{137}Cs and ^{239,240}Pu in similar proportions, with a median ^{239,240}Pu/^{137}Cs ratio of $32 \cdot 10^{-3}$. This suggests that the ultimate source of most ^{239,240}Pu and ^{137}Cs in the SIS, and therefore in the bottom sediments mostly delivered by rivers of continental shelves, is the same around the Arctic Ocean. In fact, the average ^{239,240}Pu/^{137}Cs ratio is in good agreement with the global fallout value, ~ $34 \cdot 10^{-3}$ in 2007, based upon decay correction of data in *Beck and Krey* [1983]. This conclusion is reasonable because global fallout is regarded as the main source of both radionuclides to the Arctic Ocean [*JNREG*, 1996, *Oughton et al*., 1999]. However, it is necessary to use caution when using the ratio to attribute the source of ^{137}Cs and ^{239,240}Pu to global fallout. The ^{239,240}Pu/^{137}Cs ratio in bottom sediments depends on many factors: decay, scavenging of the radionuclides by particles during sedimentation, water column depth and proximity to river outflows, sediment characteristic and composition or radionuclide chemical features. In particular the distribution coefficients (K_d) for Pu and Cs in the marine environment are significantly different ($1 \cdot 10^5$ and $2 \cdot 10^3$, respectively; [*IAEA* 1985]), as Pu is more particle reactive than ^{137}Cs.

In spite of the good general correlation between ^{137}Cs and ^{239,240}Pu concentrations, slight differences were observed, suggesting that SIS were imprinted by secondary sources in addition to global fallout (Figure 4.3). This is markedly the case for samples considered as anomalous based on the criteria of higher activities (>45 Bq·kg^{-1} for ^{137}Cs and >1.4 Bq·kg^{-1} for ^{239,240}Pu).

4.4.2. Distribution of ^{240}Pu/^{239}Pu atom ratios in sea-ice sediments

The ^{240}Pu/^{239}Pu atom ratio can be used to identify local sources of Pu other than global fallout. Although the main source of Pu isotopes to the Arctic Ocean is global fallout from the nuclear weapons testing [*Oughton et al*., 2004; *Skipperud et al*., 2004], additional local and regional sources, including local fallout from tropospheric weapons testing, dumping of nuclear waste, marine and terrestrial transport

from the reprocessing plants, and input from nuclear accidents that occurred in proximity to the Arctic Ocean (Tomsk-7) have all contributed to enhancing ^{239,240}Pu and ^{137}Cs activities and modifying the ^{240}Pu/^{239}Pu atom ratios in specific areas of the Siberian shelves [*Cochran et al*., 2000]. In general, the ^{240}Pu/^{239}Pu atom ratio is relatively uniform in the bottom sediments along the continental shelves of the Arctic Ocean [*Skipperud et al*., 2004] and is comparable to the characteristic ratio of global fallout, (0.183 ± 0.009). However, low ^{240}Pu/^{239}Pu atom ratios have been reported in bottom sediments from areas such as Kara Sea and Novaya Zemlya archipelago, ranging from 0.03 at Chernaya Bay to 0.16 ± 0.03 at the Kara Gate [*Smith et al*., 2000; *Oughton et al*., 2004]. On the other hand, ratios slightly higher than the global fallout (0.1939 ± 0.0013) were measured in sediments at Point Barrow, Alaska [*Kelley et al*., 1999].

Huh et al. [1997] suggested that ^{240}Pu/^{239}Pu atom ratios in sediment cores from the deep Arctic Basin correspond to a mixture of global fallout inputs, which decreases with increasing latitudes, and discharges from reprocessing plants in Russia and in the Atlantic area. *Cooper et al*. [2000] suggested that Pu associated with SIS can be considered as a source of Pu to the bottom sediments, although the total flux of Pu from SIS to the deep sea would be relatively small. Recent studies of ^{240}Pu/^{239}Pu atom ratios in bottom sediments in the Fram Strait have provided evidence of the long distance dispersion of Pu in the Arctic Ocean associated to sea-ice sediments [*Masqué et al*., 2003]. This demonstrates that sea-ice is an efficient transport agent of Pu associated with sediments and the fate of sea ice and associated radionuclides to sea-ice sediments is closely coupled.

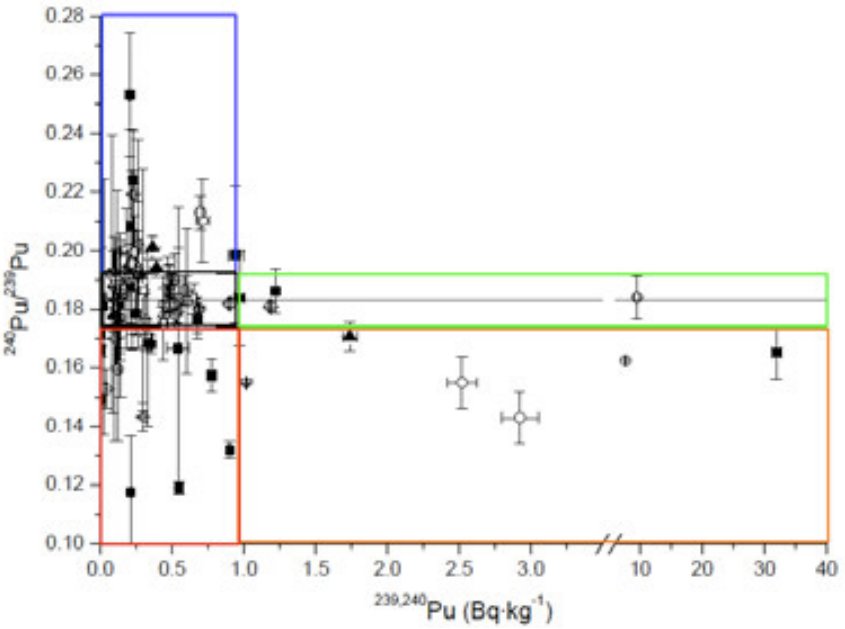

Figure 4.4 Relationship of all available data of ^{137}Cs activities vs ^{240}Pu/^{239}Pu atom ratios in sea-ice sediments collected in the Arctic Ocean including data from this study and from *Meese et al*. [1997], *Landa et al*. [1998], *Cooper et al*. [1998] and *Masqué et al*. [2003, 2007]. Samples are divided according to the mean sea ice drift patterns: Fram Strait (circles), Siberian (solid squares), Laptev Sea (reversed triangle), Polar-central Arctic (triangle), Beaufort (rhombus) and Alaska continental shelves (solid triangle). Five clusters are identified using a ^{240}Pu/^{239}Pu atom ratio of 0.183 ± 0.009 and a ^{137}Cs activity of 20 Bq kg−1 as limits. These clusters are used to hypothesize source areas for sea-ice sediments (see text for details).

The ^{240}Pu/^{239}Pu atom ratios in SIS are generally comparable to that of global fallout (0.18, [*Krey et al*., 1985]). This is expected because most of the continental shelves have been affected by Pu derived from global fallout (Figure 4.4). Deviations from it have been observed at the Fram Strait (0.14 – 0.21) and the Eurasian Basin (0.12 – 0.22) due to the fact that the former area is the region where all drift pathways merge while the latter is influenced by the extensive source areas of the Siberian shelves [*Nürnberg et al*., 1994; *Eicken et al*., 1997]. In the western Arctic Ocean, in contrast, ^{240}Pu/^{239}Pu atom ratios range from 0.17 to 0.19, showing clearly the signature of global fallout. However, the exceptions

to this trend are two samples, 218-1 and 234-1, collected close to the North Pole. These samples likely originated in the vicinity of the Kara Sea, as inferred from their lower $^{240}Pu/^{239}Pu$ atom ratios. The ice floes carrying these SIS could reach the western Arctic as a result of exchange between TPD and Beaufort Gyre. Also, $^{240}Pu/^{239}Pu$ atom ratios slightly higher than global fallout were found in SIS in the Alaska coast [*Landa et al*., 1998]. Those are comparable to $^{240}Pu/^{239}Pu$ atom ratios determined in the sediments of Point Barrow, suggesting that their origin was close to the site of sampling.

4.4.3. Linking radionuclide signatures of SIS to areas of sea ice origin

As shown in Figure 4.4 and noted above, most SIS samples have $^{240}Pu/^{239}Pu$ atom ratios comparable to that of stratospheric bomb fallout (0.183 ± 0.009), irrespectively of their ^{137}Cs concentrations. In particular, samples with elevated ^{137}Cs concentrations are not necessarily characterized by non-global fallout Pu atom ratios, implying that ^{137}Cs alone cannot be used to identify an origin area of sea ice. The combination of both datasets may allow us to identify source areas of the SIS and thus of sea ice. Several clusters of radionuclide signature can be identified according to two criteria (Figure 4.4): deviations of the $^{240}Pu/^{239}Pu$ atom ratios relative to the global fallout value (0.183 ± 0.009) and ^{137}Cs activities higher or lower than 20 $Bq{\cdot}kg^{-1}$, as it has been reported that concentrations of ^{137}Cs originated from global fallout in most continental shelf sediments are <20 $Bq{\cdot}kg^{-1}$ [*AMAP*, 2002]. These clusters include: i) samples with $^{240}Pu/^{239}Pu$ atom ratios <0.174 and ^{137}Cs activities >20 $Bq{\cdot}kg^{-1}$; ii) samples with $^{240}Pu/^{239}Pu$ atom ratios lower than 0.174 and ^{137}Cs activity <20 $Bq{\cdot}kg^{-1}$; iii) samples with $^{240}Pu/^{239}Pu$ atom ratios within the range of global fallout and ^{137}Cs activities >20 $Bq{\cdot}kg^{-1}$; iv) samples with $^{240}Pu/^{239}Pu$ atom ratio greater than global fallout but with low ^{137}Cs activities (<20 $Bq{\cdot}kg^{-1}$) and v) samples with $^{240}Pu/^{239}Pu$ atom ratio comparable to the global fallout and ^{137}Cs activities < 20$Bq{\cdot}kg^{-1}$.

Kara Sea

As shown in Figure 4.4, cluster (i) (yellow-orange line), a group of SIS samples is characterised by $^{240}Pu/^{239}Pu$ atom ratios lower than the global fallout value (< 0.174) and ^{137}Cs activities greater than 20 $Bq{\cdot}kg^{-1}$. Low $^{239}Pu/^{240}Pu$ atom ratios correspond to a mixture between global fallout and low-yield nuclear testing fallout or material released from nuclear reprocessing plants. Among the Arctic continental shelves, low $^{240}Pu/^{239}Pu$ atom ratios have been reported only in the Kara Sea and the Novaya Zemlya archipelago, as a result of local fallout, discharge from rivers and nuclear waste dumping [*Smith et al*., 2000; *Skipperud et al*., 2004]. ^{137}Cs and $^{239,240}Pu$ activities in SIS are greater than those typical for continental shelf sediment affected by global fallout (20 $Bq{\cdot}kg^{-1}$ for ^{137}Cs and 1 $Bq{\cdot}kg^{-1}$ for $^{239,240}Pu$; Smith *et al*., 2000). Previous studies have reported elevated activities of ^{137}Cs and $^{239,240}Pu$ (>45 $Bq{\cdot}kg^{-1}$ and >1 $Bq{\cdot}kg^{-1}$, respectively) in bottom sediments of the Kara Sea [*AMAP*, 1998; *Baskaran et al*., 1995; *Smith et al*., 2000], and thus this could be a likely origin area for SIS with low $^{239}Pu/^{240}Pu$ atom ratios and high ^{137}Cs and $^{239,240}Pu$ activities. The SIS samples showing these isotopic signatures were collected in the west side of the Fram Strait and in the Siberian Branch of the TPD, regions that are principally within the drift path for sea ice formed along the western Arctic shelves, particularly between the Laptev Sea and the Novaya Zemlya Archipelago [*Pfirman et al*., 2004; *Wadhams*, 1983].

Another group of samples are characterized by low Pu atom ratios (< 0.174) but also low ^{137}Cs specific activities (<20 $Bq{\cdot}kg^{-1}$), cluster (ii) (Figure 4.4, red line). Given the low $^{240}Pu/^{239}Pu$ atom ratios of these samples, the most probable source area would also be the Kara Sea and its surrounding areas. The low ^{137}Cs specific activities are likely due to the other factors that affect specific activity (described in section 4.1), and in any case are within the range of activities found in surface bottom sediments [2-33 ^{137}Cs $Bq{\cdot}kg^{-1}$, *Livingston and Povinec*, 2000]. This reinforces the concept that the $^{240}Pu/^{239}Pu$ atom ratio is a better indicator of SIS source than the ^{137}Cs specific activity.

Laptev-Kara Sea

A number of SIS samples display $^{240}Pu/^{239}Pu$ atom ratios typical of global fallout and high ^{137}Cs activities (>20 $Bq{\cdot}kg^{-1}$), cluster (iii) (Figure 4.4, green line). The $^{240}Pu/^{239}Pu$ atom ratios suggest that any

continental shelf area might be the origin of the sediments. High ^{137}Cs activities were measured in bottom sediments in the western Kara and Laptev Seas [*AMAP*, 1998; *Baskaran et al*., 1995; *Smith et al*., 2000, personal communication by A. *Johnson-Pyrle* in *Meese et al*., 1997], although elevated inventories of ^{137}Cs in bottom sediments could result from a combination of processes related to the sedimentation dynamics, *Johnson-Pyrle et al*. [2001] hypothesized that elevated ^{137}Cs inventories in bottom sediments may be the result of ^{137}Cs origin other than direct atmospheric fallout, indicating the Lena river as a secondary source. In the absence of any other direct source of ^{137}Cs in its drainage basin, it is likely that ^{137}Cs introduced into the Lena river comes from the erosion of global fallout and possibly from Chernobyl derived contamination.

Several SIS samples with these characteristics were collected in the Laptev Sea and along the northwest of Franz Josep Land. The Franz Josef Land is within the Siberian Branch of the TPD. Prior studies have considered the Laptev Sea as the major source of sea ice to the Siberian Branch of the TPD, with the Kara Sea as a secondary source [*Nünrberg et al*., 1994; *Pfirman et al*., 1997].

Back trajectory analysis of three samples [sample coded PS93-235-1-2; *Landa et al*., 1998 and 212-2 and 218-1; *Cooper et al*., 2000] collected in the western part of the Arctic Ocean suggested that they originated from the Canadian archipelago and the Beaufort Sea [*Tucker et al*., 1999]. However, the ^{137}Cs and ^{240,239}Pu activities and ^{240}Pu/^{239}Pu atom ratios of these samples argue against these areas as the origin, as no elevated ^{137}Cs and ^{239,240}Pu concentrations have been reported in North American continental shelves [*Meese et al*., 1997; *Landa et al*., 1998]. It is more likely that these sediments originated and were incorporated into sea ice in the Laptev Sea, and reached the western basin by exchange between the TPD and the Beaufort Gyre. The most likely scenario for the transport of Laptev Sea-derived SIS into the Beaufort Gyre occurs when a positive Arctic Oscillation (AO), which favours strong advection of ice away from the Siberian shelves into the central Arctic, is followed by negative AO conditions, increasing the size of the Beaufort Gyre and capturing sea ice into the Beaufort Gyre. The three samples from the western part of the Arctic Ocean were collected in 1994 [*Cooper et al*., 1998]. The years immediately preceding the sampling activities (1989 to 1995) were mostly years of a +AO [*Mysak*, 2001], supporting the hypothesis that they could have originated in the Laptev Sea. During these years, the TPD would be strengthened and pushed closer to Beaufort Sea, making the transport of Laptev Sea into the Beaufort Gyre more likely.

North American Shelves

Most of the samples collected in the western part of the Arctic Ocean close to the Alaska coast, as well as samples collected on the western side of the Fram Strait form another cluster with ^{240}Pu/^{239}Pu atom ratios greater than global fallout (0.19-0.25) and ^{137}Cs activities mostly below 10 Bq·kg^{-1}, cluster (iv) (Figure 4.4, blue line). North American shelves are likely the origin area for such SIS: relatively elevated ^{240}Pu/^{239}Pu atom ratios were measured in bottom sediments from Point Barrow [*Kelley et al*., 1999], while average activities of ^{137}Cs in surface bottom sediments in the Bering and Chukchi Seas and in the East Chukchi Sea are low (4.2 ± 2.8 Bq·kg^{-1}, *Meese et al*., [1997] and 2.9 ± 0.7 Bq·kg^{-1}, *Baskaran and Naidu* [1995], respectively). The high ^{240}Pu/^{239}Pu atom ratios in samples from the western Fram Strait highlight the importance of long-distance transport SIS from the Beaufort Sea across the Arctic Ocean. These sea ice floes and their contained SIS would have originated in the shallow parts of the Beaufort and Chukchi Seas, close to the shore, and drifted eastward, traversing the Arctic Ocean via the Beaufort Gyre and being captured by the Polar Branch of the TPD before finally reaching the Fram Strait. Indeed, this is supported by *Pfirman et al*. [1997], which concluded that North American shelves were the origin for sea ice that flows into western Arctic Ocean and the western part of the Fram Strait.

Unidentifiable source areas

Approximately 50% of the analysed samples have ^{240}Pu/^{239}Pu atom ratios comparable to that of global fallout and ^{137}Cs specific activities lower than < 20 Bq·kg^{-1}, cluster (v), (Figure 4.4, black line). The anthropogenic radionuclide distributions in most of the continental shelves of the Arctic Ocean are typical of global fallout origin, and thus the isotopic signature is not distinct as to identify the source areas of SIS. Additional analyses, such as Fe oxide mineral grains [*Darby*, 2003], planktonic diatom

species [*Abelmann*, 1992], or smectite and illite analysis [*Wollenburg*, 1993; *Delhleff et al*., 1993; *Nürnberg et al*., 1994] may help to constrain more accurately the origin of these samples.

4.5. Conclusions

Based on a combined dataset of previously published and new analyses of ^{137}Cs and $^{239,240}Pu$ and the $^{240}Pu/^{239}Pu$ atom ratios in Arctic sea-ice sediments (SIS), we conclude that these anthropogenic radionuclides can be used in many instances to determine the geographical source area in which the sediments were incorporated into the ice. This information, in addition, can be used to elucidate the sea ice floes formation areas. The $^{240}Pu/^{239}Pu$ atom ratio, in combination with the ^{137}Cs or $^{239,240}Pu$ activity, is especially useful in this regard. SIS originating in the Laptev and Kara Seas have $^{240}Pu/^{239}Pu$ atom ratios lower than those imprinted by global fallout (<0.18), while SIS originating from the Alaskan shelf is characterised by $^{240}Pu/^{239}Pu$ atom ratios greater than global fallout. The specific activities of ^{137}Cs and $^{239,240}Pu$ are less diagnostic of sea-ice origin, because many processes in addition to source can affect their values; however, sediments of the Kara and Laptev Seas can have markedly elevated specific activities of ^{137}Cs that are imprinted on SIS originating in those areas. In approximately 50% of the samples analyzed, the isotopic signatures are not distinctive as to SIS origin and additional approaches are required to better resolve possible source areas.

Chapter 5.

Interception of atmospheric fluxes by Arctic sea ice: evidence from cosmogenic ^{7}Be

5.1. Introduction

Sea ice plays an important role in the climate system in the Arctic Ocean, regulating the ocean-atmosphere interaction and controlling heat exchange [*Thomas and Dieckmann*, 2003]. It is formed mainly along the continental shelves and from its formation until its inevitable melting, sea ice is subject to diverse chemical, physical and structural processes that affect its properties. Initially, during the formation of new sea ice, solutes are excluded and particulate matter (and associated chemical species such as nutrients, pollutants, and radionuclides) is entrained [*Weeks and Ackley*, 1986; *Kempema et al*., 1989; *Reimnitz et al*., 1992]. In the open Arctic Ocean, sea ice also can intercept the atmospheric fluxes of particles, contaminants and other chemical species that then become incorporated into the ice. Presumably to a lesser extent, sea ice may also incorporate chemical species by scavenging them from the surface waters onto sediment carried in the ice [*Baskaran et al*., 2005]. Thus, sea ice drift becomes an important transport pathway for both particles and chemical species that otherwise would not be transported as far away from the source areas [e.g. *Pfirman et al*., 1995]. These components are released to the surface ocean as the ice melts, mainly in ablation areas such as the Fram Strait [*Masqué et al*., 2003, 2007] but also to a lesser extent in the central Arctic Ocean. This release occurs over a short timescale and may coincide with a burst in biological activity [*Melnikov*, 1991]. Indeed, *Granskog et al*. [2003] indicated that atmospherically derived nutrients accumulated in sea ice may enhance the magnitude of ice algae blooms in the Baltic Sea and potentially also in under-ice waters, due to the downward flushing of surface deposited nutrients during periods when sea ice is permeable.

The Arctic Ocean presently displays significant changes, especially concerning the extent and thickness of sea-ice [*Kwok et al*., 2009]: the extent of multi-year sea-ice is decreasing and shifting to the Western Arctic [*Nghiem et al*., 2007], the freezing-up period occurs later and sea ice drifting patterns are subject to changes [*Pfirman et al*., 2004]. *Nghiem et al*. [2007] and *Gascard et al*. [2008] suggest that an increase in the sea ice flux through the Fram Strait is a consequence of an acceleration of the

Transpolar Drift (TPD), and as a consequence there is a reduction in the transit time for sea ice to reach the Fram Strait from its formation areas. The acceleration of the TPD and enhancement of sea ice efflux can increase the fluxes of ice-borne particles and chemical species in ablation areas. In the event of a completely ice-free Arctic in the summer, sea ice would release associated sediments and chemical species all along the central Arctic Basin, likely reducing the fluxes released in the Fram Strait. For these reasons it is of interest to seek a better understanding of the processes related to sea-ice as an accumulation and transport medium of atmospheric fluxes of trace metals, contaminants, etc. Here we use the cosmogenic radionuclide ^{7}Be ($T_{1/2}$= 53.4 d) to determine the efficiency with which sea ice intercepts the atmospheric fluxes of chemical species and their subsequent fate as they are released in ablation areas.

^{7}Be is produced in both the troposphere and the stratosphere through interactions of cosmic-rays with nitrogen and oxygen at rates that are dependent in both latitude and altitude. It rapidly becomes adsorpbed with aerosols [*Bondietti et al*., 1987] and its flux to the Earth's surface is controlled primarily by wet precipitation [*Brown et al*., 1989]. Although ^{7}Be is somewhat particle-reactive and can be scavenged onto particles in coastal waters [*Kadko and Swart*, 2004], it tends to remain in solution in open ocean waters and is rapidly homogenized within the mixed layer with respect to is decay rate [*Silker*, 1972; *Young and Silker*, 1980; *Kadko and Olson*, 1996]. Indeed, it has been used in this context to model mixed layer history, oxygen utilization rates [*Kadko*, 2000; 2009] and upwelling of equatorial waters of the North Atlantic [*Kadko*, 2011].

5.2. Methods and area sampling

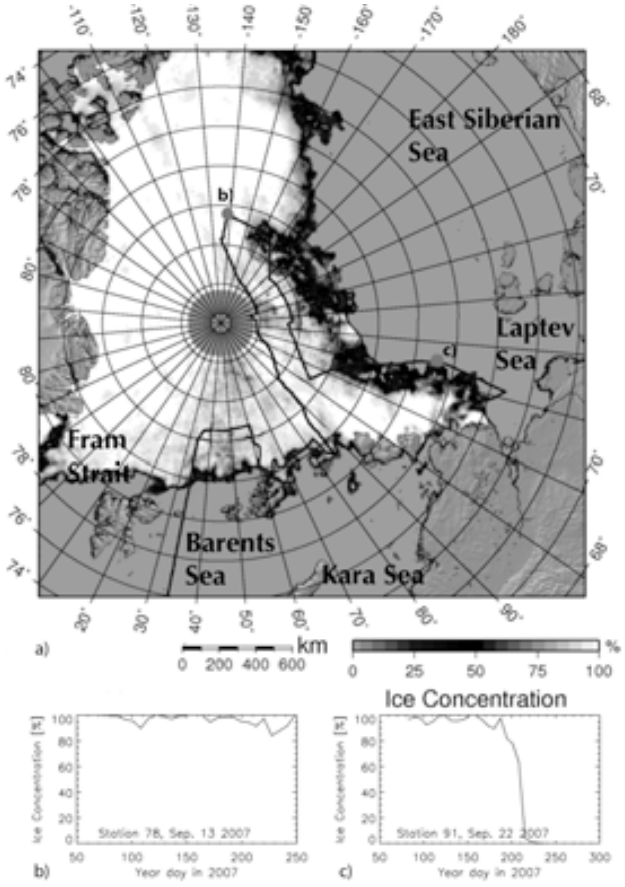

Figure 5.1 a) Map of the Arctic Ocean showing the sea ice coverage and concentration on September 2007. The black line denotes that part of the track of the cruise IPY-SPACE-ARK XXII/2 that was in or close to ice-covered waters (Aug. 1 to Sep. 24). Also shown two examples of time series of the weekly mean ice concentration at stations SWBe-78 and SWBe-91 (labelled with b) and c), respectively).

The study area comprises the Eurasian Basin of the Arctic Ocean, from the shelves of the Barents, the Kara and the Laptev Seas across the Nansen, the Amundsen and the Makarov Basins beyond the Alpha Ridge and the Canada Basin (black line, Figure 5.1). A total of 90 samples of sea ice (n=18), sea-ice sediments (n=16), water beneath the ice (n=10), precipitation (n=18) and surface water (n= 28) were collected during expedition ARK XXII/2-IPY-SPACE of the German R/V *Polarstern* from July 28 to October 7, 2007. Sea-ice sediment samples collected during R/V *Polarstern* expeditions ARK XVII/2 (n=10) and ARK XV/3 to the Nansen Basin and Fram Strait [n=12, *Masque et al*., 2007] are also included for purposes of completeness.

5.2.1. Sea ice concentration analysis

The sea ice coverage at the locations the samples were taken was derived from daily average sea-ice concentrations, i.e. the percentage areal fraction of sea ice. These were calculated using the ARTIST Sea Ice (ASI) algorithm [*Kaleschke et al*., 2001; *Spreen et al*., 2008] applied to brightness temperature polarization differences measured at a frequency of 89 GHz by the polar orbiting Advanced Microwave Scanning Radiometer aboard EOS-Terra (AMSR-E). The grid resolution of the obtained ice concentration maps was 6.25 km. Details about the algorithm and its performance in comparison to other ice-concentration retrieval algorithms like the NASA-Team algorithm [*Cavalieri et al*., 1984] and its enhanced version [*Markus and Cavalieri*, 2000] or the Comiso Bootstrap algorithm [*Comiso,* 1986], can be found in *Kaleschke et al*. [2001], *Kern et al*. [2003], *Andersen et al*. [2007], and *Spreen et al*. [2008].

The sampling position was co-located with the nearest ice concentration data grid cell, which was in polar-stereographic projection true at 70°N. Ice concentration values of a 3 x 3 grid cell area centred at the ship's position were averaged and the respective standard deviation is calculated (from nine values). Subsequently the weekly average ice concentrations and weekly average standard deviations were computed for a period of six months previous to the respective sampling date. For each sampling location the resulting time series of weekly average ice concentration data can be subsequently used to investigate the temporal variation of the ice cover at that location (see Figures 5.2 - 5.3). Two examples of such time-series are given in Figure 1 b) and c) for stations SWBe-78 and 91.

5.3. Results

5.3.1. Sea ice environment and weather conditions

During the 2007 cruise, sea ice extent in the Arctic dropped from $8.1 \cdot 10^6$ km^2 to $4.3 \cdot 10^6$ km^2 from July to September, the minimum extent of ice coverage ever recorded [NSIDC, National Snow and Sea Ice Data Center]. Figure 1a displays the minimum September sea ice extent as given by the ASI algorithm 60% ice-concentration iso-line. Sea ice coverage was above 90% for most of the stations until the beginning of July, and declined swiftly, falling below 70% in some stations by early August and as low as 30% from the central Arctic to the Laptev Sea by the end of August - beginning of September (Figure 5.1 b, c).

Sea ice observation was visually and routinely recorded from the R/V *Polarstern's* bridge during the whole cruise [*Schauer*, 2008]. Sea ice concentration was assessed for the local area surrounding the ship, estimated to be 5 km diameter in good weather conditions and less than 1 km in foggy conditions. The average concentration was ~81% of the total track-sampling area, which is comparable with satellite images showing 70% coverage. However, some variations were observed along the cruise track, such as consolidated pack ice (100%) around 84ºN and low ice concentrations along the St. Anna and the Voronin Troughs and also along the section from the Amundsen Basin toward the Laptev shelf. The concentrations of melt ponds on the ice floes ranged widely, from >60% of the ice coverage in the central Arctic Basin and the Nansen Basin in early August to <10% at the end of September along the Amundsen Basin toward the Laptev Sea. This low occurrence is coincident with the formation of new

ice, even though melt ponds generally were frozen from mid-August onwards [*Schauer*, 2008]. The average concentration of melt ponds along the cruise track was 30%.

5.3.2. ^{7}Be flux from precipitation

The ^{7}Be fluxes in total (wet and dry) and wet precipitation along the cruise track from end of July to September were 1.6 ± 0.3 and 1.7 ± 0.2 Bq·m^{-2}·d^{-1}, respectively. The agreement between integrated fluxes of total and wet precipitation confirms that the dry component of ^{7}Be deposition is not dominant in controlling the atmospheric ^{7}Be fluxes. However, some degree of variability is observed in comparing single precipitation events; wet precipitation ranged from 0.72 ± 0.25 to 4.3 ± 1.4 Bq·m^{-2}·d^{-1}, while total precipitation ranged from 0.97 ± 0.08 to 2.80 ± 0.18 Bq·m^{-2}·d^{-1} (Table 5.1).

Our measured fluxes are in agreement with previous studies: *Kadko and Swart* [2004] reported a total atmospheric flux of ^{7}Be to be 2.03 Bq·m^{-2}·d^{-1}, with values ranging from 0.46 to 3.8 Bq·m^{-2}·d^{-1} in July-August, 1998 at the SHEBA station, located in the Canada Basin. At the same station in October 1997, the ^{7}Be flux varied from 0.0083 to 0.53 Bq·m^{-2}·d^{-1}, averaging 0.33 Bq·m^{-2}·d^{-1} [*Kadko,* 2000]. *Cooper et al*. [2005] reported fluxes ranging from 0.95 to 1.04 Bq·m^{-2}·d^{-1} in July-August, 2002 in the Chukchi Sea. Daily fluxes were measured in Greenland by *Dibb* [1990], who estimated a mean ^{7}Be atmospheric flux ranging from 0.31 to 0.36 Bq·m^{-2}·d^{-1} at Dye 3 station and from 0.45 to 0.89 Bq·m^{-2}·d^{-1} at Summit station in June-July, 1989. These fluxes were estimated assuming a dry fall was 50% of the total precipitation. A significant degree of variability in single events was also observed in this study, with daily fluxes ranging from 0.05 to 3.33 Bq·m^{-2}·d^{-1}. *Dibb* [1990] also suggested that the wet deposition fluxes of ^{7}Be in June and July might be representative of the flux throughout the year.

Table 5.1 Daily and integrated atmospheric fluxes of ^{7}Be (Bq·m^{-2}·d^{-1}) of wet and total (wet and dry) precipitation in the central Arctic Ocean in August and September 2007.

Code	Sampling period		^{7}Be (Bq·m^{-2}·d^{-1})
Wet precipitation			
ARKP-1	12 Aug 16:00	· 12 Aug 22:50	4.3 ± 1.4
ARKP-2	15 Aug 11:15	· 16 Aug 9:10	0.72 ± 0.25
ARKP-3	18 Aug 11:00	· 19 Aug 9:30	2.17 ± 0.59
ARKP-6	12 Sept 10:00	· 16 Sept 8:55	0.98 ± 0.08
ARKP-7	21 Sept 13:20	· 22 Sept 15:00	1.49 ± 0.16
Integrated wet precipitation flux			**1.6 ± 0.3**
Total (wet +dry) precipitation			
ARK W-2	13 Aug 11:30	· 14 Aug 8:30	1.57 ± 0.60
ARK W-3	14 Aug 11:36	· 16 Aug 9:10	1.36 ± 0.22
ARK W-4	17 Aug 15:00	· 19 Aug 9:30	1.94 ± 0.29
ARK W-7a	29 Aug 0:00	· 3 Sept 10:40	1.26 ± 0.11
ARK W-7b	4 Sept 16:30	· 16 Sept 8:55	0.97 ± 0.08
ARK W-8	18 Sept 10:25	· 22 Sept 15:00	2.80 ± 0.18
Integrated total precipitation flux			**1.7 ± 0.2**

5.3.3. ^{7}Be concentration in sea ice, sea water and sea-ice sediments

^{7}Be concentrations in the upper 10 cm of sea ice ranged from 10 to 427 Bq·m^{-3} (Table 5.2). These concentrations are comparable to the range reported by *Eicken et al*. [2002] in the brine channels of sea ice floes (8.3 to 50 Bq·m^{-3}) and in melt ponds (17 to 183 Bq·m^{-3}).

^{7}Be concentrations at 8 m water column depth (Table 5.3) ranged between 1.5 and 9.1 Bq·m^{-3}, about 1-2 orders of magnitude lower than those in sea ice. There is few water column ^{7}Be data from the Arctic Ocean with which to compare these values. The only data available are from *Kadko and Swart* [2004],

who reported ^{7}Be concentrations ranging from 0.8 to 1.5 Bq·m^{-3} at 7 - 10 m depth in leads, whereas at 0.5 m the ^{7}Be concentration was significantly higher (44 Bq·m^{-3}).

Table 5.2 Concentrations of ^{7}Be in the upper 10 cm of sea ice. Samples are gathered in two clusters according to ^{7}Be concentrations (Student's t-test, $p<0.05$).

Code	Lat	Long	Date	Cluster	^{7}Be (Bq·m^{-3})	
SIBe-2	82.792	33.750	04 Aug	1	10	± 3
SIBe-3	83.505	33.973	05 Aug	1	33	± 3
SIBe-4	84.505	36.085	06 Aug	1	61	± 5
SIBe-5	83.608	60.395	12 Aug	1	35	± 3
SIBe-6	82.502	60.791	15 Aug	1	99	± 3
SIBe-7	82.502	65.756	18 Aug	1	105	± 5
SIBe-8	82.143	86.320	20 Aug	1	33	± 2
SIBe-9	83.296	86.189	22 Aug	1	99	± 4
SIBe-10	84.563	89.764	24 Aug	2	253	± 11
SIBe-12	87.034	104.972	27 Aug	1	60	± 2
SIBe-13	87.498	109.556	28 Aug	1	68	± 2
SIBe-14	88.254	150.134	31 Aug	1	126	± 2
SIBe-15	87.827	170.321	02 Sept	2	427	± 10
SIBe-16	84.694	-145.429	05 Sept	2	282	± 3
SIBe-17	88.499	-137.611	07 Sept	1	56	± 2
SIBe-18	86.642	-177.545	10 Sept	2	228	± 3
SIBe-19	86.393	135.817	13 Sept	2	288	± 11
SIBe-20	84.667	102.779	16 Sept	1	68	± 3

Table 5.3 Concentrations of ^{7}Be in the water column at 8 m depth and inventories in the mixed layer. Samples are gathered in two clusters according to ^{7}Be inventories in areas where sea ice coverage during the 4 weeks preceding to sampling was >80% (cluster 1) and <40% (cluster 2).

Code	Lat	Long	Date	Cluster	Mixed layer depth (m)	^{7}Be (Bq·m^{-3})	^{7}Be (Bq·m^{-2})
SWBe-28	81.236	86.288	17 Aug	1	23.4	1.5 ± 0.5	36 ± 12
SWBe-39	83.807	87.099	21 Aug	1	21.8	3.0 ± 0.8	65 ± 18
SWBe-40	85.921	91.238	23 Aug		11.9	< 9.4	< 112
SWBe-42	86.706	99.272	26 Aug	1	15.9	3.1 ± 1.8	49 ± 28
SWBe-43	88.152	119.883	27 Aug		24.0	< 9.0	< 215
SWBe-51	88.211	139.410	29 Aug		26.7	< 9.0	< 239
SWBe-53	88.038	169.988	30 Aug	1	22.8	3.2 ± 0.6	70 ± 12
SWBe-56	87.027	-146.384	01 Sept	1	17.8	5.7 ± 1.4	102 ± 25
SWBe-65	86.363	-139.321	04 Sept		20.8	< 5.0	< 104
SWBe-66	85.693	-134.971	05 Sept		20.8	< 5.3	< 111
SWBe-67	84.499	-138.389	06 Sept	1	18.8	2.2 ± 0.7	41 ± 14
SWBe-68	84.694	-145.429	07 Sept	1	19.8	3.0 ± 0.8	60 ± 17
SWBe-74	85.074	-164.550	08 Sept	1	22.8	5.6 ± 1.8	127 ± 40
SWBe-75	85.751	-170.803	09 Sept	1	18.8	3.9 ± 1.0	74 ± 19
SWBe-76	86.642	-177.545	09 Sept	1	32.0	2.0 ± 0.8	46 ± 18
SWBe-77	86.512	151.952	10 Sept	2	14.0	6.8 ± 2.2	95 ± 31
SWBe-78	86.406	140.959	12 Sept	1	22.8	5.6 ± 1.6	128 ± 36
SWBe-79	86.409	127.433	12 Sept	1	15.8	4.0 ± 1.1	48 ± 13
SWBe-81	84.667	102.779	15 Sept	1	22.8	1.9 ± 1.0	43 ± 22
SWBe-82	83.834	112.719	16 Sept		15.8	< 4.5	< 71
SWBe-84	82.865	117.833	17 Sept	2	12.9	5.2 ± 0.6	66 ± 8
SWBe-86	81.357	120.718	18 Sept	2	17.0	6.1 ± 1.2	104 ± 21
SWBe-88	80.659	122.221	19 Sept	2	21.8	7.2 ± 1.3	157 ± 27
SWBe-90	79.346	124.342	20 Sept	2	13.9	8.6 ± 2.0	120 ± 28
SWBe-91	78.356	124.529	21 Sept	2	14.0	8.3 ± 2.1	116 ± 29
SWBe-93	77.365	123.423	22 Sept	2	15.0	9.1 ± 0.6	136 ± 9
SWBe-100	76.181	122.129	23 Sept	2	17.8	7.7 ± 1.1	137 ± 19
SWBe-102	75.201	121.363	23 Sept	2	19.2	7.7 ± 1.0	147 ± 18

Table 5.4 Concentrations of ^{7}Be in water samples collected at 1m beneath sea ice.

Code	Lat	Long	Date	^{7}Be (Bq·m^{-3})
WunderBe-1	81.952	34.076	02 Aug	2.9 ± 1.2
WunderBe-2	83.505	33.973	07 Aug	< 1.5
WunderBe-3	88.254	150.134	12 Aug	5.3 ± 1.2
WunderBe-4	84.505	36.085	15 Aug	< 2.7
WunderBe-6	86.642	-177.545	24 Aug	4.4 ± 1.1
WunderBe-7	82.143	86.320	28 Aug	4.5 ± 1.0
WunderBe-8	86.393	135.817	31 Aug	2.4 ± 0.4
WunderBe-9	84.563	89.764	10 Aug	4.7 ± 0.9
WunderBe-10	86,393	135,817	12 Sept	4.8 ± 0.7
WunderBe-11	87.034	104.972	16 Sept	5.5 ± 0.9

Table 5.5 Concentrations of ^{7}Be in sea-ice sediments collected during several cruises in the Arctic Ocean: ARK XV/3 (1999), ARK XIV/1a (2001) and ARK XXII/2-IPY-SPACE (2007).

Code	Lat	Long	Date	^{7}Be (Bq·kg^{-1})
ARK XIV/1a -1999 (published in Masqué et al., 2007)				
7	80.01	-1.53	18 Sept	130 ± 5
8	80.18	-1.02	18 Sept	41 ± 3
10	78.95	-7.46	22 Sept	212 ± 6
11	79.03	-10.64	23 Sept	13 ± 2
12	78.99	-11.55	23 Sept	15 ± 2
13	79.07	-8.97	25 Sept	39 ± 4
16	78.92	-4.35	26 Sept	135 ± 5
20	77.46	-7.15	4 Oct	20 ± 2
21	77.46	-6.98	4 Oct	92 ± 6
22	75.64	-10.58	5 Oct	49 ± 3
23	75.44	-11.39	5 Oct	33 ± 5
27	74.72	-13.67	7 Oct	44 ± 4
ARK XV/3 - 2001				
217	83.95	24.25	5 Aug	278 ± 15
218	85.63	17.31	6 Aug	469 ± 27
220	84.67	5.10	8 Aug	1807 ± 84
222	84.13	0.02	10 Aug	1230 ± 67
228	83.79	-2.20	16 Aug	709 ± 36
270-2	84.29	28.26	27 Sept	110 ± 9
270-3	83.87	28.26	27 Sept	20 ± 3
270-4	83.85	27.86	27 Sept	1924 ± 97
Iceberg-5	86.72	46.65	17 Sept	641 ± 29
Iceberg-6	85.80	21.39	23 Sept	104 ± 7
ARK XXII/2-IPY-SPACE - 2007				
PS70/1.1	83.99	34.03	6 Aug	755 ± 33
PS70/1.3	83.99	34.03	6 Aug	524 ± 27
PS70/2.C.2	83.99	34.39	6 Aug	71 ± 14
PS70/2D2	83.99	34.39	6 Aug	92 ± 14
PS70/3	85.15	60.82	11 Aug	1174 ± 94
PS70/4.1	83.60	60.40	12 Aug	1263 ± 101
PS70/4.2	83.60	60.40	12 Aug	2441 ± 97
PS70/5	83.43	61.99	14 Aug	444 ± 28
PS70/6	84.50	-138.39	7 Sept	7477 ± 265
PS70/7.1.2	84.45	-147.57	8 Sept	72 ± 5
PS70/7.2.2	84.45	-147.57	8 Sept	135 ± 12
PS70/7.3.2	84.45	-147.57	8 Sept	140 ± 20
PS70/8.1	84.26	108.75	17 Sept	972 ± 54
PS70/8.2	84.26	108.75	17 Sept	92 ± 9
PS70/8.3	84.26	108.75	17 Sept	580 ± 31
PS70/9.2	84.22	108.92	17 Sept	514 ± 20

^{7}Be concentrations in seawater at 1 m beneath sea ice ranged from 2.4 to 5.5 Bq·m^{-3} (Table 5.4), with an average of 4.3 ± 1.1 Bq·m^{-3}. The only published concentrations of ^{7}Be in water below ice ranged from 1.7 to 2.2 Bq·m^{-3} at 25 m depth [*Kadko*, 2000].

Concentrations of ^{7}Be in sea-ice sediments (SIS) presented a large degree of variability, ranging from 20 to 7477 Bq·kg^{-1}, with a median of 518 Bq·kg^{-1} (Table 5.5). These values encompassed a larger range than those reported by *Masqué et al*. [2007] (13-212 Bq·kg^{-1}, median = 44 Bq·kg^{-1}, n=12). Considering all ^{7}Be published data in SIS (n=32; this study and *Masqué et al*. [2007]), the median concentration is 138 Bq·kg^{-1}.

5.4. Discussion

5.4.1. ^{7}Be concentrations in sea ice

Sea ice acts as a barrier between the ocean and the atmosphere [*Granskog et al*., 2003], and one would therefore expect to find a significant amount of ^{7}Be in sea ice. Indeed, the interception and accumulation of ^{7}Be from the atmosphere appears to be the ultimate source of this radionuclide in sea ice inasmuch as the ice expels sea-salt together with other solutes during its formation [*Weeks and Ackley*, 1986; *Eicken*, 1998]. This conclusion is reinforced by a correlation between ^{7}Be concentrations and the δ^{18}O values (range -9.6‰ to -1.1‰) of the surficial (0 - 10 cm) sea ice ($R^2 = 0.61$, regression not shown). Although sea ice formed on the shelves can contain a small fraction of river runoff, also characterized by low δ^{18}O values, direct deposition of precipitation on the sea ice contributes water with light δ^{18}O (*Bauch et al*., 1995; *Eicken et al*., 2002). The present results suggest that up to 36% of the water in ice is meteoric.

The highest ^{7}Be concentrations ought to occur in the upper part of the sea ice floes, with decreases with depth due to decay. This distribution pattern was displayed by Eicken *et al*. [2002], who measured ^{7}Be concentrations in a multiyear sea ice floe.

Concentrations of ^{7}Be in sea ice can be grouped into two significantly different clusters (Student's t-test, $p<0.05$) (Table 5.2). The first sample group, collected mainly in August, has ^{7}Be concentrations ranging from 10 to 126 Bq·m^{-3} (average 66 ± 34 Bq·m^{-3}), whereas the second cluster comprises samples mostly collected during early September, with higher concentrations ranging from 228 to 427 Bq·m^{-3} (average 295 ± 77 Bq·m^{-3}). This pattern corresponds to the development of sea ice conditions during the summer period: from the end of July to mid-to-late August, most sea ice was snow-free and there were widespread melt ponds. Under these conditions, ^{7}Be from melted sea ice could percolate through brine channels towards the bottom of the sea ice and into the underlying water. Later in summer, snow accumulated on top of the ice and melt ponds were covered by an ice layer [*Schauer*, 2008].

Sea ice also can contain significant amounts of particulate matter (SIS), reported to range from 5 to 56000 g·m^{-2} [*Nürnberg et al*., 1994; *Eicken et al*., 1995; 1997; *Pfirman et al*., 1995]. SIS consists mostly of silt and clays (<63 μm), entrained during ice formation in the shallow shelves, predominantly through the freezing process [e.g. *Nürnberg et al*., 1994; *Pfirman et al*., 1990; *Dethleff*, 2005]. We note that the ^{7}Be activities in SIS (Table 5.5) cannot reflect the original ^{7}Be concentration in sediments at the time of entrainment in the ice because ^{7}Be has a short half-life, and thus the initial concentrations would have decayed completely before the ice has arrived at the sampling locations. The large variability in ^{7}Be is thus caused by i) the various processes that the sea ice has undergone during its drifting (freezing/melting cycles, cryoconite formation), ii) the length of time during which sea ice is exposed to the atmospheric flux of ^{7}Be, iii) characteristics of the sediments (i.e. granulometry) and iv) its distribution in sea ice.

5.4.2. ^{7}Be concentrations in surface water

^{7}Be activity in the surface ocean is dependent on both atmospheric flux and mixed layer depth, which varies seasonally [*Kadko and Olson*, 1996; *Silker*, 1972]. In addition, sea ice intercepts some of the ^{7}Be atmospheric flux (see below). In order to minimize the effect of dilution due to variable mixed layer thickness, we determined ^{7}Be inventories in the upper water column by multiplying the measured surface water ^{7}Be activity by the depth of the mixed layer (Table 5.3). The mixed layer depth was calculated as the depth at which potential density has increased by 0.125 kg m^{-3} of the surface value [*Kara et al*., 2000], varying from 12 to 32 m. Thus, the variation in ^{7}Be inventory should be related to the sea ice coverage during the weeks-months before sampling.

a)

b)

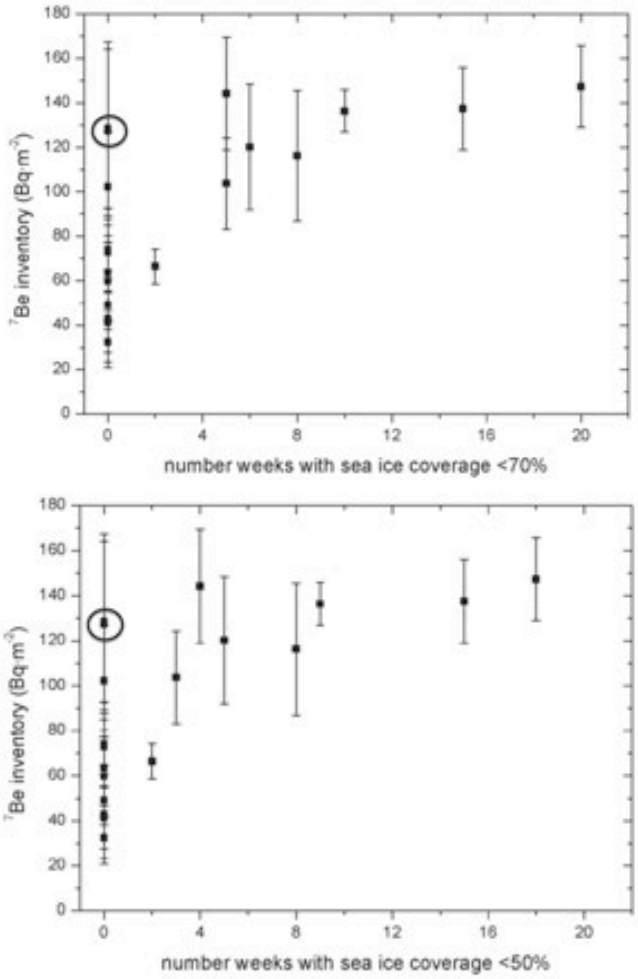

Figure 5.2 ^{7}Be inventory in the mixed layer of the water column as a function of the number of preceding weeks with a) sea ice coverage <70% and b) with sea ice coverage <50%. Samples with inventories of ^{7}Be below the detection limit are not plotted. The circles indicate samples SWBe-74 and 78.

The ^{7}Be inventory in the water column increases as the number of weeks with <70% ice coverage increases (Figure 5.2 a). Maximum inventories are attained after about four weeks of exposure to direct atmospheric inputs, reflecting a quasi-equilibrium between atmospheric inputs and decay. Similar results are observed taking as a limit sea ice coverage of <50% (Figure 5.2 b), partly because the sea ice underwent a rapid decline over nearly two weeks and we have no samples to record this shift. Some degree of variability of ^{7}Be inventories was observed at those stations with ice coverage >70% during the previous six months before sampling (e.g., SWBe-74 and 78) (Figure 5.2 a,b). Proximity of the stations to the ice edge and the presence of leads might explain the surface water enrichment and thus

the divergence from the main trend. However, the apparent lack of agreement between salinity and water column ^{7}Be inventory suggests that ice melt does not contribute significantly to increasing ^{7}Be in the adjacent waters. In contrast, the presence of leads together with the occurrence of precipitation events at the time of sampling can explain the water column data (Table 5.1). We conclude that the decoupling between surface water ^{7}Be inventory and ice coverage seen at specific stations can be explained by the presence of leads that cannot be resolved in the satellite microwave radiometry used to estimate ice concentrations.

Water column ^{7}Be inventories decrease when average sea-ice coverage during the preceding four weeks increases, (Figure 5.3). The exceptions to this trend are two samples, which have ^{7}Be concentrations greater than 120 Bq·m^{-2} yet were collected when ice coverage was above 80% (SWBe-74 and 78) (Figure 5.3). Two clusters of samples can be identified with significantly different ^{7}Be inventories (Student's t-test, $p<0.05$), taking as a limit any value between 40 and 80%: we note that the lack of samples with ice coverage of 40 to 80% does not allow being more specific. Taking different limits within this range leads to variations in the average inventories of less than 5%. For conditions of extensive ice coverage (i.e. >80% in the preceding four weeks) the inventory is 58 ± 20 Bq·m^{-2} (range 32 – 102 Bq·m^{-2}) and in areas with limited ice coverage (i.e. <40%), it is 130 ± 19 Bq·m^{-2} (range 94 – 157 Bq·m^{-2}) (Table 5.3).

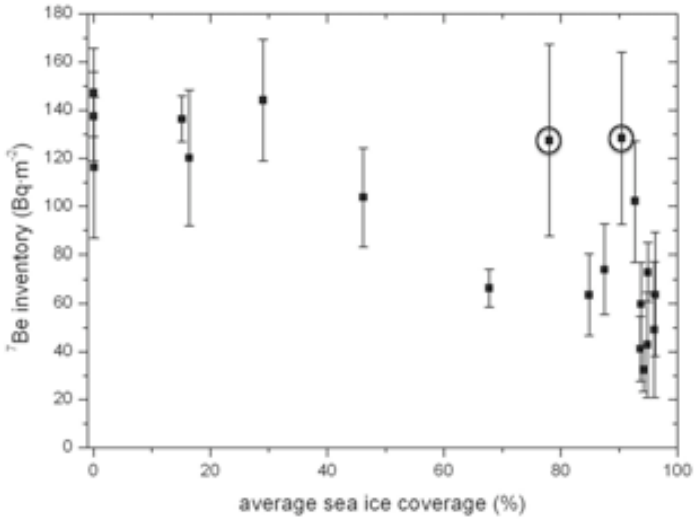

Figure 5.3 ^{7}Be inventory in the mixed layer of the water column as a function of the average of sea ice coverage during the 4 weeks preceding sample collection. Samples with inventories of ^{7}Be below the detection limit are not plotted. The circles indicate samples SWBe-74 and 78.

The ^{7}Be concentration in water beneath ice should reflect input from melting snow and ice (Table 5.4). At the time of sampling, sea-ice temperatures exceeded -5ºC and salinities were <5. Under these conditions, water underneath might receive an extra ^{7}Be supply from ice melt. However the ^{7}Be concentrations measured under the ice are in agreement with values at those locations where sea ice coverage had been >80% during the previous four weeks (1.9 - 5.7 Bq·m^{-3}). As well, no correlation with salinity was observed for the under-ice samples.

5.4.3. Efficiency with which sea ice intercepts the atmospheric flux of ^{7}Be

We can use a mass balance for ^{7}Be to determine the efficiency of interception of the atmospheric ^{7}Be flux by sea ice. Figure 5.4 summarizes the inventories of ^{7}Be in the different reservoirs. For the atmospheric flux of ^{7}Be, we use the integrated value obtained during the cruise from July to October 2007 (1.7 ± 0.2 Bq·m^{-2}·d^{-1}) yielding a steady state inventory of 128 ± 21 Bq·m^{-2}.

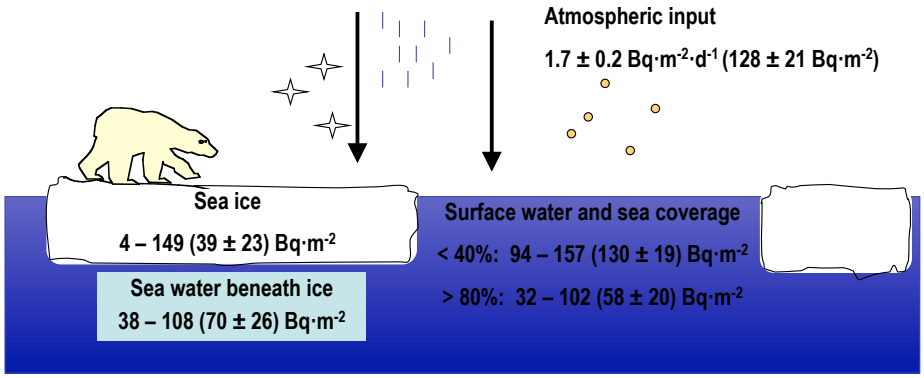

Figure 5.4 Diagram of the ^{7}Be mass balance in the Arctic Ocean, including the atmospheric flux and the ranges and averages (± SD) of the inventories of ^{7}Be for each compartment: sea ice and mixed layers of the water column beneath the ice and ice-free water.

The ^{7}Be inventory in sea ice is estimated as the product of the average concentration of ^{7}Be in sea ice, 112 ± 92 Bq·m^{-3}, and the sea ice thickness over which ^{7}Be is distributed, 0.35 cm. This latter value is assessed from the vertical distribution model of ^{7}Be in sea ice developed by *Eicken et al*. [2002], which takes into account the downward advection of ^{7}Be deposited on the surface, decay and core depth. Accordingly, the estimated inventory of ^{7}Be in sea ice is 39 ± 23 Bq·m^{-2}.

As noted above, the ^{7}Be inventory in the surface water is strongly controlled by sea ice coverage, and two clusters of stations were identified according to the average sea ice coverage during the month prior to sampling: thus the ^{7}Be inventory in surface water is 130 ± 19 Bq·m^{-2} when sea ice coverage is <40%, while under sea ice-covered (>80%) conditions ^{7}Be inventory is 58 ± 20 Bq·m^{-2} while the ^{7}Be inventory beneath sea ice ranges from 38 to 108 (70 ± 26 Bq·m^{-2}).

We note that the ^{7}Be inventory in the water column under conditions of low ice coverage, 130 ± 19 Bq·m^{-2}, is in good agreement with the inventory derived from the atmospheric flux, 128 ± 21 Bq·m^{-2}. Under conditions of greater ice coverage, the ^{7}Be is distributed between the ice and water. Our results show that the sum of the ^{7}Be inventory in these two reservoirs is 97 ± 30 Bq·m^{-2}, with the uncertainty in relatively good agreement with that expected from the atmospheric input. Discrepancies in the balance, especially when considering the ranges of inventories in the ice and water under the ice can be attributed to 1) the way the inventories were calculated (i.e. using an average depth of distribution of ^{7}Be in the ice and the mixed layer thickness in water below the ice) or 2) the possibility of decay of ^{7}Be in water beneath the ice and this somewhat isolated from the atmospheric input. Nevertheless, these inventories provide a means of assessing the efficiency with which sea ice in intercepts the atmospheric flux of ^{7}Be. The inventory in the ice (39 ± 23 Bq·m^{-2}) divided by the atmospheric-derived inventory (or, equivalently, the inventory in surface water when the sea ice coverage is small) (128 ± 21 Bq·m^{-2}) yields a value of 30 ± 18% for studied period. This result suggests that sea ice can accumulates a significant fraction of the total atmospheric deposition of ^{7}Be in the Arctic Ocean. Such inputs to the ice are then subject to transport and ultimate release when melting occurs, largely in the Fram Strait and to a lesser extent in the central Arctic Ocean. In a previous study, *Masqué et al*. [2007] also referred to the role of sea ice intercepting atmospheric fluxes. They showed that the atmospheric fluxes of ^{210}Pb and ^{7}Be to sea ice are effectively imprinted on sea-ice sediments (SIS) through scavenging, and thus the ^{7}Be/^{210}Pb activity ratio in SIS can be used to estimate the transit time of the sea ice, assuming that this ratio is dominated by the supply of both radionuclides to the ice from the atmosphere. Here, we provide for the first time an estimate of the efficiency of the interception of atmospheric fluxes by sea ice, supporting the idea that sea ice is a relevant temporal boundary between the ocean and the atmosphere.

We can use our data to calculate the contribution of sea-ice melting to the ^{7}Be flux in the Fram Strait. The mean annual area of ice fluxing through the Fram Strait has been estimated to be 0.86·10^{6} km^{2}·y^{-1} [*Smedsrud et al*., 2011] and a ^{7}Be inventory of 39 ± 23 Bq·m^{-2} in the sea ice gives a ^{7}Be flux of 34 ± 28 TBq·y^{-1}. Taking an ablation area of ~0.5·10^{6} km^{2} in the Greenland Sea [*Eicken et al*., 2000], the

dissolved ^{7}Be flux to the water column due to sea-ice melting equals 67 ± 55 Bq·m^{-2}·y^{-1}. This value is approximately 50% of the direct ^{7}Be atmospheric flux to the area (113 – 131 Bq·m^{-2}·y^{-1}; *Dibb*, [1990]), suggesting that ice transport and melting can significantly elevate the flux of atmospherically transported chemical species to ice ablation areas.

5.4.4. Load and flux of sediments through the Fram Strait

Sea ice contains ^{7}Be derived from the interception of its atmospheric flux. If particulate matter is present in the ice, atmospherically supplied ^{7}Be can be scavenged onto it via melt-refreeze cycles as the ice moves. Assuming that SIS scavenge all the ^{7}Be supplied to the ice from the atmosphere, a rough estimate of the SIS load in sea ice can be made by dividing the ^{7}Be inventory in sea ice (39 ± 23 Bq·m^{-2}) by the ^{7}Be activity in SIS (range 20 - 7477 and median 138 Bq·kg^{-1}). We use the median ^{7}Be activity in SIS, rather than the mean, because the values are not distributed normally. An upper estimate of the SIS load thus is 284 g·m^{-2} (range 5 – 1960 g·m^{-2}), consistent with previous estimates based on individual measurements in sea ice cores that obtained SIS loads ranging from 8 to 800 g·m^{-2} [e.g. *Barnes et al.*, 1982; *Eicken et al.*, 1997; *Nürnberg et al.*, 1994].

The SIS load estimated from the ^{7}Be data, coupled with the mean annual ice area efflux through the Fram Strait (0.86·10^{6} km^{2}·y^{-1}, *Smedsrud et al.*, 2011), can be used to estimate the sediment flux to the Fram Strait associated with ice melting. In doing so, we acknowledge the uncertainties derived from the large degree of variability of ^{7}Be activities in SIS and its inventories in sea ice, and thus this becomes a rough estimate. The annual export of sediments would be 240 (4.5 - 1700)·10^{6} tons, which is comparable to the range of 7 - 150·10^{6} tons per year reported by *Larssen et al.* [1987] and *Wollenburg* [1993], although *Eicken et al.* [2000] and *Dethleff* [2005] suggested that a more realistic figure would be in the order of 250·10^{6} tons. As a reference, the discharge of sediment load from Arctic rivers is of about 115·10^{6} tons per year [*AMAP*, 1998].

The annual sediment flux from sea ice to the surface waters of the Fram Strait, considering the melting area of 0.5·10^{6} km^{2} in the Greenland Sea, would be of 489 (9-3371) g·m^{-2}·y^{-1}. This flux compares well with sediment fluxes measured using sediments traps deployed in the eastern part of the Fram Strait between 1987 and 1990, which showed fluxes ranging from 122 to 231 g·m^{-2}·y^{-1}, with maximum values of 1300 mg·m^{-2}·d^{-1} [*Hebbeln*, 2000]. *Ramseier et al.* [1999] and *Hebbeln and Wefer* [1991] noted that the variability in sediment flux is directly related to the sea ice distribution, with increases in sedimentation rates being linked to the intensity of the melting of sea ice and release of the sediments. Other measurements using sediment traps across the Fram Strait yielded lower fluxes: *Bauerfeind et al.* [2009] measured fluxes varying from 13 to 32 g·m^{-2}·y^{-1} in the eastern side of Fram Strait (79º02 N, 4º20 E) during the period 2000 - 2005, with a maximum flux about 500 mg·m^{-2}·d^{-1} during May and April. Our results based on ^{7}Be suggest that present-day sedimentation in the Fram Strait can be significantly influenced by sea-ice transport and release of particulate matter originating in the continental shelves.

5.5. Conclusions

This study has shown that sea ice in the Arctic Ocean intercepts and accumulates 30 ± 18% of the atmospheric flux of ^{7}Be for the studied period and that 67 ± 55 Bq·m^{-2} of ^{7}Be would be annually released in the Fram Strait due to ice melting. The transport and release of ^{7}Be in the Fram Strait augments the direct atmospheric deposition there by ~50%, suggesting that sea ice is an important source of ^{7}Be to ablation areas. Our data also provide a first-order assessment of the sediment load in sea ice (284 g·m^{-2}) and sediment flux in the Fram Strait (489 g·m^{-2}·y^{-1}). The results suggest that sea ice is an effective accumulation agent of atmospheric fluxes and can be an important factor in sedimentation rates in ice ablation areas. In the same way that sea ice accumulates and stores ^{7}Be, it can also intercept other atmospherically transported species. Iron is of especial interest in this regard because it is an important micronutrient: similarly, contaminants that bioaccumulate, such as PCBs, can

be atmospherically transported by sea ice. As with ^{7}Be, which is released into surface waters during melting, these other species can also be released and their concentration in surface waters can thus increase over short time periods encompassing ice melt. For Fe and N, at least, such releases can help trigger blooms and modify biogeochemical cycling [*Melnikov*, 1991]. However, changes in the timing over which sea ice melts in ablation areas may produce nutrient releases that are decoupled from biological blooms, and this decoupling may have consequences in the whole Arctic ecosystem.

Chapter 6.

Scavenging from seawater or atmospheric fluxes as mechanisms of radionuclide enrichment in sea-ice sediments

6.1. Introduction

Sea ice contains chemical species both dissolved or associated to sea-ice sediments (SIS). In fact, recent studies have pointed out that sea ice and SIS are enriched respect to surface waters in some chemical species, such as trace metals, nutrients or radionuclides [e.g. *Meese et al.*, 1997; *Measures et al.* 1999*; Grankrog* 2003; *Masqué et al*., 2007*; Tovar-Sanchez et al*., 2010]. These SIS and chemical species transported by sea ice are eventually discharged onto the surface water during sea ice melting, linking the final fate of sea ice to them. Discharge process takes place in relatively short-time scales, releasing a massive particle and chemical species flux onto surface water. The current accelerated shifts that Arctic Ocean is undergoing, in particular changes related to the declining of sea ice extent, later freezing-up, or the alterations in the melting patterns [e.g. *Nghiem et al.*, 2007; Comiso, 2008; *Kwok et al.*, 2009], might entail thoughtful consequences which include the detachment between light and nutrient availability for microorganisms, the increase of toxic chemical species that could inhibit production, the fostering or inhibiting production of minority communities, impact in the biogeochemical cycles in the water column [e.g. *Arrigo et al*., 2008; *Melnikov,* 1991; *Aguilar-Islas et al*., 2008; *Tovar-Sanchez et al*., 2010]. Consequently, improving the knowledge about the mechanisms through which chemical species are enriched in sea ice and SIS is required.

During sea ice formation, only between 15 and 30% of seawater salts remain in sea ice due to segregation process [*Ackley and Weeks*, 1986]. The amount of particle matter that is incorporated varies according to the conditions and location in which sea ice is formed. For instance, the suspension freezing process predominates in the continental shelves (Chapter 2) [e.g. *Kempema et al*., 1989*; Reimnitz et al*., 1992]. During ageing and drifting, sea ice undergoes different physical (atmospheric interception, melting, flushing), chemical (precipitation) and biological (algae bloom) processes that

might contribute to enhance the amount of chemical species, such as trace metals and radionuclides, contained both in sea ice and SIS [*Grankrog*, 2004]. In fact, the interception of atmospheric fluxes has been identified as a relevant source of chemical species to sea ice [*Grankrog,* 2003; *Masqué et al*., 2007; *Tovar-Sanchez et al.,* 2010; *Cámara-Mor et al*, 2011]. For example, *Cámara-Mor et al*. [2011 in Chapter 5] estimated that about 30% of the atmospheric flux of ^{7}Be is intercepted and accumulated into sea ice While the main source of dissolved radionuclide concentrations into sea ice is relatively well known, it is not clear which the main process that explain the radionuclide enrichment in SIS. These mechanisms can be direct uptake in the geographical areas of origin of sea ice, atmospheric deposition onto sea ice or scavenging from dissolved sea ice and/or surface seawater. *Cooper et al*. [1998] and *Cámara-Mor et al*. [2010] stated that bottom sediments from the areas where SIS are entrained in sea ice are the main sources of ^{137}Cs and ^{239,240}Pu activity in SIS; *Masqué et al*. [2007] suggested that scavenging from atmospheric deposition on sea ice could be considered as the most significant source of ^{7}Be and ^{210}Pb in SIS. However, *Baskaran* [2005] stated that surface seawater is likely the major source of ^{210}Pb measured in SIS.

The aim of this chapter is to assess the relative significance of the mechanisms that are potentially responsible for the enrichment of several radionuclides in SIS. These radionuclides are either of natural or artificial origin, and are instrumental as tracers of a variety of processes in the Arctic:

i) ^{7}Be ($T_{½}$= 53 d), a natural radionuclide that is formed in the upper part of the atmosphere. Its presence in the surface of the Earth (continent or ocean) is almost exclusively driven by the atmospheric deposition [*Brown et al*., 1989].
ii) ^{210}Pb ($T_{½}$= 22.3 y), a natural radionuclide that is formed from ^{226}Ra decay. Its presence in the atmosphere is regulated by the ingrowth from ^{222}Rn exhaled from soil and lithogenic dust. Its distribution in the ocean is governed by atmospheric deposition and by in situ ^{226}Ra decay in the water column [e.g. *Broecker et al*., 1967, *Moore et al*., 1974; *Turekian et al*., 1977; *Cochran*, 1992].
iii) ^{234}Th ($T_{½}$=24.1 d), a natural radionuclide that is continuously produced throughout the oceans from the decay of ^{238}U at almost a uniform rate. In general, ^{234}Th is in secular equilibrium with ^{238}U in the water column, excluding sites of high particle flux such as productive surface waters, where a deficit in respect to ^{238}U can exist [*Rutgers van der Loeff and Geibert*, 2008].
iv) Artificial radionuclides, such as ^{137}Cs ($T_{½}$=30.1 y) and Pu isotopes (^{239}Pu, $T_{½}$=24110 y and ^{240}Pu, $T_{½}$= 6560 y). They were introduced in the Earth in the earliest 50s-60s, albeit nowadays their atmospheric deposition is negligible [*UNSCEAR,* 2000*, AMAP,* 1998]. In the Arctic Ocean, other sources have been also significant: the Chernobyl accident had a large impact, particularly of ^{137}Cs; nuclear wastes from reprocessing facilities also contributed to the overall inventories of ^{137}Cs and Pu, including discharges from Sellafield (UK) and, to a lesser extent, from La Hague (France) [*Holm*, 1994; *Aarkrog*, 2003]. Also, the terrestrial run-off from the Ob and Yenisey rivers that has received radionuclides from weapons testing at Semipalatinsk and discharges from nuclear facilities located near or on the rivers (Tomsk-7 and Mayak) [e.g. *JRNEG*, 1994, 1996, *Oughton et al*. 1999; *Smith et al*., 1995].

6.2. Results

The concentrations of ^{7}Be, $^{210}Pb_{xs}$ (^{210}Pbxs = $^{210}Pb_{total}$ – ^{226}Ra), ^{137}Cs and ^{239,240}Pu as well as the ^{240}Pu/^{239}Pu atom ratios in SIS samples collected from the Nansen and Makarov Basins, the central Arctic Basin and the Fram Strait are given in Table 6.1.

SIS samples obtained in 2007 were measured by gamma spectrometry after collection and four years after sampling to determine the excess of ^{234}Th relative to ^{238}U ($^{234}Th_{xs}$ = ^{238}U - ^{234}Th). Concentrations of ^{238}U were also determined by alpha spectrometry in a selection of the samples to confirm the gamma measurements, obtaining a good agreement between the two methods. ^{238}U concentrations ranged from 16 to 69 Bq·kg^{-1}, and $^{234}Th_{xs}$ was not detected in any sample.

Table 6.1 Activities of ^{7}Be, ^{137}Cs, ^{210}Pb, $^{239,240}Pu$ ($Bq \cdot kg^{-1}$) and $^{240}Pu/^{239}Pu$ atom ratios in sea ice sediments collected during several oceanographic expeditions in the Arctic Ocean: ARK XIV/1a (1998), ARK XVII/2 (2001), ARK XVIII/1 (2002), ARK XVIX/4 (2003) and ARK XXII (2007). n.m.: not measured. ^{137}Cs and $^{239,240}Pu$ data published by *Cámara-Mor et al.*, [2010]; ^{7}Be data from ARK XII/2 published by *Cámara-Mor et al.,* [2011]; ^{7}Be, ^{210}Pb, ^{137}Cs and $^{239,240}Pu$ data from cruise XV/3 published by *Masqué et al.,* [2003; 2007]).

Code	Lat.	Long.	Date	^{7}Be ($Bq \cdot kg^{-1}$)	^{137}Cs ($Bq \cdot kg^{-1}$)	$^{210}Pb_{xs}$ ($Bq \cdot kg^{-1}$)	$^{239.240}Pu$ ($Bq \cdot kg^{-1}$)	$^{240}Pu/^{239}Pu$
ARK XIV/1a- 1998 (Central Arctic Ocean)								
5	86.658	7.690	8-Jul	n.m.	13.3±0.7	228±10	0.26±0.02	0.20±0.04
8	88.073	-89.887	10-Jul	n.m.	9.9±0.5	104±8	0.06±0.03	0.19±0.18
11	87.572	-115.094	12-Jul	n.m.	13.2±0.9	144±6	0.14±0.01	0.19±0.02
12	87.578	-116.606	12-Jul	n.m.	15.4±0.9	110±4	0.18±0.01	0.19±0.02
14	87.520	-118.825	12-Jul	n.m.	14.3±0.8	117±5	0.09±0.02	0.19±0.09
15	86.992	-143.379	13-Jul	n.m.	8.3±0.7	229±8	0.10±0.01	0.17±0.04
17	86.457	-147.240	13-Jul	n.m.	8.0±0.9	1202±58	0.30±0.03	0.19±0.04
18	86.373	-148.478	14-Jul	n.m.	n.m.	304±14	0.11±0.01	0.18±0.02
23	85.673	-176.937	18-Jul	n.m	n.m.	315±15	0.03±0.01	0.19±0.13
25	85.653	-177.862	18-Jul	n.m.	n.m.	26±2	0.16±0.05	0.17±0.11
27	83.560	144.983	21-Jul	n.m.	n.m.	180±10	0.08±0.01	0.18±0.06
29	81.473	145.065	23-Jul	n.m.	n.m.	288±19	0.17±0.01	0.17±0.02
ARK XV/3- 1999 (Fram Strait)								
6	79.921	-1.980	18-Sep	131±5	17.8±0.7	394±19	0.844±0.003	0.138±0.002
7	80.015	-1.537	18-Sep	41±3	15.0±0.5	303±13	0.484±0.006	0.185±0.005
8	80.183	-1.022	18-Sep	n.m.	n.m.	134±5	0.580±0.007	0.187±0.005
9	79.038	-5.733	20-Sep	212±6	15.2±0.7	414±25	0.862±0.005	0.189±0.002
10	78.947	-7.458	22-Sep	13±2	10.0±0.5	350±17	0.469±0.008	0.177±0.007
11	79.024	-10.644	23-Sep	15±2	14.2±0.5	86±4	0.140±0.008	0.183±0.025
12	78.995	-11.547	23-Sep	39±4	15.3±0.5	125±8	0.604±0.010	0.189±0.007
13	79.072	-8.969	25-Sep	n.m.	n.m.	248±12	0.487±0.007	0.190±0.006
15	78.922	-4.324	26-Sep	135±5	13.5±0.5	337±18	0.612±0.004	0.183±0.003
16	78.915	-4.346	26-Sep	20±6	2.2±0.3	62±3	0.472±0.032	0.190±0.031
20	77.462	-7.151	4-Oct	92±3	16.0±0.7	44±6	0.114±0.005	0.183±0.018
21	77.460	-6.984	4-Oct	49±5	15.2±0.5	144±5	0.543±0.009	0.185±0.007
22	75.643	-10.576	5-Oct	33±4	13.5±0.7	131±5	0.487±0.007	0.171±0.006
23	75.443	-11.392	5-Oct	n.m.	12.5±0.5	83±6	0.318±0.007	0.176±0.009
24	75.336	-11.511	5-Oct	n.m.	n.m.	47±6	0.315±0.007	0.190±0.009
26	74.759	-13.676	7-Oct	44±4	17.3±0.7	116±8	0.617±0.032	0.180±0.023
27	74.720	-13.667	7-Oct	n.m.	n.m.	118±5	0.521±0.006	0.178±0.005
28	74.675	-13.878	7-Oct	n.m.	n.m.	307±12	0.469±0.033	0.180±0.031
ARK XVII/2- 2001 (Nansen Basin)								
217	83.950	24.250	5-Aug	278±15	3.7±0.3	669±32	0.136±0.007	0.18±0.02
218	85.633	17.313	6-Aug	469±27	4.1±0.4	783±35	0.083±0.010	0.19±0.05
220	84.667	5.100	8-Aug	1807±84	14.4±1.0	6258±255	0.97±0.04	0.184±0.016
222	84.133	0.017	10-Aug	1230±67	25.2±1.6	4571±184	1.22±0.02	0.186±0.008
223?	83.636	-2.975	11-Aug	n.m.	11.9±0.7	161±9	0.474±0.011	0.189±0.009
228	83.791	-2.199	16-Aug	709±36	4.2±0.4	359±17	0.21±0.01	0.118±0.019
270-2	84.289	28.258	27-Sep	110±9	14.2±0.8	337±17	0.54±0.08	0.17±0.05
270-3	83.873	28.258	27-Sep	20±3	4.3±0.3	56±4	0.246±0.005	0.179±0.008
270-4	83.853	27.855	27-Sep	1924±97	13.8±1.4	2853±104	0.94±0.05	0.20±0.02
Iceberg1	85.050	11.040	21-Aug	n.m.	n.m.	190±9	0.67±0.03	0.18±0.02
Iceberg2	86.333	37.767	29-Aug	bdl	1.8±0.2	47±3	0.021±0.002	0.18±0.04
Iceberg5	86.720	46.653	17-Sep	641±28	4001±78	7126±284	31.9±0.8	0.165±0.009
Iceberg6	85.800	21.390	23-Sep	104±7	4.2±0.3	98±7	0.205±0.008	0.25±0.02
ARK XVIII/1-2002 (Fram Strait)								
01-1	75.123	-16.528	30-Jul	n.m.	n.m	37±2	0.044±0.004	n.m
02-1	75.009	-13.641	30-Jul	n.m.	10.1±0.4	103±6	0.24±0.009	0.189±0.017
03-1	79.200	2.672	8-Aug	n.m.	6.0±0.7	n.m.	0.223±0.017	0.19±0.03
05-2	78.967	0.655	12-Aug	n.m.	6.4±0.5	148±7	0.71±0.05	0.210±0.024

Table 6.1 (cont.)

Code	Lat.	Long.	Date	^{7}Be (Bq·kg^{-1})	^{137}Cs (Bq·kg^{-1})	^{210}Pb$_{xs}$ (Bq·kg^{-1})	$^{239.240}$Pu (Bq·kg^{-1})	^{240}Pu/^{239}Pu
06-2	78.782	-2.002	13-Aug	n.m.	3.5±0.2	474±19	0.70±0.03	0.217±0.010
07-1	78.943	-4.600	14-Aug	n.m.	7.7±0.3	161±8	0.086±0.005	n.m
08-1	78.756	-7.113	14-Aug	n.m.	480.6±2.3	705±23	7.69±0.3	0.166±0.007
08-3	78.756	-7.113	14-Aug	n.m.	651.7±3.3	751±28	9.5±0.4	0.187±0.007
10-1	78.844	-17.657	15-Aug	n.m.	136.3±0.5	510±18	2.52±0.10	0.155±0.009
ARK XIX/4-2003 (Fram Strait)								
01-1B	76.127	-18.602	13-Aug	n.m.	n.m.	28 ± 2	n.m.	n.m.
01-2A	76.114	-18.509	13-Aug	n.m.	n.m	106 ± 8	n.m	n.m
02-2	76.380	-4.654	15-Aug	n.m.	3.9±0.7	326 ± 19	0.144±0.008	0.187±0.017
03-1	76.918	-6.529	16-Aug	n.m.	n.m.	1295 ± 40	n.m.	n.m.
04-1	76.750	-5.480	16-Aug	n.m.	5.4±0.8	358 ± 14	0.262±0.017	0.19±0.02
04-2	76.747	-5.459	16-Aug	n.m.	4.2±0.4	153 ± 7	0.254±0.012	0.193±0.013
05-1	77.150	-1.172	20-Aug	n.m.	5.6±0.3	133 ± 7	0.144±0.011	0.17±0.02
06-1	77.150	-1.201	20-Aug	n.m.	5.6±0.3	173 ± 8	0.186±0.015	n.m
07-1	75.586	-8.048	25-Aug	n.m.	4.5±0.6	89 ± 4	0.124±0.010	0.16±0.03
08-1	75.058	-18.764	26-Aug	n.m.	n.m.	11 ± 6	n.m.	n.m.
08-2	75.100	-17.864	26-Aug	n.m.	n.m.	24 ± 2	n.m.	n.m.
09-1	74.976	-19.979	29-Aug	n.m.	n.m.	65 ± 7	n.m.	n.m.
09-2A	75.013	-20.101	29-Aug	n.m.	22.4±0.2	141 ± 6	0.141±0.012	n.m
11-3	76.216	-8.999	5-Sep	n.m.	126.2±8.	491 ± 17	2.92±0.13	0.143±0.009

Table 6.1 (cont.)

Code	Lat.	Long.	Date	^{7}Be (Bq·kg^{-1})	^{137}Cs (Bq·kg^{-1})	^{210}Pb$_{xs}$ (Bq·kg^{-1})	$^{239.240}$Pu (Bq·kg^{-1})	^{240}Pu/^{239}Pu
12-1	75.704	-19.602	6-Sep	n.m.	23.1±0.2	31 ± 6	n.m	n.m
12-2	75.622	-19.735	6-Sep	n.m	8.7±1.5	49 ± 3	n.m	n.m
12-3	75.261	-20.905	6-Sep	n.m.	n.m.	49 ± 7	n.m.	n.m.
13-1	74.138	-21.430	8-Sep	n.m.	n.m.	75 ± 7	n.m.	n.m.
13-2	74.170	-22.326	8-Sep	n.m.	n.m.	12 ± 6	n.m.	n.m.
14-1	73.400	-24.257	14-Sep	n.m.	n.m.	17 ± 6	n.m.	n.m.
14-2A	73.357	-23.818	14-Sep	n.m.	n.m.	20 ± 6	n.m.	n.m.
ARK XXII/2- 2007 (Along Tanspolar Drift)								
1.1	83.994	34.026	6-Aug	755 ± 33	31.8±1.3	4637 ± 140	n.m	n.m
1.3	83.994	34.026	6-Aug	524 ± 27	29.9±2.8	1747 ± 110	0.78±0.03	0.157±0.006
2.C.2	83.993	34.385	6-Aug	71 ± 14	29.6±0.9	269 ± 9	0.68±0.02	0.177±0.007
2.D.2	83.993	34.385	6-Aug	92 ± 14	19.2±0.5	243 ± 9	0.66±0.02	n.m.
4.1	83.604	60.399	12-Aug	1174 ± 94	4.8±1.0	2366 ± 95	0.210±0.018	0.21±0.03
4.2	83.604	60.399	12-Aug	1263 ± 101	9.7±1.4	6590 ± 243	0.210±0.011	0.188±0.014
5	83.425	61.986	14-Aug	2441 ± 97	4.5±1.0	274 ± 26	n.m	0.180±0.018
3	85.145	60.815	11-Aug	444 ± 28	11.2±1.9	428 ± 17	n.m	n.m
6	84.499	-138.389	7-Sep	7477 ± 265	15.1±6.0	548 ± 29	n.m	n.m
7.1.2	84.450	-147.572	8-Sep	72 ± 5	2.5±0.3	144 ± 7	0.229±0.014	0.22±0.02
7.2.2	84.450	-147.572	8-Sep	135 ± 12	5.2±0.7	219 ± 9	0.246±0.017	n.m
7.3.2	84.450	-147.572	8-Sep	140 ± 20	2.7±0.9	227 ± 14	0.226±0.018	0.20±0.03
8.1	84.261	108.746	17-Sep	972 ± 54	16.6±3.8	203 ± 9	n.m	n.m
9.1.2	84.215	108.916	17-Sep	92 ± 9	8.1±0.9	153 ± 7	n.m	n.m

Results in SIS samples showed a large variability of concentrations for all radionuclides except for ^{234}Th$_{xs}$. Since concentrations do not follow normal distributions, we calculated the median concentration for all radionuclides.

Measured ^{7}Be activities in SIS varied from 20 to 7477 Bq·kg^{-1} (n=25), albeit only 20% of the samples presented activities higher than 1230 Bq·kg^{-1}. The median concentration of ^{7}Be was137 Bq·kg^{-1} (Figure 6.1a).

The $^{210}Pb_{xs}$ activities ranged from 20 to 7125 Bq·kg^{-1} (n=69). The median ^{210}Pb concentration in SIS was180 Bq·kg^{-1} (Figure 6.1b). The highest concentrations were of the same order of magnitude than those measured in the Arctic Ocean by *Baskaran* [2005], who reported ^{210}Pb activities ranging from 123 to 2916 Bq·kg^{-1} (n=10).

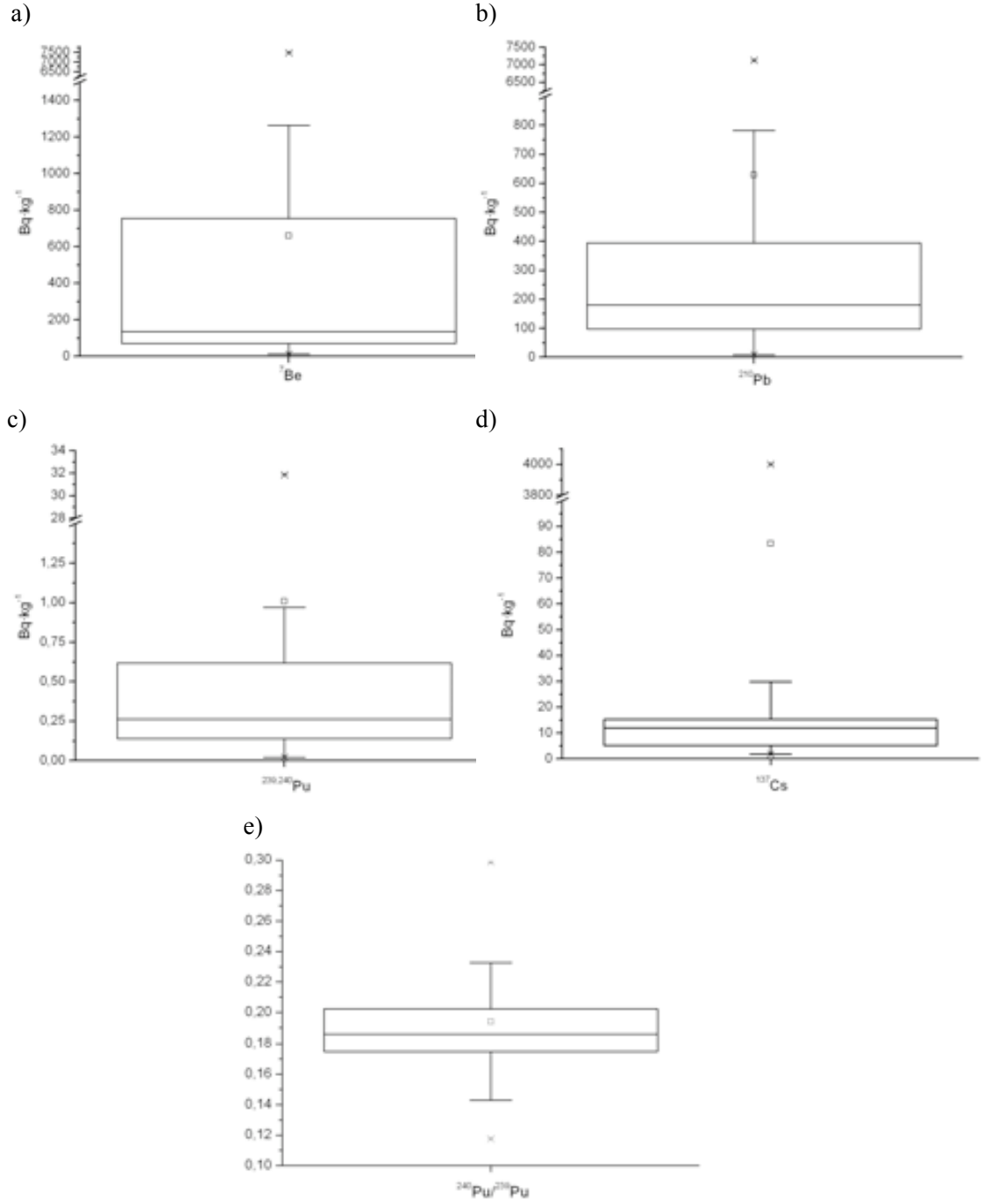

Figure 6.1 Box chart of concentrations of ^{7}Be (a), ^{210}Pb (b), ^{239,240}Pu (c), ^{137}Cs (d) and the ^{240}Pu/^{239}Pu atom ratio (e) in SIS in the Arctic Ocean.

The ^{239,240}Pu activities varied from 0.018 to 31.8 Bq·kg^{-1}, with a median value of 0.29 Bq·kg^{-1}. Most of the samples (88%) had ^{240,239}Pu activities <1 Bq·kg^{-1} (Figure 6.1c). Previous studies [*Landa et al*., 1998; *Cooper et al*., 1998; *Masqué et al*., 2007] obtained similar results, ranging from 0.09 to 1.84 Bq·kg^{-1}. The ^{240}Pu/^{239}Pu atom ratios ranged from 0.112 to 0.224 (Figure 6.1d). Although most of the published ^{240}Pu/^{239}Pu atom ratios are comparable to the global fallout value of 0.183 ± 0.009 [*Krey et*

al., 1976], other studies [e.g. *Landa et al*. 1998, *Cooper et al.,* 1998] also measured lower $^{240}Pu/^{239}Pu$ atom ratios in some samples. The median of the $^{240}Pu/^{239}Pu$ atom ratios was 0.183. This value is consistent with the global fallout value, reflecting that 46% of all analysed samples contain Pu exclusively derived from global fallout.

The ^{137}Cs activities also presented a large variability, ranging from <3.5 to $4 \cdot 10^3$ Bq·kg^{-1}, with a median of 12.2 Bq·kg^{-1} (Figure 6.1e). Most ^{137}Cs activities are comparable to previous published data in SIS from the Arctic [*Landa et al*., 1998; *Cooper et al*., 1998; *Baskaran,* 2005; *Masqué et al*., 2007], and the highest ^{137}Cs activity is of the same order of magnitude than the greatest activity reported by *Cota et al.* [2008] (2528 Bq·kg^{-1}).

6.3. Discussion

Radionuclides can be present in sea ice via incorporation during ice formation or from atmospheric deposition. Sea ice excludes salts together with other impurities during its formation and growth due to segregation process [*Weeks and Ackley*, 1986]. For that reason, sea ice is less salty than seawater. Indeed, salinity values measured in full sea ice cores collected during the expedition ARK XXII/2 in 2007 were one order the magnitude lower than surface seawater, ranging from 0 to 4.4. Assuming that radionuclides have the same geochemical behavior as salts (REF), only 15 - 30% of the total amount of radionuclides in sea water would be retained in newly grown sea ice on account of solute segregation: the ice crystal lattice restricts the accommodation of sea ice ions or ions molecules in the voids or the structure itself due to the constraints in size and electric charge imposed on these ions. The major ions present in seawater, such as Na^+, K^+, Ca^{2+}, Mg^{2+}, Cl^-, SO_4^{2-}, CO_3^{2-}, are not incorporated into the ice crystal lattice and therefore, are rejected [*Eicken*, 2003]. For ^{137}Cs, that does not have an atmospheric component, we were not able to determine the concentrations but only maximum detectable activities, which ranged from 0.37 to 0.98, with an median of 0.57 Bq·m^{-3} (MDA) (Table 6.2). These concentrations would correspond to, at most, 30% of the average concentration of ^{137}Cs in seawater (2.0 ± 0.3 Bq·m^{-3}, Table 6.3). This is in agreement with the assumption stated above about incorporation of radionuclides in sea ice from seawater during formation.

Table 6.2 Minimum detectable activities (MDA) of ^{137}Cs (Bq·m^{-3}) and concentration of ^{210}Pb (Bq·m^{-3}) in the upper 10 cm of sea ice samples collected along the Transpolar Drift (ARK XXII/2, 2007). n.m.: not measured.

Sample code	Lat.	Long.	Date	^{137}Cs	^{210}Pb
SI_1	81.952	34.076	02-Aug	< 0.60	87 ± 5
SI-2	82.792	33.750	04-Aug	< 0.58	n.m.
SI _3	83.505	33.973	05-Aug	< 0.98	n.m.
SI _4	84.505	36.085	06-Aug	< 0.56	n.m.
SI _5	83.608	60.395	12-Aug	< 0.71	37 ± 2
SI _6	82.502	60.791	15-Aug	< 0.63	31 ± 1
SI _7	82.502	65.756	18-Aug	< 0.53	n.m.
SI _8	82.143	86.320	20-Aug	< 0.57	42 ± 3
SI _9	83.296	86.189	22-Aug	< 0.52	n.m.
SI-10	84.563	89.764	24-Aug	n.m.	75 ± 3
SI _11	85.565	90.439	25-Aug	< 0.76	n.m.
SI _12	87.034	104.972	27-Aug	< 0.57	75 ± 3
SI _13	87.498	109.556	28-Aug	< 0.59	62 ± 3
SI _14	88.254	150.134	31-Aug	< 0.52	54 ± 3
SI _15	87.827	170.321	02-Sep	< 0.40	n.m.
SI _16	84.694	-145.429	05-Sep	< 0.59	n.m.
SI _17	88.499	-137.611	07-Sep	< 0.57	n.m.
SI _18	86.642	-177.545	10-Sep	< 0.37	67 ± 4
SI _19	86.393	135.817	13-Sep	< 0.38	71 ± 3
SI _20	84.667	102.779	16-Sep	< 0.40	83 ± 4

Table 6.3 Concentrations of ^{137}Cs and ^{239,240}Pu and ^{240}Pu/^{239}Pu atom ratios in surface seawater (upper 7 m) collected along the Transpolar Drift (ARK XXII/2, 2007). n.m.: not measured.

Sample Code	Lat	Long	Date	^{137}Cs (Bq·m^{-3})	^{239,240}Pu (mBq·m^{-3})	^{240}Pu/^{239}Pu
SW236	77.504	33.975	31-Jul	2.03 ± 0.16	4.39 ± 0.13	0.185 ± 0.005
SW260	84.493	36.089	09-Aug	2.02 ± 0.16	5.38 ± 0.13	0.191 ± 0.003
SW271	82.502	60.791	15-Aug	1.76 ± 0.08	n.m.	n.m.
SW273	82.086	68.950	16-Aug	1.60 ± 0.13	5.82 ± 0.13	0.189 ± 0.003
SW276	82.085	68.952	17-Aug	1.83 ± 0.14	5.11 ± 0.13	0.183 ± 0.004
SW279	81.236	86.288	19-Aug	2.13 ± 0.16	3.33 ± 0.13	0.186 ± 0.006
SW310	87.671	111.693	29-Aug	2.42 ± 0.15	2.75 ± 0.11	0.174 ± 0.006
SW328	87.827	170.321	02-Sep	2.40 ± 0.15	2.15 ± 0.11	0.188 ± 0.006
SW342	84.499	-138.389	07-Sep	1.42 ± 0.11	1.20 ± 0.07	0.199 ± 0.009
SW400	77.365	123.423	22-Sep	1.90 ± 0.13	3.12 ± 0.11	0.191 ± 0.006
SW411	75.201	121.363	22-Sep	2.40 ± 0.15	1.99 ± 0.07	0.186 ± 0.005

For radionuclides with an atmospheric input to the sea surface (or sea ice), it would be expected to observe greater activities in sea ice than those predicted from incorporation during sea ice formation. For ^{210}Pb, the average concentration in surface seawater during the expedition ARK XXII/2 in 2007 was 0.81 ± 0.22 Bq·m^{-3} [*Roca et al*., 2012]. Even through a 100% incorporation of ^{210}Pb from surface seawater took place, this source would represent a small fraction of the ^{210}Pb activities measured in full sea ice cores: 1.02 to 12.6 Bq·m^{-3} (average: 5.1 ± 3.4 Bq·m^{-3}, Table 6.4), and even higher lower proportion compared with the ^{210}Pb concentration in the upper 10 cm of sea ice (31 - 87 Bq·m^{-3}, Table 6.2). Furthermore, ^{210}Pb sea ice profiles presented larger concentrations in the upper cm corresponding with low salinity values and d^{18}O too. These ^{210}Pb concentrations in the upper cm and concentration profiles in full sea ice core are of the same order as those reported by *Masqué et al*. (2007). Concentrations of ^{210}Pb in melt-ponds were comparable to those the upper 10 cm of sea ice (Table 6.2), besides salinity values were also lower than surface seawater, ranging from 4 to 6. These results confirm that atmospheric deposition is the most likely source of the major fraction of ^{210}Pb to sea ice.

Table 6.4 Concentrations of ^{210}Pb in sea ice cores collected along the Transpolar Drift (ARK XXII/2, 2007).

Code	Lat	Long	Date	^{210}Pb (Bq·m^{-3})
Core_1	81,952	34,076	03-Aug	1.2 ± 0.1
Core_2	83,505	33,973	06-Aug	1.3 ± 0.1
Core_3	84,505	36,085	07-Aug	1.0 ± 0.1
Core_5	82,502	60,791	16-Aug	3.5 ±0.3
Core_6	82,143	86,320	21-Aug	2.9 ± 0.2
Core_7	84,563	89,764	25-Aug	4.8 ±0.2
Core_8	87,034	104,972	29-Aug	6.5 ± 0.2
Core_9	88,254	150,134	01-Sep	8.0 ± 0.2
Core_11	84,694	-145,429	06-Sep	6.9 ± 0.6
Core_12	86,642	-177,545	11-Sep	7.1 ± 0.4
Core_13	86,393	135,817	14-Sep	12.6 ± 0.6
Core_14	84,667	102,779	17-Sep	4.8 ± 0.2

Regarding ^{7}Be and ^{234}Th$_{xs}$, and due to their short half-lives, any activity of both isotopes incorporated during sea ice formation in the continental shelves would have decayed completely at the time of sampling in the central Arctic Ocean or in the Fram Strait. Even though bottom layers of sea ice (lamellae structure interface see chapter 1.2.1) could contain both radionuclides, ^{7}Be and ^{234}Th, due to newly sea ice grows from bottom freezing of sea water. It is noteworthy that in the case of ^{7}Be with an atmospheric input surface sea ice exhibits relatively large ^{7}Be activities (10 - 427 Bq·m^{-3}) in comparison with surface seawater (1.5 - 9.1 Bq·m^{-3}) (Chapter 5). Indeed, *Eicken et al.* [2002] argued that ^{7}Be in sea ice is derived from direct atmospheric deposition onto the sea ice, showing that the concentrations decrease exponentially with depth, the penetration depth depending on flushing/freezing period. This conclusion is reinforced by the correlation between ^{7}Be concentrations and d^{18}O (R^2 = 0.62), as a signal of direct deposition of precipitation onto sea ice (Chapter 5). Furthermore, ^{7}Be concentration in sea ice

implies that sea ice acts a barrier between atmosphere and ocean, accumulating chemical atmospheric fluxes. This is corroborated with the fact that ^{7}Be inventory in the water column is regulated by ice coverage (Figure 5.2a, Chapter 5).

Table 6.5 Concentrations of ^{210}Pb in melt ponds sampled along the Transpolar Drift (ARK XXII/2, 2007).

Code	Lat	Long	Date	^{210}Pb (Bq·m^{-3})
melting_1	81,952	34,076	03-Aug	15.8 ± 0.7
melting_2	83,505	33,973	08-Aug	37.6 ± 1.5
melting_3	84,505	36,085	13-Aug	23.5 ± 1.1
melting_4	83,608	60,395	16-Aug	11.8 ± 0.6
melting_5	82,502	60,791	25-Aug	37.1 ± 0.9
melting_6	82,143	86,320	28-Aug	12.5 ± 0.3
melting_7	84,563	89,764	01-Sept	23.1 ± 0.6
melting_8	87,034	104,972	03-Sept	63.7 ± 1.3
melting_9	88,254	150,134	06-Sept	86.6 ± 2.2
melting_10	88,499	-137,611	08-Sept	72.1 ± 1.8

Radionuclide concentration in SIS can be accounted partially by the geographical origin of the SIS (e.g. artificial radionuclides) [*Cooper et al*., 1998; *Landa et al.,* 1998; *Cámara-Mor et al*., 2010]. Several processes and mechanisms could modify this initial concentration of radionuclides in SIS during sea ice formation and sea ice drifting [e.g. *Pfirman et al.*, 1995; *Cooper et al*., 1998; Masqué et al., 2003, 2007; Baskaran, 2005]. The potential sources of radionuclides are the entrained concentration in sea ice during its formation, surface seawater and atmospheric deposition.

Baskaran [2005] suggested that the enrichment of radionuclides in SIS is largely driven by direct scavenging from surface seawater, on the basis of high activities of ^{210}Pb in 10 SIS samples (up to ~2900 Bq·kg^{-1}). This mechanism implies that each gram of SIS has to scavenge ^{210}Pb from a determined amount of seawater, which contains dissolved ^{210}Pb, for a prolonged period of time to allow the equilibrium between dissolved ^{210}Pb and the fraction attached to SIS. This scavenging was suggested to occur while SIS are at the ice/water interface, or as a consequence of movement of SIS caused by collisions or melting or even as a result of submerging of SIS within sea ice due to solar melting that place them where seawater may pass through. *Masqué et al.* [2007] argued that atmospheric deposition in sea ice is the main source of ^{210}Pb measured in sea ice, being several orders of magnitude higher than surrounding surface seawater. Therefore, scavenging of ^{210}Pb deposited onto sea ice by SIS can explain the activities in SIS.

If this mechanism was predominant for the enrichment of $^{210}Pb_{xs}$ in SIS, the $^{210}Pb_{xs}$ in SIS would be generated by the scavenging a certain amount of surface seawater in contact with SIS. Equally, SIS could also scavenge other radionuclides present in surface seawater such as ^{7}Be, ^{234}Th, ^{137}Cs and ^{239,240}Pu. Taking ^{210}Pb as a reference, a correspondence between the concentrations of the different radionuclides in SIS and the volume of seawater needed to explain ^{210}Pb concentration in SIS should exist. This relationship should be present despite of differences in the affinity of each of the elements for particles (expressed using the distribution coefficient, K_d), hence we can use the ratio between respective K_ds (Table 6.6). In order to confirm the relative importance of scavenging from seawater as a source of enrichment of each radionuclide in SIS, we applied the same reasoning as *Baskaran* [2005]: we estimated the volume of seawater per gram of SIS needed to explain all our measured $^{210}Pb_{xs}$ activities in SIS. The amount of seawater scavenged by each gram of SIS is calculated dividing the concentrations of ^{210}Pb in each sample of SIS (Bq·kg^{-1}) by the average concentration of ^{210}Pb in surface seawater along the Transpolar Drift (0.81 ± 0.22 Bq·m^{-3} [*Roca et al*., 2012] (Figure 6.2). In most of the cases (88%), the estimated k_d is lower than the value reported by *IAEA* [1985]. It is noteworthy to mention that this mechanism [*Baskaran*, 2005] is based on i) the volume required to explain the concentration in SIS is constantly in contact with SIS during all sea ice lifespan and ii) the activity of the radionuclide in surface waters does not vary as a function of the sea ice extent, despite of the fact that sea ice modifies atmosphere-ocean interaction [*Cámara-Mor et al.*, 2011]. Therefore, based on these assumptions these seawater volumes estimated to explain ^{210}Pb in SIS per gram would correspond

to the minimum amount of water needed.

The expected activities in SIS for the rest of radionuclides studied here (^{7}Be, $^{234}Th_{xs}$, ^{137}Cs and ^{239,240}Pu) (Table 6.6) were determined applying the equation 6.1, where $A_{r\text{-}sis}$ is the expected radionuclide activity in SIS; V_{sw} corresponds to the required seawater volume per kg to explain $^{210}Pb_{xs}$ activity in SIS, $A_{r\text{-}sw}$ is the average activity of the radionuclide in surface seawater and k_d is the coefficient distribution value of the radionuclide, R, and ^{210}Pb. In the case of ^{7}Be and $^{234}Th_{ex}$, decay corrections have to be considered. The correction implies that scavenging by SIS is constant through the considered period of time, that we take as 1 year for samples collected during ARK XXII/2, and as 3 years for samples collected during ARK XV/3 and ARK XVII/2).

$$A_{r-SIS}\ [Bq \cdot kg^{-1}] = V_{sw}{}^{210}Pb\ [m^{-3}] \cdot \frac{kd\ R}{kd\ {}^{210}Pb} A_{r-sw}[Bq \cdot m^{-3}] \qquad Eq.\ 6.1$$

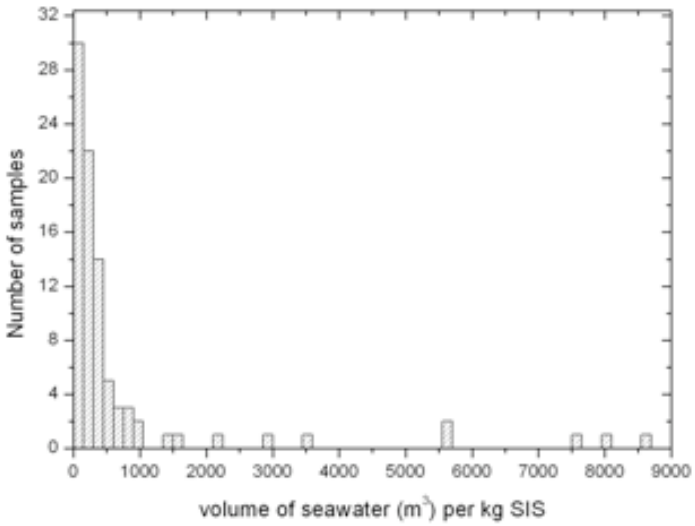

Figure 6.2 Histogram of the needed volume of seawater (m^3) per kg de SIS in order to explain the $^{210}Pb_{xs}$ activity in SIS. The vertical axis represents the percentage of the total samples explained by the corresponding range of volume.

Table 6.6 Distribution coefficients (recommended and range) and average concentration in surface seawater for each radionuclide. Values used to estimate the volume of seawater needed to explain the ^{210}Pb concentration in SIS if scavenging from seawater was the main mechanism of enrichment, and the expected activities in SIS for the rest of radionuclides corresponding to this seawater volume.

Radionuclide	**K_d ($m^3 \cdot kg^{-1}$)**	**Average activity in surface seawater ($Bq \cdot m^{-3}$)**
^{7}Be	100 (37 - 810)[1]	7.9 ± 1.3 [*Cámara-Mor et al.,* 2011; Chapter 5]
^{137}Cs	2 (0.03 - 3)[2]	2.0 ± 0.3
^{210}Pb	10000 (100 - 50000)[3]	0.81 ± 0.22 [*Roca et al.,* 2012]
^{234}Th	5000 (500 - 7900)[3]	32 ± 4 [*Cai et al.,* 2010]
^{239,240}Pu	100 (60 - 100)[4]	$(3.9 \pm 1.4) \cdot 10^{-3}$

[1] *You et al.* [1989], *Olsen et al.* [1986] and *Ciffrog et al.* [2003]
[2] *IAEA 422* [1985] and *Layton et al.* [1997]
[3] *IEAE 422* [1985] and *Wei and Hung* [1998]
[4] *IEAE 422* [1985] and *Layton et al.* [1997]

Concerning artificial radionuclides, ^{239,240}Pu and ^{137}Cs in SIS can only be incorporated in sea ice in formation areas or from scavenging from surface waters, since atmospheric flux is considered negligible nowadays [e.g. *UNSCEAR*, 2000; *Masqué et al.*, 2003]. The fraction of Pu and ^{137}Cs in SIS explained by seawater scavenging using the recommended values of K_d present a relatively large variability, even through for most the samples (90%), less than 20% and 7% of the Pu and ^{137}Cs

activities in SIS are explained, respectively (Figure 6.3 a and b, respectively). However, on median only 4% and 2% for Pu and ^{137}Cs activities in SIS are explained, respectively (Table 6.7). Whereas if the the lowest K_d values are considered, the median percentage explained by scavenging increases up to 2% for ^{137}Cs and could be as high as 238% for ^{239,240}Pu. This last plutonium result points out that the measured concentrations of ^{239,240}Pu in SIS would be much lower than the expected ones. Nevertheless, the medians of the explained percentages are 0.3% and 0.8% for ^{137}Cs and ^{239,240}Pu, respectively, when the highest values of K_d were used. Overall, the results imply that a small percentage of the activities of Pu and ^{137}Cs in SIS are derived from scavenging from seawater (Table 6.7).

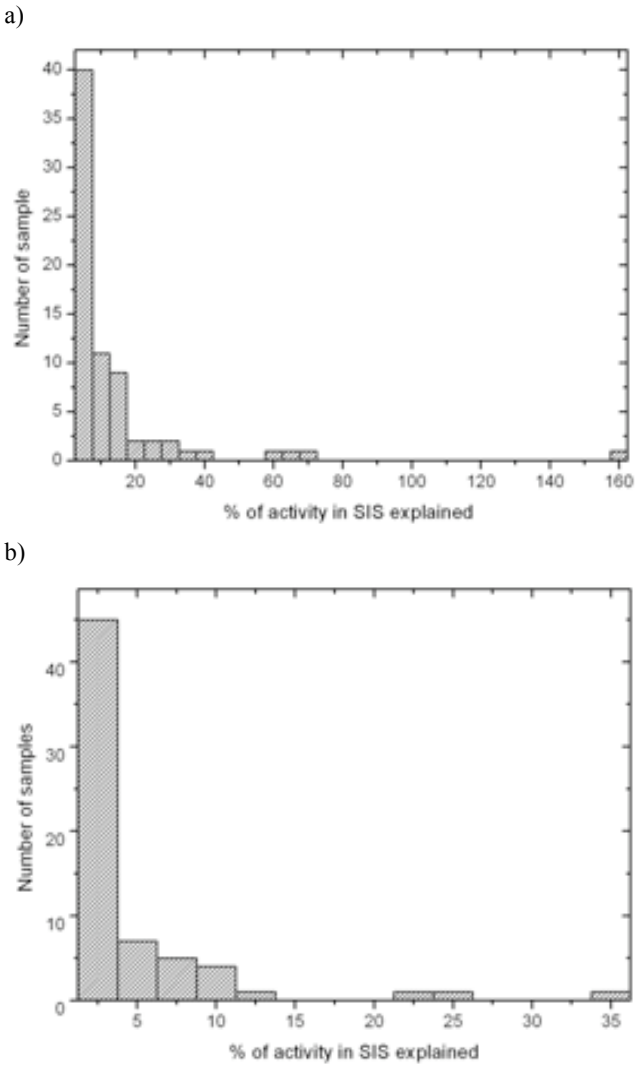

Figure 6.3 Histogram of the percentage of measured radionuclide activity in SIS (Bq·kg^{-1}) a) ^{239,240}Pu and b) ^{137}Cs explained from the corresponding seawater volume needed to explain the measured ^{210}Pb in SIS according to recommended k_ds values. Values greater than 100% indicate that the measured activities in SIS are lower than the expected.

Table 6.7 Percentage of measured radionuclide activity in SIS (median and range) explained by the scavenging from corresponding seawater volume needed to explain the measured ^{210}Pb concentration in SIS, according to different K_d values: low, recommended and high. For the ^{234}Th, the absence of $^{234}Th_{xs}$ in analysed SIS samples implies that the scavenging from seawater is negligible.

Radionuclide	Low K_d values	Recommended K_d values	High K_d values
^{7}Be	68 (5 – 454)%	2 (0.2 – 12)%	3 (0.08 – 19)%
^{137}Cs	2 (0.08 – 50)%	2 (0.06 – 33)%	0.3 (0.02 – 10)%
^{239,240}Pu	238 (4 – 11499)%	4 (0.5 – 191)%	0.8 (0.10 – 38)%

a)

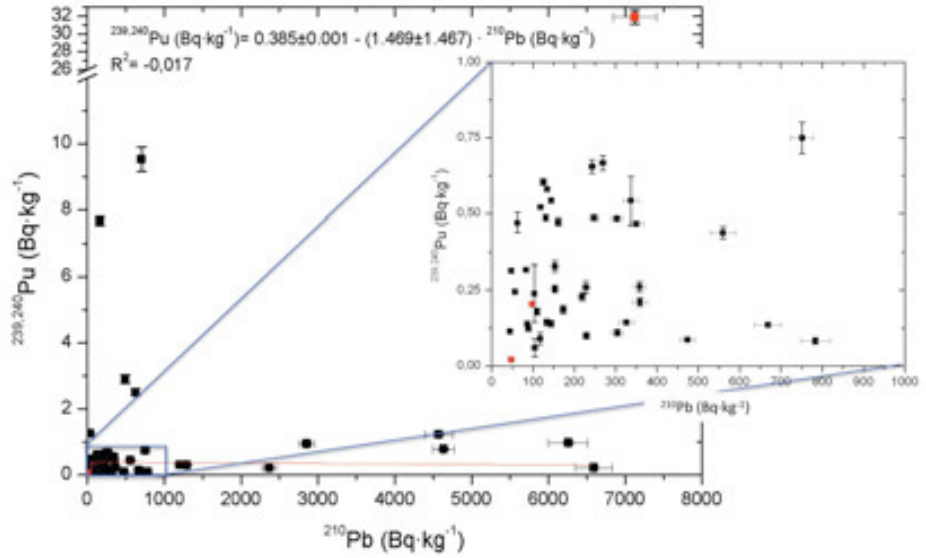

b)

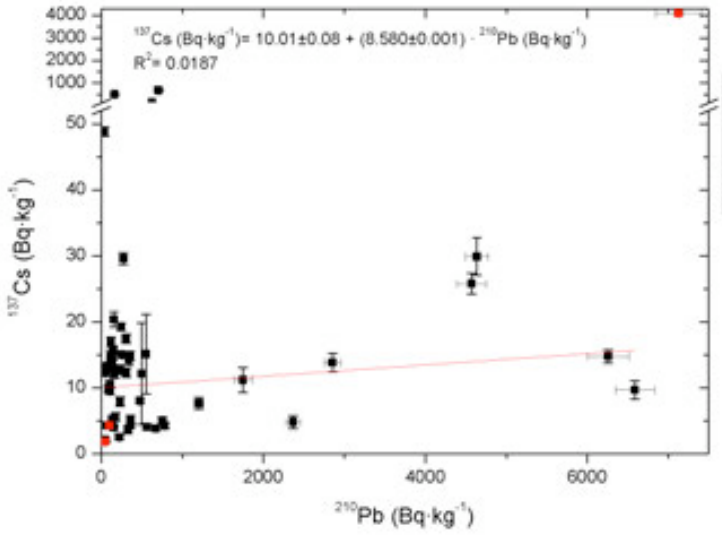

Figure 6.4 a) Excess $^{210}Pb_{xs}$ versus $^{239,240}Pu$ and b) Excess ^{210}Pb versus ^{137}Cs. Red dots correspond to iceberg samples and were not included into the regression

If scavenging from seawater was the dominant mechanism of enrichment of radionuclides in SIS, certain relationship between the concentrations of $^{210}Pb_{xs}$ and the other radionuclides could be expected. However, no correlation is found between the concentrations of $^{210}Pb_{xs}$ and $^{239,240}Pu$ (Figure 6.4 a) or $^{210}Pb_{xs}$ and ^{137}Cs (Figure 6.4b). Indeed, *Cooper et al.* [1998], *Masque et al*., [2003] concluded that $^{239,240}Pu$ and ^{137}Cs in SIS derived from continental shelves since were comparable to those in bottom sediments of the continental shelves and together with the $^{240}Pu/^{239}Pu$ atom ratios allowed constraining the geographical source area in which the sediments were incorporated into the sea ice *Cámara-Mor et al.* [2010, in Chapter 4]. This conclusion also reinforced by the following arguments:

i) The geographical distributions of $^{239,240}Pu$ and ^{137}Cs activity in SIS mirror the main patterns of sea ice motion: the TPD and the Beaufort Gyre (Chapter 4). If scavenging from surface water was a significant mechanism, it would homogenise the signal from the continental shelves.
ii) The correlation between $^{239,240}Pu$ and ^{137}Cs activities in SIS presented slight differences respect to global fallout as the ultimate source of both radionuclide in the SIS (Figure 4.3), implying a contribution from additional sources distinct from global fallout: local sources such as local fallout,

dumping of nuclear waste, etc. This finding would be largely masked if scavenging from seawater was the main mechanism of enrichment.

The $^{240}Pu/^{239}Pu$ atom ratio in SIS was proposed as a tracer to distinguish the geographical source area by comparing it with those in bottom sediments [*Cámara-Mor et al*. 2010, Chapter 4]. Most sediments in the continental shelves are characterized by $^{240}Pu/^{239}Pu$ atom ratios comparable to the global fallout, 0.18 [*JRNEG*, 1996; *Krey et al.*, 1976]. However, deviations from global fallout were observed in particular areas of the continental shelves [*Smith et al.,* 2000; *Skipperud et al*. 2004; *Kelley et al*., 1999]. The scavenging of Pu from seawater, were it a relevant mechanism, would disturb and homogenise the $^{240}Pu/^{239}Pu$ atoms ratio signal to approximately 0.18, since this value is the atom ratio characteristic of the Arctic surface waters [table 7.3; *Josefsson*, 1998; *Cooper et al*., 1999; *León-Vintro et al.,* 2002]. Nevertheless, several SIS samples contain $^{240}Pu/^{239}Pu$ atoms ratios as low as 0.118 or as high as 0.253 [*Cooper et al.*, 1998; *Landa et al.*, 1998; *Masqué et al*., 2003, 2007 and *Cámara-Mor et al*., 2010]. Besides, these samples were placed in the most probable path of sea ice from those defined continental shelves with similar range of values (Chapter 4).

The presence of ^{234}Th in SIS can be supported by the decay of ^{238}U, which is present in the SIS since it is a lithogenic material. Any enrichment of ^{234}Th in SIS in respect to ^{238}U concentrations should be due to scavenging from surface water or melting of sea ice if any excess ^{234}Th present in sea ice at formation areas would have decayed by the time the samples were collected, since atmospheric deposition is negligible. *Not et al.* [2011] measured ^{238}U in sea ice and sea ice brines from the Arctic Ocean. Data showed the conservative behaviour of U in relation to changes in salinity during sea ice formation and melting. For that reason, despite of the fact that sea ice brines contains three times higher concentrations ^{238}U respect to surface water, the ^{238}U concentrations in sea ice was 10 times lower than in surface waters. Similar results were observed for salinity. Therefore, the enrichment of ^{234}Th in SIS by the scavenging from sea ice can be ruled out in comparison with seawater. If the scavenging by SIS from seawater was an enrichment source of ^{234}Th, according to the estimated volumes of seawater required to explain the $^{210}Pb_{xs}$ concentrations in SIS by this mechanism and using the recommended K_d values, SIS should contain $^{234}Th_{xs}$ concentrations ranging from 100 to 5000 $Bq \cdot kg^{-1}$ (Figure 6.5). Based on low K_d values, concentrations of $^{234}Th_{xs}$ would range from 3000 to 150000 $Bq \cdot kg^{-1}$, and taking the high K_d values, the concentrations would vary between 100 and 4800 $Bq \cdot kg^{-1}$. These results imply that $^{234}Th_{xs}$ should be present that for any amount of seawater scavenged by SIS. Nevertheless, $^{234}Th_{xs}$ was not detected in any of the SIS samples analysed in this work. Consequently, this clearly evidences that scavenging from seawater by SIS is not a significant mechanism of enrichment of radionuclides in SIS.

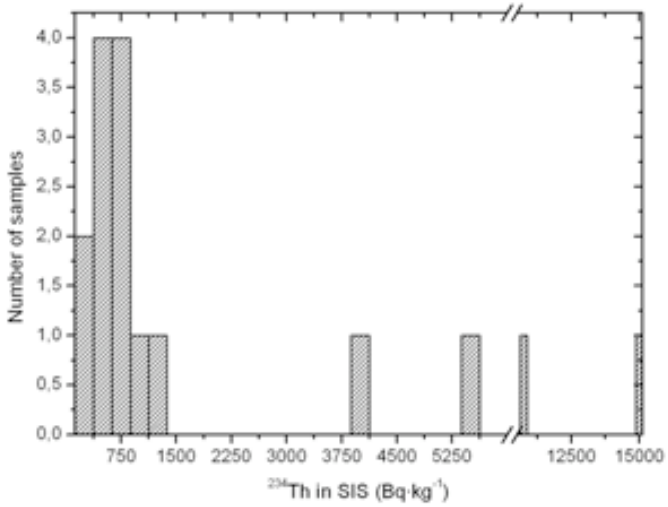

Figure 6.5 Histogram of the expected $^{234}Th_{xs}$ activity in SIS ($Bq \cdot kg^{-1}$) according to amount of sea water per gram needed to explain the measured ^{210}Pb activity in SIS based on recommended kd values .

^{7}Be could be incorporated by SIS by direct scavenging from surface seawater or by scavenging from sea ice during formation of cryoconite holes, where it would have been deposited by atmospheric deposition. As for ^{234}Th, any initial activity of ^{7}Be in SIS from their geographical source area in which

the sediments were incorporated into the sea ice would have been decayed at the time of sampling. The fraction of measured ^{7}Be activity in SIS that could be explained by scavenging based on recommended K_d values is shown in Figure 6.6. In this case, scavenging from seawater would account for 0.2 - 12% of the measured ^{7}Be activities, with a median of 1.6%. Instead, considering the highest K_d values, the percentage explained would vary between 0.08 and 19%, with a median value of 3%, while considering the lowest K_d values, the median percentage increases to 68 with a range 5 - 454% (Table 6.7). These last estimates, however, are not consistent with the findings for the rest of the radionuclides when considering their respective lowest K_d values: i) we did not detect excess ^{234}Th in SIS and ii) measured ^{239,240}Pu concentrations in SIS are much lower than the concentrations expected from the corresponding seawater volume of ^{210}Pb according to the lowest K_ds values (Table 6.7).

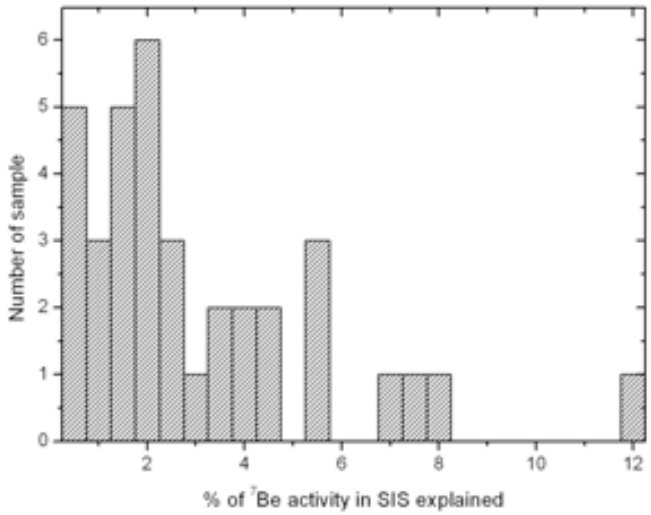

Figure 6.6 Histogram of the percentage of measured ^{7}Be activity in SIS (Bq·kg^{-1}) explained from the scavenging of the corresponding seawater volume per kg of SIS needed to explain the measured ^{210}Pb activity in SIS according to recommended k_ds values

The comparison between estimated and measured concentrations of radionuclides in SIS shows that the needed volume of seawater to explain ^{210}Pb activities is not consistent with the data for the other radionuclides studied here, suggesting that the scavenging from seawater is not the main responsible to enhance their concentration in SIS. Atmospheric deposition and scavenging from sea ice is a plausible mechanism to explain the ^{210}Pb and ^{7}Be activities in SIS, as previously proposed by *Masqué et al.* [2007].

Sea ice acts as a barrier between the ocean and the atmosphere, intercepting atmospheric fluxes [*Granskog et al*., 2003]. In fact, the concentrations of ^{7}Be and ^{210}Pb in the upper layers of sea ice are clearly higher than in surface seawater (Chapter 5 and table 6.2 and 6.3) and originate from atmospheric deposition. SIS, mostly present in the upper layer as a consequence of the continuous freezing/melting cycles, could scavenge the radionuclides from the surrounding melting sea ice. The amount of melting sea ice that should be in contact to each kg of SIS to explain the median ^{210}Pb concentration in SIS (180 Bq·kg^{-1}) if a quantitative scavenging takes place would be approximately 5 m^{3}. This median k_d value is several order of magnitude lower than the recommended value reported by the IAEA [1985] (table 6.6), showing the large influence of the atmospheric flux in enriching SIS. This required amount of melting sea ice would also explain the concentrations of ^{7}Be measured in SIS. Furthermore, this mechanism would also explain why ^{239,240}Pu and ^{137}Cs activities in SIS are not significantly enriched, and the signal of both radionuclides in SIS and the ^{240}Pu/^{239}Pu atom ratios can be used to determine the regional area of origin of sea ice floes.

Moreover, ^{7}Be and ^{210}Pb concentration in SIS were used to estimate the transit time of the sea ice floes in the Arctic Ocean [*Masqué et al*., 2007], obtaining average transit time ranging from 3 to 5 years, consistent with the sea ice drift patterns [*Pfirman et al*., 1997]. The back-trajectory model was

applied for the samples collected in the Siberia branch of the Transpolar Drift, estimating average transit times of about 3-4 years, and for samples closer to the Kara Sea, for which transit times were of about half a year, also coherent with the drifting patterns of sea ice [*Pfirman et al*., 1997].

6.4. Conclusions

Data showed that SIS contained ^{7}Be, ^{137}Cs, $^{210}Pb_{xs}$ and $^{239,240}Pu$ concentration, but any $^{234}Th_{xs}$ was measured in SIS. These concentrations respond to different mechanisms, which happen along the sea ice lifespan. Whereas the geographical origin of SIS probably plays some role in determining the radionuclide activity in SIS; it is not enough to explain the whole content of radionuclide. Scavenging from surface water is neither accountable for radionuclide enrichment since any $^{234}Th_{xs}$ is present in SIS. Furthermore, it would invalidate the use of $^{240}Pu/^{239}Pu$ atom ratios in SIS to identify sea ice origin due to the homogenization to the seawater signal as the same as $^{7}Be/^{210}Pb_{xs}$ activity ratio to estimate transit time. Instead, the atmospheric deposition and the scavenging from sea ice endorses all requirements; since sea ice is almost free for those radionuclide without atmospheric input while it contains larger concentrations of radionuclides with atmospheric input respect to surface seawater. The scavenging from sea ice and atmospheric deposition would explain why $^{239,240}Pu$ and ^{137}Cs activities in SIS are not significantly enriched, since its atmospheric deposition is negligible, and the signal of both radionuclides and the $^{240}Pu/^{239}Pu$ atom ratios in SIS can be used to determine the regional area of origin of sea ice floes, and it would also account for the enrichment of ^{7}Be and ^{210}Pb in SIS but not for $^{234}Th_{xs}$ hence sea ice does not almost contain ^{238}U. Atmospheric deposition appears as the most plausible enrichment source of radionuclides, although scavenging from surface seawater is not the main mechanism is not discardable and further research should be done in order to constrain/get an accuracy estimation of the contribution of each mechanism, and determine under which condition each mechanism is more significant.

Chapter 7.

Conclusions

The main objective of this thesis was to study the relevance of the sea ice as an important agent of transport and distribution of particulate matter and chemical species along the Arctic Ocean through the use of natural and artificial radionuclides.

To evaluate/comprehend the role of the sea ice as a particulate matter transport, it was firstly necessary to identify the origin of sea ice. Sea ice pack is formed by an aggregation of diverse floes, most of them formed in the shallow areas of the Siberian shelves, that can incorporate fine sediments that will named sea ice sediments (SIS). Its final destination is related to sea ice drift path, which relies on geographical origin of sea ice. Eventually exported sea ice floes from shelves would leave the Arctic Ocean though the Fram Strait. The necessary time and the path followed to reach the Fram Strait vary according to both source area and Arctic Oscillation (AO). The origin of sea ice gives us relevant information to improve the possible implications in the Arctic system of the climate change. If sea ice does not contain SIS, its origin is difficult to determine since it can be either formed in the continental shelves or in the deep basin, however that does not happen when sea ice contains SIS. Clay mineralogy, diatoms, Fe grains are used to distinguish between each one however, no all continental shelves can be distinguish with these parameters. A combination of artificial radionuclides (especially $^{240}Pu/^{239}Pu$ atom ratio, in combination with the ^{137}Cs or $^{239,240}Pu$ activity) measured in SIS allowed constraining the geographical origin of the sea ice floes. SIS originating in the Laptev and Kara Seas have $^{240}Pu/^{239}Pu$ atom ratios lower than those imprinted by global fallout (0.18), while SIS originating from the Alaskan shelf is characterised by $^{240}Pu/^{239}Pu$ atom ratios greater than global fallout. The specific activities of ^{137}Cs and $^{239,240}Pu$ are less diagnostic of sea-ice origin, because many processes in addition to source can affect their values; however, sediments of the Kara and Laptev Seas can have markedly elevated specific activities of ^{137}Cs that are imprinted on SIS originating in those areas. In approximately 50% of the samples analysed, the isotopic signatures are not distinctive as to SIS origin and additional approaches are required to better resolve possible source areas.

The second study embraced the evaluation of the mechanisms by sea ice incorporate chemical species; in particular determine the role in intercepting atmospheric fluxes. To quantify these processes in the whole sea ice system, a natural radioactive tracer was used. Results showed that sea ice is enriched in ^{7}Be. In fact, any ^{7}Be from sea ice formation is present in sea ice at sampling time due to its

short half-life (53 days). Therefore, atmospheric interception appears as the most likely source. Based on ^{7}Be concentration results, we concluded that the sea ice intercepts and accumulates circa 30% of the atmospheric fluxes of ^{7}Be. Although the data is no used to elucidate the transformation processes along the transport path of the sea ice, it shows that sea ice is an effective accumulation agent of atmospheric fluxes in the Arctic Ocean. In this context, chemical species in sea ice and SIS are strong influenced by atmospheric deposition. In the same way that ^{7}Be is accumulated and stored in sea ice, ice floes can also intercept other atmospherically transported species. Thus, the accumulation of iron is of especial interest in thisregard because it is an important micronutrient: similarly, contaminants that bioaccumulate, such as PCBs, can be atmospherically transported by sea ice. The importance of sea ice as extra source of chemical species as a consequence of its melting was also assessed, on average 67 ± 55 Bq·m^{-2} of ^{7}Be would be annually discharged in the Fram Strait due to sea ice melts. That value is comparable to ^{7}Be atmospheric flux in this area, suggesting sea ice is a relevant source of ^{7}Be in the ablation areas and also in the entire Arctic Ocean. As with ^{7}Be, which is released into surface water during melting, these other species can also be released and their concentration on surface water can thus increase in short time periods. For Fe at least and N, this discharge can help trigger blooms and modify biogeochemistrical cycling [*Melnikov*, 1991]. However, changes in the timing over which sea ice melts in ablation areas may produce that nutrient releases are decoupled from biological blooms, and this decoupling may have consequences in the whole Arctic ecosystem.

Data showed in the present study was also used to provide with a first order assessment of the sediment load in sea ice; an upper estimate of the SIS load thus would be 284 g·m^{-2} (range 5 - 1960 g·m^{-2}), consistent with previous estimates based on individual measurements in sea ice cores that obtained SIS loads ranging from 8 to 800 g·m^{-2} [e.g. *Barnes et al.,* 1982; *Nürnberg et al*., 1994; *Eicken et al*., 1997]. These data allowed estimating the annual sediment flux to the surface waters of the Fram Strait in 489 (9 - 3371) g·m^{-2}·y^{-1}. This flux compares well with sediment fluxes measured using sediments traps deployed in the eastern part of the Fram Strait between 1987 and 1990, which showed fluxes ranging from 122 to 231 g·m^{-2}·y^{-1}, with maximum values of 475 g·m^{-2}·y^{-1} [*Hebbeln*, 2000]. These results showed the useful of tracers such as natural radionuclides to determine the importance of sea ice as an important transport of particulate matter along the Arctic Ocean and a source of particulate matter to the water column.

In addition, sea ice seems presumably to be a source and transport of chemical species. The entrainment of these chemical species into sea ice is poorly understood. Once its formed, sea ice starts undergoing a gathered of chemical and physical processes that contribute to enhance the concentration of chemical species in sea ice and SIS. The last topic was related to elucidate which are the mechanisms of chemical species enrichment into sea ice after its formation. Despite of the fact that the geographical origin of those sediments probably plays some role in determining the radionuclide activity in SIS in the Arctic Ocean, it is not enough to explain the whole content of radionuclide in SIS. The hypothesis of the scavenging from surface water proposed by *Baskaran* [2005] is neither wholly satisfactory since it does not match between different radionuclides measured in SIS mainly because; i) SIS does not contain $^{234}Th_{xs}$ when it should; ii) ^{137}Cs and ^{239,240}Pu does do not show any relationship with ^{210}Pb, and combination of both is used to identify sea ice origen; iii) ^{239}Pu/^{240}Pu ratio is an useful tracer to identify the SIS origin and iv) a small fraction of ^{7}Be activity in SIS is explained if all ^{210}Pb activity in SIS was explained. Sea ice acts a barrier between ocean and atmosphere, intercepting and accumulating atmospheric fluxes. Radionuclide activity in sea ice is almost negligible compared with surface seawater for those radionuclides without atmospheric input (^{239,240}Pu, ^{238}U, ^{234}Th and ^{137}Cs). However, radionuclides with atmospheric input, such as ^{210}Pb and ^{7}Be, sea ice presents activities several orders of magnitude higher than in surface water [*Eicken et al.,* 2002; *Masqué et al.,* 2007 and *Cámara-Mor et al*., 2010]. Atmospheric fluxes and subsequently scavenging from sea ice appears as a main mechanism that would explain the radionuclide enrichment in SIS since it responds why SIS does not contain $^{234}Th_{xs}$ or why ^{239,240}Pu and ^{137}Cs activities in SIS can be used to estimate the sea ice origin. Besides, it would explain the $^{210}Pb_{xs}$ and ^{7}Be activities, enabling to use the activity ratio between both in SIS to estimate the transit time of the sea ice [*Masqué et al.,* 2007]. Nevertheless, further investigation should be done in order to constrain/get an accuracy estimation of the contribution of each mechanism, and determine under which condition each mechanism is more significant

Bibliografy

Aagaard K. (1981). On the deep circulation of the Arctic Ocean. Deep-Sea Res. 82: 251-268.

Aagaard K. (1989). A synthesis of the Arctic Ocean circulation. Rapports et proces-verbaux des Reunions, Conseil International pour l'Exploration de la Mer 188, 11-22.

Aagaard, K., J. H. Swift and E. C. Carmack (1985). Thermohaline circulation in the Arctic Mediterranean seas, Journal Geophysical Research 90:4833-4846, doi:10.1029/JC090iC03p04833.

Aagaard K. and E.C. Carmack (1989). The role of sea ice and other fresh water in the Arctic circulation. Journal Geophysical Reseach 94: 14485-14498.

Aagaard K., L.A. Barrie, E.C. Carmack, C. Garrity, E.P. Jones, D. Lubin, R.W. Macdonald, J.H Swift, W.B. Tucker, P.A. Wheeler and R.H. Whritner (1996). U.S., Canadian Researchers Explore the Arctic Ocean. Eos 177, 209-213.

Aarkrog A. (2003). Input of anthropogenic radionuclides into the World Ocean. Deep- Sea Research II: Topical Studies in Oceanography 50(17-21):2597-2606.

Abelmann, A. (1992). Diatom assemblages in Arctic sea ice-indicator for ice drift pathways. Deep Sea Research 39(2):S525-S538.

Aguilar-Islas A.M., R.D. Rember, C.W. Mordy and J. Wu (2008). Sea ice-derived dissolved iron and its potential influence on the spring algal bloom in the Bering Sea. Geophysical Research Letters 35,l24601, doi:10.1029/2008GL035736.

AMAP (1998). Arctic Pollution Issues: A State of the Arctic Environment Report. Arctic Monitoring and Assessment Programme, P.O. box 8100 Dep., N-0032 Oslo, Norway.

AMAP (2002). Arctic Pollution Issues: A State of the Arctic Environment Report. Arctic Monitoring and Assessment Programme. AMAP Assessment 2002: Radioactivity in the Arctic.

Andersen S., R. Tonboe, L. Kaleschke, G. Heygster and L.T. Pedersen (2007). Intercomparison of passive microwave sea ice concentration retrievals over the high-concentration Arctic sea ice. Journal Geophysical Research 112(C08004), doi:10.1029/2006JC003543.

Anderson L. G., E.P. Jones, K.P Koltermann, P. Schlosser, J.H. Swift and D.W Wallace (1989). The first oceanographic section across the Nansen Basin in the Arctic Ocean. Deep-Sea Research 36:475-482.

Anderson L.G., G. Bjork, O. Holby, E.P. Jones, G. Kattner, K.P. Koltermann, B. Liljeblad, R. Lindegren, B. Rudels and J.H Swift (1994). Water masses and circulation in the EurasianBasin: results from the Oden 91 expedition. Journal Geophysical Research 99(C2):3273-3283.

Arrigo, K. R., G. V. Dijkin, and S. Pabi (2008). Impact of a shrinking Arctic ice cover on marine primary production, Geophysical Research Letters 35, L19603, doi: 10.1029/2008GL035028

Assur A. (1960). Composition of sea ice and its tensile strength. SIPRE research report, 44.

Azahra M., A. Camacho-García, C. González-Gómez, J. J. López-Peñalver and T. El Bardouni (2003). Seasonal ^{7}Be concentrations in near-surface air of Granada (Spain) in the period 1993–2001. Applied Radiation and Isotopes 59(2-3):159-164.

Bacon M.P., C.A Huh and R.M. Moore (1989). Vertical profiles of some natural radionuclides over the Alpha ridge, Arctic Ocean. Earth and Planetary Science Letters 95:15-22.

Barnes P., E. Reimnitz and D.H. Fox (1982). Ice rafting of fine grained sediment, a sorting and transport mechanism, Beaufort Sea, Alaska. Journal Sedimentology Petrology 52(2): 493–501.

Barrie L., E. Falck, D. Gregor, T. Iverson, H. Loeng and R. Macdonald (1998). The influence of physical and chemistry processes on contraminant transport into and within the Arctic. In: Gregor D., Barrie L., Loeng H., editors. The AMAP assessment, 25-116.

Baskaran M. (2005). Interaction of sea ice sediments and surface sea water in the Arctic Ocean: Evidence from excess ^{210}Pb. Geophysical Research Letters 32: LI2601, doi:10.1029/2004GL022191.

Baskaran M. and J. Naidu (1995). ^{210}Pb-derived chronology and the fluxes of ^{210}Pb and ^{137}Cs isotopes into continental shelf sediments, East Chukchi Sea, Alaska Arctic. Geochimica et Cosmochimica Acta 59:4435-4448.

Baskaran M., A. Shaunna, P. Santschi, J. Brooks, M. Champ, D. Adkinson, M.R. Colmer and V. Makeyev (1996). Pu, ^{137}Cs and excess ^{210}Pb in the Russian Arctic sediments. Earth and Planetary Science Letters 140:243-257.

Baskaran M., S. Asbill, J. Schwantes, P.H. Santschi, M.A. Champ, J.M. Brooks, D. Adkinson and V. Makeyev (2000). Concentrations of ^{137}Cs, ^{239,240}Pu, and ^{210}Pb in sediment samples from the Pechora Sea and biological samples from the Ob, Yenisey Rivers and Kara Sea. Marine Pollution Bulletin 40:830–838.

Bauch D., P. Schlosser and R.G. Fairbanks (1995). Freshwater balance and the sources of deep and bottom waters in the Arctic Ocean inferred from the distribution of $H_2{}^{18}O$. Progress in Oceanography 35:53-80.

Bauerfeind E.M., E.A. Nöthig, A. Beszczynska, K. Fahl, L. Kaleschke, K. Kreker, M. Klages, T. Soltwedel, C. Lorenzen and J. Wegner (2009). Particle sedimentation patterns in the eastern Fram Strait during 2000–2005: Results from the Arctic long-term observatory HAUSGARTEN. Deep-Sea Research I 56(9):1471-1487.

Baxter M.S., S.W. Fowler and P.P. Povinec (1995). Observations on plutonium in the oceans. Applied Radiation Isotopes 46(11):1213–23.

Beck, H.L. and P.W. Krey (1983). Radiation exposure in Utah from Nevada Nuclear Tests. Science 220:18–24

Bennington K.O. (1963). Some chemical composition studies on Arctic sea ice. (In Kingery, W. D., ed. lee andBsnow; properties, processes and applications: proceedings if a conference held at the Massachusetts Institute of Technology,BFebruary 12-16,1962. Cambridge, Mass., M.LT. Press. P.248-57.

Berner H. and G. Wefer (1990). Physiographic and biological factors controlling surface sediment distribution in the Fram Strait. In: Geological history of the Polar Oceans: Arctic versus Antartic. U. Bleil and J. Thiede, editors, Klower, Dordrecht, 317-335.

Bondietti E.A., C. Papastefanou and C. Rangarajan (1987). Aerodynamic size associations of natural radioactivity with ambient aerosols. In: P.K. Hopke (editor), Radon and its decay products: Occurrence, properties and health effects. ACS Symposium Series 331, American Chemical Society, Washington, D.C., 377–397.

Bönisch, G. and P. Schlosser (1995). Deep water formation and exchange rates in the Greenland/Norwegian Seas and the Eurasian Basin of the Arctic Ocean derived from tracer balances, Progress in Oceanography 35:29-52

Brown L., G.L. Stensland and R. Middleton (1989). Atmospheric deposition of ^{7}Be and ^{10}Be. Geologic Cosmochemical Acta. 53, 135-149.

Buesseler K.O. (1986). Plutonium isotopes in the North Atantic. PhD. Thesis, Massachussets Institute of Technology/Woods Hole Oceanographic Institution Joint Program in Oceanography, pp. 220.

Cámara-Mor P., P. Masqué, J. Garcia-Orellana, J.K. Cochran, J.L. Mas, E. Chamizo, C. Hanfland (2010). Arctic Ocean sea ice drift origin derived from artificial radionuclides. Science of the Total Environment 15: 408(16):3349-58.

Cámara-Mor P., P. Masque, J. Garcia-Orellana, S. Kern, J.K. Cochran and C. Hanfland (2011). Interception of atmospheric fluxes by Arctic sea 1 ice: evidence from cosmogenic 7Be. Journal Geophysical Research 16:C12041,doi:10.1029/2010JC006847

Campbell N.J. and A.E. Collin (1958). The discoloratioonf Foxe Basin ice. Journal Fisheries Research Board of Canada 15(6):1175-1188

Carmack E. (1990). Large-scale oceanography of polar oceans. In: W. O. Smith [ed.] Polar Oceans. Academic, pp.171-222.

Carmack E. C. (1986). Circulation and mixing in ice covered waters, in The Geophysics of Sea Ice, edited by N. Untersteiner, Plenum Press, New York. pp. 641-712.

Carmack E.C. and J.H. Swift (1990). Some aspect of the large-sclae physical oceanography of the Arctic Ocean influencing biological distributions. In Polar Marine Diatoms, L.K. Medlin and J- Priddle, editors, British Antarctic Survey, Cambridge, UK, pp. 35-46.

Carmack E. C., R. W. Macdonald, R. G. Perkin, F. A. McLaughlin and R. J. Pearson (1995). Evidence for warming of Atlantic Water in the southern Canadian Basin of the Arctic Ocean: Results from the Lasen- 93 Expedition, Geophysical Research Letters 22:1061-1064, doi:10.1029/95GL00808.

Carmack E.C., K. Aagaard, J.H. Swift, R.W. Macdonald, F.M. McLaughlin, E.P. Jones, R.G. Perkin, J.N. Smith, K.M. Ellis and L.R. Killius (1997). Changes in temperature and tracer distributions within the Arctic Ocean: results from the 1994 Arctic Ocean section. Deep-Sea Research II 44:1487-1502.

Carmack, E. and P.Wassmann. 2006. Food webs and physical-biological coupling on pan-Arctic shelves: Unifying concepts and comprehensive perspectives. Progress in Oceanography. 71: 446-477. doi: 10.1016/j.pocean.2006.10.004.

Cavalieri D. J., P. Gloersen and W. J. Campbell (1984). Determination of sea ice parameters with the NIMBUS 7 SMMR. Journal Geophysical Reseach 89(D4):5355-5369.

Chamizo E., S.M. Enamorado, M. García-León, M. Suter and L. Wacker (2008b). Plutonium measurements on the 1 MV compact AMS system at the Centro Nacional de Aceleradores (CNA), Nuclear Instruments and Methods in Physics Research Section B 266:4948-4954.

Chamizo E., M.C. Jimenez-Ramos, R.L. Wacke, I. Vioque, A. Calleja, M. García-León and R. García-Tenorio (2008ª). Isolation of Pu-isotopes from environmental simples using ion chromatography for accelerator mass spectrometry and alpha spectrometry, Analytica Chimica Acta 606:239-245.

Christensen G.C., G.N. Romanov, P. Strand, B. Saibu, S.V. Malyshev, T.D. Bergan, D. Oughton, E.G. Drozhko, Y.V. Glagolenko, I. Amundsen, L.A. Rudjord, T.O. Bjerk and B. Lind (1997). Radioactive contamination in the environment of the nuclear enterprise "MAYAK" PA. Results from the joint Russian–Norwegian field work in 1994. The Science of the Total Environment 202:237–248.

Coachman L. K. and C. A. Barnes (1961). The contribution of Bering Sea water to the Arctic Ocean. Arctic 14:147-161.

Coachman L.K. and C.A. Barnes (1963). The movement of Atlantic water in the Arctic Ocean. Arctic 16:8–16.

Coachman L. K. and K. Aagaard. (1974). Physical Oceanography of Arctic and Subarctic Seas. In Marine Geology and Oceanography of the Arctic Seas, edited by Y. Herman. New York: Springer-Verlag.

Cochran, J. K., S.B. Moran, N.S. Fisher, T.M. Beasley and J.M. Kelley (2000). Sources and transport of anthropogenic radionuclides in the Ob River system, Siberia. Earth and Planetary Science Letters 179:125-137

Colony, R., and A. S. Thorndike (1985). Sea ice motion as a drunkard's walk. Journal Geophysical Research 90:965-974.

Comiso J. C. (1986). Characteristics of arctic winter sea ice from satellite multispectral microwave observations. J. Geophys. Res. 91(C1), 975–994.

Comiso J.C. (2002). A rapidly declining perennial sea ice cover in the Arctic. Geophys. Res. Lett. 29, DOI:1029/2002gl015650

Comiso J. C., C. L. Parkinson, R. Gersten and L. Sock (2008). Accelerated decline in the arctic sea ice cover, Geophysical Reseach Letters 35, L01703, doi:10.1029/2007GL031972.

Cooper L.W., C. R. Olsen, D. K. Solomon, I. L. Larsen, R. B. Cook and J. M. Grebmeier (1991). Stable Isotopes of Oxygen and Natural and Fallout Radionuclides Used for Tracing Runoff During Snowmelt in an Arctic Watershed. Water resources research 27(9):2171-2179.

Cooper L.W., I.L. Larsen, T.M. Beasley, S.S. Dolvin, J.M. Grebmeier, J.M. Kelley, M. Scott and A. Jonhson-Pyrtle (1998). The distribution of radiocesium and plutonium in Sea Ice-entrained Arctic sediments in relation to potential sources and sinks. Journal of Environmental Radioactivity 39(3):279-303.

Cooper L.W., J.M. Kelley, L.A. Bond, K.A. Orlandini and J.M. Grebmeier (2000). Sources of the transuranic elements plutonium and neptunium in arctic marine sediments. Marine Chemistry 69:253-276.

Cooper L.W., A. Ingvar, L. Larsen, J. M. Grebmeier and S. B. Moran (2005). Detection of rapid deposition of sea ice-rafted material to the Arctic Ocean benthos using the cosmogenic tracer ^{7}Be. Deep-Sea Research II 52:3452–3461.

Cornwell J.C. (1985). Sediment accumulation rates in ana Alaska Arctic lake using a modied ^{210}Pb technique. Candian Journal Fisheries and Aquatic Science 42:809-814.

Cota G.F., L.W. Cooper, D.A. Darby and I.L. Larsen (2006). Unexpectedly high radioactivity burdens in ice-rafted sediments from the Canadian Arctic Archipelago. The Science of the Total Environment 366:253-261.

Cox G.F.N. and W.F. Weeks (1983). Numerical simulations of the profile properties of undeformed first-year sea ice during the growth season. Journal Geophysical Research 93: 12449-12460.

Damm E., S. Helmke, U. Thoms, U. Schauer, E. Nöthig, K. Bakker and R.P. Kiene (2009). Methane production in aerobic oligotrophic surface water in the central Arction Ocean. Biogeosciences Discussion 6:1-25.

Darby D. A, L.H. Burckle, and D.L. Clark, (1974). Airborne dust on the Arctic pack ice: its composition and fallout rate. Earth and Plan. Science Report 477:1-13.

Darby D.A. (2003). Sources of sediments found in sea ice from the western Arctic Ocean, new insights into processes of entrainment and drift pattern. Journal of Geophysical Research 108(C8)3257.

Dethleff D. (2005), Entrainment and export of Laptev Sea ice sediments, Siberian Arctic. Journal of Geophysical Research 110:C07009, doi:10.1029/2004JC002740.

Dethleff D., D. Nürnberg, E. Reinmitz, M. Saarso and Y.P. Savchenko (1993). East Siberian Arctic Region Expedition '92. The Laptev Sea-its significantce for Arctic sea-ice formation and transpolar sediments flux. Report of Polar Research, 120pp.

Dethleff, D., D. Nürnberg and E. Gorth (1993). East Siberian Arctic region expedition '92: the Laptev Sea: its significance for Arctic sea-ice formation and transpolar sediment flux. Reports on Polar Research 20, 44pp.

Dethleff D., P. Loewe and E. Kleine (1998). The Laptev Sea flaw lead - Detailed investigation on ice formation and export during 1991/92 winter season. Cold Region Science Technology 27(3):225-243.

Dehtleff D. and E.W. Kempema (2007). Langmuir circulation driving sediment entrainment into newly formed ice: Tank experiment results with application to nature (Lake Hattie, United States; Kara Sea, Siberia). Journal of Geophysical Research 112, C02004, doi:10.1029/2005JC003259.

Dethleff D. and G. Kuhlmann (2010). Fram Strait sea-ice sediment provinces based on silt and clay compositions identify Siberian Kara and Laptev seas as main source regions. Polar Research. doi : 10.1111/j.1751-8369.2010.00149.

Dibb J.E. (1990), Beryllium-7 and ^{210}Pb in the atmosphere and surface snow over the Greenland ice sheet in the summer of 1989. Journal of Geophysical Research 95, 407-422

Dibb J.E. (1992). The accumulation of ^{210}Pb at Sumit, Greenland since 1885. Tellus 44B, 72-79.

Dickmann G.S. and H.H. Hellmer (2003). The importante of sea cie: an overview. In Sea Ice. An introduction to its physics, chemistry, biology and geology. Thomas D.N. and Dieckmmann G.S. Ed. Backwell Publising.

Efurd E.D., R.E. Steiner, F.R. Roensch, S.E. Glover and J.A. Musgrave (2005). Determination of the ^{240}Pu/^{239}Pu atom ratio in global fallout at two locations in the Northern Hemisphere. Journal of Radioanalytical and Nuclear Chemistry 263(2):387-391.

Eicken H. (1998), Factors determining microstructure, salinity and stable-isotope composition of Antarctic sea ice: Deriving modes and rates of ice growth in the Weddell Sea. AGU Antarctic Research Series, 74 (Antarctic Sea Ice Physical Processes).

Eicken H. (2003). From the microscopic, to the macroscopic, to the regional scale: growth, microstructure and properties of sea ice. An Introduction to its Physics, Biology, Chemistry and Geology (Ed. by D.N. Thomas & G.S. Dieckmann), Blackwell Scientific, 82-111.

Eicken H. and M. A. Lange (1989). Development and properties of sea ice in the coastal regime of the southeastern Weddell Sea. Journal Geophysical Research 94, 8193-8206

Eicken H., M. Lensu, M. Lepparanta, W.B. Tucker III, A.J. Gow and O. Salmela (1995). Thickness, structure and properties of level summer multi-year ice in the Eurasian sector of the Arctic Ocean. Journal Geophysical Research 100:22697- 22710.

Eicken H., E. Reimnitz, V. Alexandrov, T. Martin, H. Kassens and T. Viehoff (1997). Sea-ice processes in the Laptev Sea and their importance for sediment export. Continental Shelf Research 17 (2):205-233.

Eicken H., J. Kolatschek, F. Lindemann, I. Dmitrenko, J. Freitag and H. Kassens (2000). A key source area and constraints on entrainment for basin-scale sediment transport by Arctic sea ice. Geophysical Research Letters 27(13):1919-1922.

Eicken H., H. R. Krouse, D. Kadko and D. K. Perovich (2002). Tracer studies of pathways and rates of meltwater transport through Arctic summer sea ice. Journal Geophysical Research 107(C10), doi:10.1029/2000JC000583.

Eicken H., R. Gradinger, A. Gaylord, A. Mahoney, I. Rigor, H. Melling, (2005). Sediment transport by sea ice in the Chukchi and Beaufort Seas: Increasing importance due to changing ice conditions? Deep-Sea Research II 52:3281-3302.

Garimella S., K. Koshy and S. Singh (2003). Concentration of 7Be in surface air at Suva, Fiji. Sourth Pacific. Journal Nature Science 21:5-19.

Gascard J.C., J. Festy, H. Goff, M. Weber, B. Bruemmer, M. Offermann, M. Doble, P. Wadhams, R. Forsberg, J.P. Metaxian, J. Grangeon, J. Haapala, E. Rinne, C. Haas, G. Heygster, E. Jakobson, T. Palo, J. Wilkinson, L. Kaleschke, K. Claffey, B. Elder and J. Bottenheim (2008). Exploring Arctic Transpolar Drift During Dramatic Sea Ice Retreat. EOS, Transaction American Geophyssical Union 89(3), 21.

Gerasopoulos E., P. Zanis, A. Stohl, C.S. Zerefos, C. Papastefanou, W. Ringer, L. Tobler, S. Hubener, H.W. Gaggeler, H.J. Kanter, L. Tositti, S. Sandrini (2001). A climatology of 7Be at four high-altitude stations at the Alps and the Northern Apennines. Atmospheric Environment 35:6347-6360.

Gerdes R. L and U. Schauer (1997). Large-scale circulation and water mass distribution in the Arctic Ocean from model results and observations. Journal Geophysical Research 102(C4):8467-8483.

Golden K.M., M. Cheney, A.K. Ding, A.K. Fung, T.C. Grenfell, D. Isaacson, J.A Kong, S.V. Nghiem J. Sylvester and D.P. Winebrenner (1998). Forward electromagnetic scattering models for sea ice. IEEE Trsnsactions on Geoscience and Reomte Sensing 36:1655-1674.

Granskog M.A (2004). Investigations into the Physical and Chemical Properties of Baltic Sea Ice. PhD thesis.University of Helsinki. ISBN 952-91-6613-3

Granskog M.A, H. Kaartokallio and K. Shirasawa (2003). Nutrient status of Baltic Sea ice: Evidence for control by snow-ice formation, ice permeability, and ice algae. Journal Geophysical Research 108(C8),3253, doi:10.1029/2002JC001386.

Grebmeier J.M., L.W. Cooper, L.A. Codispoti, R., Benner (2004). Benthic carbon cycling and nutrient exchange in the western Arctic shelf-basin interactions (SBI) study area. ASLO/TOS Meeting, Honolulu, HI 59.

Haas C. (2003). Dynamics versus thermodynamics: The sea-ice thickness distribution. In: D.N. Thomas and G.S. Dieckmann (editors), Sea Ice - An Introduction to its Physics, Biology, Chemistry and Geology, Blackwell Scientific,82-111.

Haas C. (2004). Late-summer sea ice thickness variability in the Arctic Transpolar Drift 1991--2001 derived from ground-based electromagnetic sounding. Geophysical Research Letters 31, L09402, doi:10.1029/2003GL019394

Haas C., S. Gerlandz, H. Eicken and H. Miller (1997). Comparison of sea-ice thickness measurements under summer and winter conditions in the Arctic using a small electromagnetic induction device. Geophysical 62(3):749–757.

Haas C., D.N. Thomas, J. Bareiss (2001). Surface properties andprocesses of perennial Antarctic sea ice in summer. Journal Glaciology 47:613–625.

Hams I.H., M.J. Karcher, and D. Dethleff (2000). Modelling Siberian river runoff-implications for contaminant transport in the Arctic Ocean. Journal of Marine Systems 27:95-115.

Harvey M.J. and K.M. Matthews (1989). 7Be deposition in a high-rainfall area of New Zeland. Journal Atmospheric Chemistry 8:299-306.

Hebbeln D. and G. Wefer (1991). Effects of ice coverage and ice-rafted material on sedimentation in the Fram Strait. Nature 350:409-411.

Hebbeln D. (2000), Flux of ice-rafted detritus from sea ice in the Fram Strait. Deep-Sea Research I 47:1773-1790.

Hirche H.J. and K.N. Kosobokova (2007). Distribution of Calanus finmarchicus in the northern North Atlantic and Arctic Ocean – expatriation and potential colonization, Deep-Sea Research Part II 54:2729–2747.

Holm E. (1994). Sources and distribution of anthropogenic radionuclides in the marine environment in radioecology: lectures in Environmental Radioacitivity, ed. E. Holm, Vol. 65, pp. 279. World Scientist, Singapore.

Huh C., N.G. Pisias, J.M. Kelley, T.C. Maiti and A. Grantz (1997). Natural radionuclides and plutonium in sediments from the western Arctic Ocean: sedimentation rates and pathways of radionuclides. Deep-Sea Research II 44(8):1725-1743.

IAEA (1985). Sediment Kds and Concentration. Factors for Radionuclides in the Marine Envi- ronment, IAEA Technical Report Series. No. 247, Vienna.

IAEA (1998). Radiological Conditions of the Western Kara Sea. Assessment of the Radiological Waste in the Arctic Seas—Report of the International Arctic Seas Assessment Project (IASAP), Radiological Assessment Reports Series, IAEA, Vienna.

Ioannidou A. and C. Papastafanou (2006). Precipitation scavenging of 7Be and 137Cs radionuclides in air. Journal Environmental Radiactivity 85:121-136.

Johnson-Pyrtle A. and M. Scott (2001). Distribution of ^{137}Cs in the Lena River Estuary-Laptev Sea system. Marine Pollution Bulletin 42(10):912-926

JRNEG (1994). Radioactive contamination at dumping sites for nuclear waste in the Kara Sea. Results from the Russian– Norwegian 1993 expedition to the Kara Sea. Joint Russian– Norwegian Expert Group for Investigation of Radioactive Contamination of the Northern Areas. (ISBN 82-993079-3-7)

JRNEG (1996). Dumping of radioactive waste and investigation of radioactive contamination in the Kara Sea. Results from 3 years of investigations (1992–1994) performed by the Joint Norwegian–Russian Expert Group. Joint Russian–Norwegian Expert Group for Investigation of Radioactive Contamination of the Northern Areas. (ISBN 82-993079-4-5).

Kabakchi S.A, A.V. Putilo. And E.R. Nazin (1995). Data analysis and physicochemical modelling of the radiation accident in the southern Urals in 1957, Atomnaya Energiya 78(1):46–50

Kadko D (2000). Modeling the evolution of the Arctic mixed layer during the fall 1997 Surface Heat Budget of the Arctic Ocean (SHEBA) Project using measurements of 7Be. Journal Geophysical Research 105(C2):3369–3378.

Kadko D. (2009). Rapid oxygen utilization in the ocean twilight zone assessed with the cosmogenic isotope 7Be. Global Biogeochemistry Cycles, 23, GB4010, doi:10.1029/2009GB003510.

Kadko D. and D. Olson (1996). Beryllium-7 as a tracer of surface water subduction and mixed-layer History. Deep-Sea Research I 43(2), 89-l 16.

Kadko D. and P. Swart (2004). The source of the high heat and freshwater content of the upper ocean at the SHEBA site in the Beaufort Sea in 1997. Journal Geophysical Research 109, C1022, doi:10.1029/2002JC01734.

Kaleschke L., C. Lüpkes, T. Vihma, J. Haarpaintner, A. Bochert, J. Hartmann and G. Heygster (2001). SSM/I sea ice remote sensing for mesoscale ocean-atmosphere interaction analysis. Journal of Remote Sening 27(5):526– 537.

Kara AB, P.A. Rochford and H.E. Hurlburt (2000). An optimal definition for ocean mixed layer depth. Journal Geophysical Research 105:16803-16821.

Kelley J.M., L.A. Bond and T.M. Beasley (1999). Global distribution of Pu isotopes and ^{237}Np, Science of the Total Environment 237/238:483–500.

Kempema E.W., E. Reimnitz and P.W. Barnes (1989). Sea ice sediment entrainment and rafting in the Arctic. Journal of Sedimentary Petrology 59:308-317.

Kenna T. (2002). Determination of plutonium isotopes and neptunium-237 in environmental samples by inductively coupled plasma mass spectrometry with total sample dissolution. Journal of Analytical Atomic Spectrometry 17:1471-1479.

Kern S., L. Kaleschke, and D. A. Clausi (2003). A comparison of two 85GHz SSM/I ice concentration algorithms with AVHRR and ERS-2 SAR imagery, IEEE Trans. Geosci. Remote Sens. 41(10):2294-2306.

Kipput G.W. (1978). An investigation of sedimentary processes in lakes. PhD. Dissertation. Columbia University, New York.

Koch D.M., D.J. Jacob and W.C. Graustein (1996). Vertical transport of tropospheric aerosols as indicated by 7Be and 210Pb in a chemical tracer model. Journal Geophysical Research 101(D13):18651-18666.

Kovacs A. (1996). Sea Ice. Part I Bulk salinity versus ice floe thickness. CRREL report.

Krey P.W., E.P. Hardy, C. Pachucki, F. Rourke, J. Coluzza and W.K. Benson (1976). Mass isotopic composition of global fallout plutonium in soil. In: Transuranium Nuclides in the Environment, IAEA (Internal Atomic Energy Agency), Vienna IAEA-SM-199/39, pp.671-678.

Kulan A., A. Aldahan, G. Possnert and I. Vintersved (2006). Distribution of ^{7}Be in surface air of Europe. Atmospheric Environment 40(21):3855-3868.

Kwok R. (2000). Recent changes of the Arctic Ocean sea ice motion associated with the North Atlantic Oscillation, Geophysical Research Letters 27(6):775-778.

Kwok R. and D. A. Rothrock, (1999). Variability of Fram Strait ice flux and North Atlantic oscillation. Jorunal Geophysical Research 104:5177-5189.

Kwok R. and D. A. Rothrock (2009). Decline in Arctic sea ice thickness from submarine and ICESat records: 1958–2008. Geophysical Research Letters 36, L15501, doi:10.1029/2009GL039035.

Kwok R., G. F. Cunningham, M. Wensnahan, I. Rigor, H.J. Zwally and D. Yi (2009). Thinning and volume loss of the Arctic Ocean sea ice cover: 2003-2008. Journal Geophysical Research 114, C07005, doi:10.1029/2009JC005312.

Lal D., P.K. Malhotra and B. Peters (1958). On the production of radiosiotopes in the atmosphere by cosmic radiation and their application to meteorology. Journal Atmospheric and Terrestrial Physics 12:306-328.

Lal D. and B. Peters (1962). Cosmic ray produced isotopes and their application to problems in geophysics, in: Wilson J.G. (Ed.), Progress in Elementary and Cosmic Ray Physics 6, North Holland, Amsterdam, pp 1-74.

Lal D. and B. Peters (1967). Cosmic ray produced radioactivity on the Earth, in Sitte K. (Ed.), Encyclopedia of Physics. Springer-Verlag, New York, pp 551-612.

Lambert G., A. Ardouin, and G. Polian (1982). Volcanic output of long-lived radon daughters, Journal Geophysical Research 87(C13):11,103-11,108.

Landa E., E. Reimnitz, D. Beals, J. Pochkowski and I. Rigor (1998). Transport of ^{137}Cs and ^{239,240}Pu with ice-rafted debris in the Arctic Ocean. Arctic 51:27-39.

Lannuzel D., V. Schoemann, J. de Jong, B. Pasquer, P. van der Merwe, F. Masson, J.L. Tison, A.R. Bowie (2010) 'Distribution of dissolved iron in Antarctic sea ice: Spatial, seasonal, and inter-annual variability', *Journal of Geophysical Research*, 115 (3) EJ ISSN 0148-0227

Larssen B.B., A. Elverhoi and P. Aagard (1987). Study of particulate material in sea ice in the Fram Strait—a contribution to paleoclimatic research?. Polar Research 5: 313-315.

Lepore K., S.B. Moran and J.N. Smith (2008). 210Pb asatracerofshelf–basintransportandsedimentfocusingin the ChukchiSea Deep- Sea Research II. doi:10.1016/j.dsr2.2008.10.021

Lisitzin A.P (2002). Sea-ice and iceberg sedimentation in the ocean. Recent and past. Springer-Verlag, 563 pp.

Livingston H.D. and V.T. Bowen (1979). Pu and ^{137}Cs in coastal sediments. Earth and Planetary Science Letters 43:29-45.

Livingston H.D. and P.P. Povinec (2000). Anthropogenic marine radioactivity. Ocean & Coastal Management 43:689-712.

Loeng H. (1991). Features of the physical oceanographic conditions in the central parts of the Barents Sea. Polar Research 10: 5-18.

Macdonald R.W., .A. Barrie T.F. Bidleman, M.L. Diamond, D.J. Gregord, R.G. Semkine, W.M.J. Strachan, Y.F. Li, F. Wania, M. Alaee, L.B. Alexeeva, S.M. Backus, R. Bailey, J.M. Bewers, C. Gobeil, C.J. Halsall, T. Harner, J.T. Hoff, L.M.M. Jantunen, W.L. Lockhart, D. Mackay, D.C.G. Muir, J. Pudykiewicz, K.J. Reimer, J.N. Smith, G.A Stern, W.H. Schroeder, R. Wagemannk, M.B. Yunker (2000). Contaminants in the Canadian Arctic: 5 years oFf progress in understanding sources, occurrence and pathways. The Science of the Total Environment 254. 93]234

Macdonald R.W., T.T. Harner and J. Fyfe (2005). Recent climate change in the Arctic and its impact on contaminant pathways and interpretation of temporal trend data. Science of the Total Environment 342: 5-86.

Malmgren F. (1927). On the properties of sea ice. J. Geophys. Res. 105, 1918-1925,1, 1-67.

Markus T. and D. J. Cavalieri (2000), An enhancement of the NASATeam sea ice algorithm, IEEE Trans. Geoscience Remote Sensing. 38(3):1387–1398.

Masqué P., J.K. Cochran, D. Hebbeln, D.J. Hirschberg, D. Dethleff and A.Winkler (2003). The role of sea ice in the fate of contaminants in the Arctic Ocean: Plutonium atom ratios in the Fram Strait. Environment Science and Technology 37:4848-4864.

Masqué P., J.K. Cochran, D.J. Hirschberg, D. Dethleff, D. Hebbeln, A. Winkler and S. Pfirman (2007). Radionuclides in Arctic sea ice: tracers of sources, fates and ice transit time scales. Deep-Sea Research I, doi:10.1016/j.dsr.2007.04.016.

Maykut G.A. (1985). The ice environment. In Horner.R. (ed.). Sea Ice Biota. CRC Press, Boca Raton, FL, pp. 21-82.

Meausures C.I. (1999). The role of entrained sediments in sea ice in the distribution of aluminium and iron in the surface waters of the Arctic Ocean. Marine Chemistry 68:59-70.

Meese D.A., E. Reimnitz, W.B. Tucker, A.J. Gow, J. Bischof and D. Darby (1997). Evidence for radionuclide transport by sea-ice. Science of the Total Environment, 202, 267-278.

Melnikov S.A. (1991). Report on Heavy Metals. The State of the Arctic Environment Reports, Arctic Centre, University of Lapland, 2:82-153.

Moore R. M. and J. N. Smith (1986). Disequilibria between 226Ra,210Pb and 210Po in the Arctic Ocean and the implications for chemical modification of the Pacific water inflow. Earth and Planetary Science Letters 77:285-292.

Mullen R.E., D.A. Darby and D.L. Clark (1972). Significance of atmospheric dust and ice rafting for Arctic Ocean sediment. Geology Society America Bulletin 83:205-212.

Muramatsu H., S. Yoshizawa, T. Abe, T. Ishii, M. Wada, Y. Horiuchi and R. Kanekatsu (2008). Variation of 7Be concentration in surface air at Nagano, Japan. Journal of Radioanalytical and Nuclear Chemistry 275(2):299-307.

Murray, M.S., L. Anderson, G. Cherkashov, C. Cuyler, B. Forbes, J.C. Gascard, C. Haas, P. Schlosser, G. Shaver, K. Shimada, M. Tjernström, J. Walsh and J. Wandell, Z. Zhao (2010). International Study of Arctic Change: Science Plan. ISAC International Program Office, Stockholm.

Mysak L.A., (2001). Patterns of Arctic circulation. Science 293:1269-1270.

Nakawo M. and N.K. Sinha (1981). Growth rate and salinity profile of first-year sea ice in the high Arctic. Journal Glaciology 27:315-330.

Nakawo M. and Sinha N.K. (1984). A note on brine layer spacing and convection in young sea ice. Journal Geophysical Research 84:1176-1186.

Nghiem S.V., I.G. Rigor, D.K. Perovich, P. Clemente-Colon, J.W. Weatherly, and G. Neumann (2007). Rapid reduction of Arctic perennial sea ice. Geophysical Research Letters 34: L19504.

Not C., C. Hillaire-Marcel, B. Ghaleb, L. Polyak, and D. Darby (2008). 210Pb–226Ra–230Th systematics in very low sedimentation rate sediments from the Mendeleev Ridge (Arctic Ocean). Canadian Journal Earth Science 45:1207-1219.

Notz D. and M.G. Worster (2009). Desalination processes of sea ice revisited. Journal Geophysical Reseach Vol 114, c05006, doi: 10,1029/2008JC004885

NSIDC, National Snow and Sea Ice Data Center: Fetterer, F., K. Knowles, W. Meier and M. Savoie (2002), updated 2009. Sea Ice Index. Boulder, CO: National Snow and Ice Data Center. Digital media.

Nürnberg D., I. Wollenburg, D. Dethleff, H. Eicken, H. Kassens, T. Letzig, E. Reimnitz and J. Thiede (1994). Sediments in Arctic Sea ice: implications for entrainment, transport and release. Marine Geology 119:185-214.

Osterkamp T.E. (1978). Frazil ice formation: a review. Journal of Hydraulic Division. American Society of Civil Engineers, 104(HY9):1239-1255.

Oughton D.H., L.K. Fified, J.P. Day, R.C. Cresswell, L. Skipperud and B. Salbu (1999). Determination $^{240}Pu/^{239}Pu$ isotope ratio in Kara Sea and Novaya Zemlya sediments using Accelerator Mass Spectrometry. In: Symposium on Marine Pollution. IAEA-SM-354, IAEA, Vienna, pp 123-128.

Oughton, D.H., Skipperud, L., Fifield, L.K., Cresswell, R.G., Salbu, B., and Day, P., 2004. Accelerator mass spectrometry measurement of $^{240}Pu/^{239}Pu$ isotope ratios in Novaya Zemlya and Kara Sea sediments. Applied Radiation and Isotopes 61:249-253.

Pabi S, G.L.van Dijken and K.R. Arrigo (2008). Primary production in the Arctic Ocean, 1998–2006. Journal Geophysical Research 113:C08005.

Papastefanou C. (2008). Radioactive aerosols. Radiactivity in the Environment. Vol 2. Series editor: M.S. Baxter.

Pavlov, V., O. Pavlova and R. Korsner (2004). Sea ice fluxes and drift trajectories from potential sources, computed with a statistical se ice model of the Arctic Ocean. Journal Marine Systems 48:133-157.

Perovich D.K. and J. A. Richter-Menge (2009). Loss of Sea Ice in the Arctic. Annual Review Marine Science 1(4)17-41.

Pfirman, S.L., J.C. Gascard, I. Wollenburg, P. Mudie and A. Abelmann (1989). Particle-laden Euroasian Arctic sea ice: Observations from July to August 1987. Polar Research 7:59-66.

Pfirman S., M.A. Lange, I. Wollenburg and P. Schlosser (1990). Sea ice characteristics and the role of sediment inclusions in deep-sea deposition: Arctic-Antarctic comparisons. In: U. Bleil and J. Thiede (editors), Geological History of the Polar Oceans: Arctic versus Antarctic. Kluwer Academic Publishers, 187-211.

Pfirman S.L., H. Eicken, D. Bauch and W.F. Weeks (1995). The potential transport of pollutants by Arctic Sea ice. The Science of the Total Environment 159:129-146.

Pfirman S.L., J.W. Kogeler and I. Rigor (1997). Potential for rapid transport of contaminants from the Kara Sea. The Science of the Total Environment 202:111-122.

Pfirman S.L., R.I. Colony and I. Rigor (2004). Variability in Arctic sea ice drift. Geophysical Research Letters 31, doi:10.1029/2004GL020063.

Phillipes, GW. G. H. Share, S. E. King, R. A. August, A. J. Tylka, J. H. Adams Jr., M. I. Panasyuk, R. A. Nymmik, B. M. Kuzhevskij, V. S. Kulikauskas, D. A. Zhuravlev, A. R. Smith, D. L. Hurley and R. J. McDonald (2001). Correlation of upper-atmospheric Be-7 with solar energetic particle events. Geophysical Research Letters 28:939-942.

Polyakov I. V. and M. A. Johnson (2000). Arctic decadal and interdecadal variability, Geophysical Research Letters 27(24):4097-4100.

Ramseier R.O., C. Garrity, E. Bauerfeind and R. Peinert (1999). Sea-ice impact on long term particle flux in the Greenland Sea's is Odden-Nordbukta region during 1985-1996. Journal Geophysical Research 104:5329-5343.

Reinmnitz E., E.W. Kempema and P.W. Barnes (1987). Anchor ice, seabed freezing, and sediment dynamics in shallow arctic seas. Journal Geophysical Research 92(C13):14671-14678.

Reimnitz, E., E. Hayden, M. McCormick and P.W. Barnes (1991), Preliminary observations on coastal sediment loss through ice rafting in Lake Michigan. Journal Coastal Research 7: 653–664.

Reimnitz E., I. Marincovich, M. McCormick and W. Briggs (1992). Suspension freezing of bottom sediment and biota in the Northwest Passage and implications for Arctic Ocean sedimentation. Canadian Journal Earth Science 2:693-703.

Reimnitz E., L. J.R. Clayton, E.W. Kempema, J.R. Payne and W.S. Weber (1993). Interaction of rising frazil wit suspended particles: tank experiments with application to nature. Cold Regional Science and Technology 21:117-135.

Rigor I.G. and J.M. Wallace (2004). Variations in the age of Arctic sea-ice and summer sea-ice extent. Geophysical Reseach Letters 31:L0940001, doi:10,1029/2004GL019492

Rigor I.G., J.M. Wallace and R.L. Colony (2002). Response of Sea Ice to the Arctic Oscillation. Journal Climate 15:2648-2664.

Rothrock, D. A., Y. Yu, and G. A. Maykut (1999). Thinning of the Arctic sea-ice cover, Geophysical Research Letters 26(23):3469-3472, doi:10.1029/ 1999GL010863.

Rothrock, D. A., J. Zhang, and Y. Yu (2003). The arctic ice thickness anomaly of the 1990s: A consistent view from observations and models, Journal Geophysical Research 108(C3):3083, doi:10.1029/2001JC001208.

Rothrock D.A., D.B. Percival and M. Wensnahan (2008). The decline in arctic sea-ice thickness: Separating the spatial, annual, and interanual variability in a quarter century of submarine data. Journal Geophysical Research 113,C05003, doi:10.1029/2007JC004252.

Rudels B. (2001). Ocean Current: Arctic Basin circulation. In: Steele J., S. Thorpe, K. Turekian (Eds.), Encyclopedia of Ocean Sciences, Academic Press, London, pp 177-187.

Rudels B., E.P. Jones, L.G. Anderson and G. Kattner (1994). On the intermediate depth waters of the Arctic Ocean. In: Johannessen, O.M., Muench, R.D., Overland, J.E. (Eds.), The role of the Polar Oceans in Shaping the Global Climate. Geophys. Monographs, 85. American Geophysical Union, Washington, pp. 33-46.

Rudels B., L.G. Anderson and E.P. Jones (1996). Formation and evolution of the surface mixed layer and halocline of the Arctic Ocean. Journal Geophysical Research 101(C4):8807-8822.

Rudels B, R. D. Muench, J Gunn, U. Schauer and H. J. Friedrich (2000). Evolution of the Arctic Ocean boundary current north of the Siberian shelves. Journal Marine Systems 25: Issue 1, pp 77-99.

Salbu B. (2001). Actinides associated with particles. Plutonium in the environment. A. Kudo (Editor). Elsevier Science Ltd.

Sanchez-Cabeza J.A., P. Masqué and I. Ani-Ragolta (1998). 210Pb and 210Po analysis in sediments and soils by microware acid digestion. Journal Radioanalytical and Nuclear Chemistry 227(1-2):19-22.

Schauer U. (2008). The expedition ARKTIS-XXII/2 of the research vessel "Polarstern" in 2007, U. Schauer (ed.), Berichte zur Polar- und Meeresforschung = Reports on polar and marine research, Alfred Wegener Institute for Polar and Marine Research, Bremerhaven, 579, pp. 271.

Schauer U., R.D. Muench, B. Rudels and L. Timokhov (1997). Impact of eastern Arctic shelf waters on the Nansen Basin intermediate layers. Journal Geophysical Research 102(C2): 3371-3382.

Schlosser P., J.H. Swift, D. Lewis and S.L. Pfirman (1995). The role of the large-scale Arctic Ocean circulation in the transport of contaminants, Deep-Sea Research II 42(6):1341-1367.

Shy T.L.,and J.E. Walsh (1996). North Pole ice thickness and association with ice motion history 1977,1992, 1979,1986, Geophysical Research Letters 23:2975-2978.

Silker W.B. (1972). Beryllium-7 and fission products in the GEOSECS II water column and applications of their ocean distributions. Earth Planet Science Letters 16:131-137.

Sitaram Garimella, Kanayathu Koshy and Shusendra Singh (2003). Concentration of 7Be in surface air at Suva, Fiji. The South Pacific Journal of Natural Science 21(1):15-19.

Skipperud L., D.H. Oughton, L.K. Fifield, O.C. Lind, S. Tims, J. Brown and M. Sickel (2004). Plutonium isotope ratios in the Yenisey and Ob estuaries. Applied Radiation and Isotopes 60 (2-4):589-593.

Smedsrud L.H., A. Sirevaag, K. Kloster, A. Sorteberg and S. Sandven (2011), Recent wind driven high sea ice export in the Fram Strait contributes to Arctic sea ice decline. The Cryosphere Discuss 5:1311-1334.

Smith J.N. and K.M. Ellis (1995a). Radionuclide tracer profiles at the CESAR Ice Station and Canadian Ice Island in the Western Arctic Ocean. Deep Sea Research II 42(6):1447-1470.

Smith, J.N., K.M. Ellis, S. Dahle and D. Matishov (1995). Sedimentation and mixing rates of radionuclides in the Barents Sea sediments off Novaya Zemlya. Deep-Sea Research II 42: 1341-1493.

Smith J.N., S.B. Moran and R.W. Macdonald (2003). Shelf-basin interaction in the Arctic Ocean based on ^{210}Pb and Ra isotope tracer distributions. Deep-Sea Research I 50:397-416.

Smith, J.N., Ellis, K.M., Polyak, L., Ivanov, G., Forman, S.L., and Moran, S.B., 2000. ^{239,240}Pu transport into the Arctic Ocean from underwater nuclear tests in Chernaya Bay, Novaya Zemlya. Continental Shelf Research 20:255-279.

Spreen, G., L. Kaleschke and G. Heygster (2008). Sea ice remote sensing using AMSR-E 89 GHz channels. Journal Geophyssical Research 113, C02S03, doi:10.1029/2005JC003384.

Staley D.O. (1982). Strontium-90 in surface air and the stratosphere: some interpretations of the 1963-75 data. Journal Atmospheric Research 77(6):1061-1070.

Stierle A. P. and H. Eicken (2002). Sedimentary inclusions in Alaskan coastal sea ice: Smallscale distribution, interannual variability and entrainment requirements. Arctic Antarctica Alpine Research 34(4):103-114.

Stroeve, J., M. Serreze, S. Drobot, S. Gearheard, M. Holland, J. Maslanik, W. Meier, and T. Scambos (2008). Arctic sea ice extent plummets in 2007, Eos Trans. AGU, 89,13-14.

Rigaud S., V. Puigcorbé, P. Camara-Mor2,3, N. Casacuberta, M. Roca-Martí, J. Garcia-Orellana, C.R. Benitez-Nelson, P. Masque and T. Church (2012) An assessment of the methods, calculation and uncertainties in the determination of 210Po and 210Pb activities in seawater. Submitted to the Limnology and Oceanography: Methods

Thomas D.N. and G.S. Dieckmann (2003). Sea Ice: An introduction to its physics, chemistry, biology and geology. Blackwell.

Thompson D.W.J. and J.M. Wallace (1998). The Arctic Oscillation signature in the wintertime geopotential height and temperature fields. Geophysical Research Letters 25:1297-1300.

Thorndike V.T. (1986). Kinematics of sea ice. In: Untersteiner, N., Ed. Air-Sea-Ice Interactions. Plenum Press, New York, pp.489-549.

Thorndike V.T. and R.I. Colony (1982). Sea ice motion in response to geostrophic winds. *Journal Geophysical Research* 87:5845–5852.

Tison J.L., A. P. Worby, B. Delille, F. Brabant, S. Papadimitriou, D. N. Thomas, J. de Jong, D. Lannuzel, and C. Haas (2008). Temporal evolution of decay summer first-year sea ice in the western Weddell sea, Antarctica, Deep Sea Research IIA 55:975-987, doi:10.1016/j.dsr2.2007.12.021.

Tovar-Sánchez A., C. M. Duart, J. C. Alonso, S. Lacorte, R. Tauler, C. Galván-Malagón (2010). Impacts of metals and nutrients released from melting multiyear Arctic sea ice. Journal Geophysical Research -Oceans, Vol. 115, Pg. 1

Tucker III W.B, A.J. Gow, D.A. Meese, H.W. Bosworth and E. Reimnitz (1999). Physical characteristics of summer sea ice across the Arctic Ocean. Journal of Geophysical Research, 104(C1):1489-1504.

Tucker III W. B., J. W. Weatherly, D. T. Eppler, D. Farmer and D. Bentley (2001). Evidence for the rapid thinning of sea ice in the western Arctic Ocean at the end of the 1980s, Geophysical Research Letters 28(14):2851–2854.

Turekian K.K., W.C. Graustrein and J.K. Cochran (1989). Lead-210 in the SEAREX program: An aerosols tracer across the Pacific. In: Chemical Oceanography (Eds. J.P. Piley and R. Chester). Academic Press, London, 51-81.

Turekian K.K. and W.C. Graustrein (2003). Natural radionuclides in the atmosphere. In: Treatise on Geochemistry (Ed. R.K. Keeling). Elsevier Press 4:261-279.

Uematsu M., R.A. Duce and J.M. Prospero (1994). Atmospheric beryllium-7 concentrations over the Pacific Ocean. Geophysical Research Letters 21(7):561-564.

UNSCEAR (1982). Ionization Radiation: Sources and biological effects. United Nations Scientific Committee on the effects of atomic radiation, New York, United Nations. Report to the General Assembly, with annexes.

UNSCEAR (2000). Sources and effects of ionizing radiation. United Nations Scientific Committee on the effects of atomic radiation, New York, United Nations. Report to the General Assembly, with annexes.

Untersteiner N. (1968). Natrual deslination and equilibrium salinity profile of perennial sea ice. Journal Geophysical Research 73:1251-1257.

Vakulovsky SM., I.I. Kryshev, A.I. Nikitin, T.V. Savitsky, S.V. Malyshev and E.G. Tertyhnik (1995). Radioactie contamination in the Yenisey River. Journal of Environmental Radioactivity 29(3):225-236.

Vinje N. Nordlund, and A. Kvambekk (1998). Monitoring ice thickness in Fram Strait. Journal Geophysical Research 103:10.437-10 449.

Vorobiova MI., M.O. Degteva, D.S. Burmistrov, N.G. Safronova, V.P. Kozheurov, L.R. Anspauch and B.A. Napier (1999). Review of historical monitoring data on Techa River contamination. Health Physics 76(6):605-618.

Wadhams P. (1983). Arctic sea-ice morphology and its measurements, Journal of the Society of Underwater Technology 9(2):1-12.

Wadhams P. and N. R. Davis (2000). Further evidence of ice thinning in the Arctic Ocean. Geophysical Research Letters 27:3973-3976.

Wakatsuchi M. (1983). Brine exclusión process from growing sea ice. Contribution-Hokkaido University (Sapporo). Low Temperature Science, Serie A(33):29-65.

Walsh E.L, WL Chapman and TL. Shy (1995). Recent decrease of sea lvel pressure in the central Arctic. Notes and correspondence. Journal of Climate 9.

Waters R.D., K.L Compton, V. Noikov and F.L. Parker (1999). Releases of radionuclides to surface waters at Krasnoyarsk-26 and Tomsk-7. Report: International Institute for Applied Systems Analysis, Laxenburg, Austria.

Weeks W.F. and S.F. Ackley (1986). The growth, structure, and properties of sea ice. In: N. Untersteiner (editor), Geophyssics of Sea Ice, NATO ASI Series B, Physics, Plenum Press. 9-164.

Whitman W. G. (1926). Elimination of salt from sea water ice. Amer. Journal Science 5:11 (62):126-132.

Windom H.L. (1969). Atmospheric dust records in permanent snowfields; implications to marine sedimentation. Geology Society America Bulletin 80:761-782.

WMO (1970). SEA-ICE NOMENCLATURE. WMO/OMM/BMO - No.259. Edition 1970 - 2004. Terminology - Volume I.

Wollenburg I. (1993). Sediment transport by sea ice: The recent sediment load of lithogenic and biogenic material, Ber. Polarforsschung, 127:1-159.

Woo, M.K. and D.J. Gregor, (1992). Arctic environment: Past, present and future. McMaster University, Department of Geography, Hamilton, 164pp.

Woodgate R.A , K. Aagaard, R. D. Muench, J. Gunn, GoK ran Bjok, B. Rudels, A.T. Roach, U. Schauer (2001). The Arctic Ocean Boundary Current along the Eurasian slope and the adjacent Lomonosov Ridge: Water mass properties, transports and transformations from mooredinstruments Deep-Sea Research I 48:1757-7792.

Yablokov A.V., B.K. Karasev, V.M. Rumyatsev, M.E. Kokeyev, O.I. Petrov, B.N. Lystsov, A.F. Yemelyanenkov and P.M. Rubossov (1993). “White book”. Facts and problems related to radioactive waste disposal in seas adjacent to the territory of the Russian Federation. Moscow: Office of the President of the Russian Federation.

Young J.A. and W.B. Silker (1980). Aerosol deposition velocities on the Pacific and Atlantic ocean calculatd from 7Be. Earth Planet. Science Letters 50:92-104.

Yu K.N. and L.Y.L. Lee (2002). Measurements of atmospheric 7Be properties using high-efficiency gamma spectrometry. Applied Radioactivity and Isotopes 57:941-946.

Zhang J., R. Lindsay, M. Steele and A. Schweiger (2008). What drove the dramatic retreat of arctic sea ice during summer 2007?. Geophysical Research Letters 35:L11505, doi:10.1029/2008GL034005

Zhang J., D. A. Rothrock and M. Steele (2000). Recent changes in arctic sea ice: The interplay between ice dynamics and thermodynamics. Journal Climate 13:3099-3114.